

**EMPIRICAL PROCESS PLANNING FOR EXPOSURE CONTROLLED
PROJECTION LITHOGRAPHY**

A Thesis
Presented to
The Academic Faculty

by

Ying Zhang

In Partial Fulfillment
Of the Requirements for the Degree
Master of Science in Mechanical Engineering

Georgia Institute of Technology

December, 2016

Copyright © 2016 by Ying Zhang

Empirical Process Planning for Exposure Controlled Projection Lithography

Approved by:

Dr. David W. Rosen, Advisor
School of Mechanical Engineering
Georgia Institute of Technology

Dr. Amit S. Jariwala
School of Mechanical Engineering
Georgia Institute of Technology

Dr. Jonathan S. Colton
School of Mechanical Engineering
Georgia Institute of Technology

Date Approved: August 26, 2016

ACKNOWLEDGEMENTS

I would like to take this opportunity to express my sincere thanks to my Master advisor, Dr. David W. Rosen for his understanding, support, patience, and inspiration. I would also like to express my big thanks to my co-advisor, Dr. Amit S. Jariwala for guiding me through the project. His experiences and insights brought me deep to the understand of this research. I thank him for his patience, knowledge, and support. I am grateful for their nice personalities and support.

I thank Dr. Jonathan S. Colton for being my committee member. His suggestions and comments on the projects really help to think deep inside the study.

I was fortunate to have had the opportunity to thank my team members in the projects: Mr.Changxuan Zhao, Ms. Xiayun Zhao, Ms. Jenny Wang, Mr. Will Borzon, and Mr. Youssef Emam for their intelligence and contribution. Thanks for their help for the past years.

I also thank all my lab members: Chad Hume, Narumi Watanabe, John-Travis Hansen, Sang-In Park and everyone for their help and suggestions.

I thank all my friends at home and abroad for their friendship. They have been providing me an enjoyable social atmosphere. I also thank Georgia Tech for providing such a great place to me. I really enjoy the campus life and its academic support.

Finally, I would express my love and sincere thanks to my family. Without them, I cannot receive a good education and life.

Table of Contents

ACKNOWLEDGEMENTS	iii
LIST OF TABLES	viii
LIST OF FIGURES	ix
LIST OF SYMBOLS AND ABBREVIATIONS	xiii
SUMMARY	xiv
CHAPTER 1 Introduction & Motivation	16
1.1 Introduction	16
1.1.1 Stereolithography (SLA)	17
1.1.2 Mask Projection Micro Stereolithography (MP μ SLA)	18
1.2 ECPL Process Overview	22
1.3 Motivation for study	23
1.4 Research Objective	25
1.5 Organization of this thesis	25
CHAPTER 2 LITERATURE REVIEW AND RESEARCH PROBLEM STATEMENT	27
2.1 Irradiance Model	27
2.2 Photopolymerization Model	30
2.2.1 Empirical modeling approach	32
2.2.2 Monomer concentration modeling approach	33

2.3 Existing process planning method for Mask Projection System.....	36
2.4 Existing process planning method for ECPL system	38
2.5 Research questions and hypotheses.....	45
2.6 Chapter Summary.....	46
CHAPTER 3 ECPL Fabrication System Design Improvement	47
3.1 Introduction	47
3.2 Existing System Design and Experimental Procedure	48
3.2.1 Energy Apply.....	48
3.2.2 Process – Resin chamber	51
3.2.3 Post Process	53
3.2.4 Experimental Procedure	54
3.3 Intensity and System Stability Check.....	55
3.4 Pretreatment Improvement.....	58
3.5 Experimental Results.....	60
3.6 Chapter Summary.....	63
CHAPTER 4 THEORETICAL MODELLING REVISION	64
4.1 Introduction to the ECPL process planning method	64
4.2 Revised Irradiance Model	66
4.2.1 Investigation on Effects of Irradiance Model.....	67
4.2.2 Irradiance Model Revision	69

4.3 Revised Polymerization Model	70
4.3.1 COMSOL Simulation Model.....	74
4.3.2 Analysis of the existing polymerization model	75
4.3.3 Empirical model of chemical reaction rates	79
4.4 Experimental Validation with Revised Model	87
4.5 Chapter Summary.....	89
CHAPTER 5 PROCESS PLAN FORMULATION AND VALIDATION	91
5.1 Formulation of the empirical process planning method.....	91
5.1.1 Empirical process planning method	91
5.1.2 Simulation results	94
5.2 Revised process planning method	100
5.2.1 Revised process plan algorithm	100
5.2.2 Shape limitation of the ECPL system.....	104
5.3 Experimental Validation	106
5.4 Error Analysis	112
5.5 Chapter Summary.....	117
CHAPTER 6 CLOSURE AND RECOMMENDATIONS	119
6.1 Summary of the thesis	119
6.2 Evaluation of hypothesis	121
6.3 Contributions.....	123

6.4. Future Work	125
APPENDIX	127
REFERENCES	136

LIST OF TABLES

Table 1: Specification of the components [9]	53
Table 2: Existing reaction rates for ECPL system	73
Table 3: Height dimension for 8px, 10px, 12px, 14px, 16px and 20px for 10s, 20s and 30s respectively	84
Table 4: Kp and Kt value for pixel 8, 10, 12, 14 and 16 from simulation	85
Table 5: Error percentage in height and diameter for case 1, 2 and 3	113
Table 6: Allowable discrepancy for process planning method	114

LIST OF FIGURES

Figure 1: Schematics of SLA machine [1].....	18
Figure 2: Scheme of the mask projection stereolithography process [3].....	19
Figure 3: Photography of X30, Perfactory 4 DSP, Projet 1200 and M1 (from left top to right bottom) [4] [5] [6] [7].....	22
Figure 4: Block diagram of ECPL system [9]	23
Figure 5: The resin chamber [9].....	23
Figure 6: Fabricating process of the ECPL system.....	27
Figure 7: Schematic of the ray tracing method [15]	28
Figure 8: Irradiance distribution [9].....	29
Figure 9: Comparison of simulation results from Irradiance model (solid lines) with data from the camera (dashed lines). Red corresponds to 10 pixels; green to 60 pixels and blue to 90 pixels [9]	30
Figure 10: Simulation results from 1D COMSOL® simulation (Red curve shows	35
Figure 11: Experimental results from different conversion value	35
Figure 12: Schematic of the layer cure model from Limaye [27].....	37
Figure 13: The flow chart for first “layer.” [30]	40
Figure 14: The flowchart for subsequent “layer.” [30].....	41
Figure 15: Half cross section geometry of the desired sample [9]	42
Figure 16: Bitmaps generated from the process planning method [9].....	43
Figure 17: Comparison of desired geometry and experimental geometry [9]	44
Figure 18: Schematic of the ECPL system [9].....	49
Figure 19: Photograph of projection system [9]	50

Figure 20: Schematic of the resin chamber [9].....	51
Figure 21: Steps in constructing the resin chamber [9]	51
Figure 22: Photography of the entire lab setup.....	52
Figure 23: Power meter used in the lab	55
Figure 24: Sensor placing in the working space	56
Figure 25: Example power meter measurements.....	56
Figure 26: Beam conditioning system with black fiber cloth and black cardboard.....	58
Figure 27: (a) comparison of the products made by three different students (b) comparison of the products made at different times.....	62
Figure 28: Flowchart for first “layer.” [30]	65
Figure 29: Flowchart for subsequent “layers.” [30].....	66
Figure 30: Comparison of simulation results from Irradiance model (solid lines) with data from the camera (dashed lines). Red corresponds to 10 pixels; green to 60 pixels and blue to 90 pixels [9]	67
Figure 31: Dimensional Error vs. Sample Desired Height	68
Figure 32: Examples of revised irradiance model. 10 pixels (left top); 60 pixels (right top); 90 pixels (bottom)	70
Figure 33: Schematic of FE model used in COMSOL	75
Figure 34: Comparison of experimental profiles (solid lines) with simulated profiles (dashed lines) Red for 5s exposure time; Green for 10s; Blue for 30s [9]	76
Figure 35: Cured Height vs. Time (blue for simulation results and red X for experimental data).....	77

Figure 36: Cross-section profile obtained from 90px, 60px, 30px, 20px and 10px through ECPL system.....	79
Figure 37: Parameter study for (a) K_p (b) $K_{(t,O_2)}$ & (c) oxygen diffusion rate	82
Figure 38: Comparison between the simulation result before changing the rate constants (blue line) and the simulation result after using the new rate constants (red line)	83
Figure 39: Plot of Table 3	84
Figure 40: Plot of Table 4 with fitted line and equation	86
Figure 41: Comparison between experimental results and simulation results of geometry profile for 10px bitmap with exposure time of 10s, 20s and 30s.....	87
Figure 42: Comparison between experimental results and simulation results of geometry profile for 20px bitmap with exposure time of 10s, 20s and 30s.....	88
Figure 43: Comparison between experimental results and simulation results of geometry profile for 30px bitmap with exposure time of 10s, 20s and 30s.....	89
Figure 44: Flowchart for first “layer.” [9]	92
Figure 45: Flowchart for subsequent “layer.” [9]	93
Figure 46: Plots illustration for the optimization [9]	94
Figure 47: 3-dimensional view of an aspherical lens.....	95
Figure 48: Desired half cross section of the aspherical lens with 0 conic constant.....	96
Figure 49: Simulation process for case 1	97
Figure 50: Desired half cross section of the aspherical lens with -1 conic constant	98
Figure 51: Simulation process for case 2	99
Figure 52: Cured profile for pixel 30 in radius	100

Figure 53: Geometry profile for case 2 from the revised process planning algorithm (Blue line: simulated geometry profile; Black line: desired geometry profile)	105
Figure 54: Slope analysis	106
Figure 55: Bitmaps and exposure times used to fabricate the sample	107
Figure 56: Comparison of the desired geometry and experimental result for case 1	107
Figure 57: Bitmaps and exposure times used to fabricate the sample for case 2.....	108
Figure 58: Comparison of the desired geometry and experimental result (right) for case 2	109
Figure 59: Comparison of the desired geometry and experimental result for case 3	111
Figure 60: Bitmaps and exposure times used to fabricate the sample for case 4.....	112
Figure 61: Comparison of the desired geometry and experimental result for case 4	112
Figure 62: Comparison of the desired geometry and experimental result with error band for case 1, 2 and 3	116

LIST OF SYMBOLS AND ABBREVIATIONS

ECPL	Exposure Controlled Projection Lithography
UV	Ultra Violet
3D	Three-dimensional
DMD	Digital Micromirror Device
DSC	(differential scanning calorimetry)
SLA	Stereolithography Apparatus

SUMMARY

Exposure Controlled Projection Lithography (ECPL) is a mask projection stereolithography process that can be used to create microlenses on flat or curved substrates. In the ECPL process, ultraviolet light patterned by a dynamic mask passes through a transparent substrate to cure photopolymer resin to a certain shape. The process planning method for ECPL systems in the literature has a relatively large error. For this research, an empirical process planning method is discussed to develop a better estimate of the process inputs for ECPL systems.

This thesis contains six chapters. Chapter 1 and 2 introduce the knowledge related to ECPL systems. The research objective and research questions are addressed based on the research limitations and gaps in the literature. The existing process planning method is described as well in these chapters. Chapter 3 describes the design of the ECPL system, along with the improvements made to achieve a more stable and reliable system. The samples fabricated by the ECPL system show a reasonable expectation of cleanness and smoothness.

The chemical reaction inside the resin through the ECPL system is modeled using a polymerization model. The incident light is modeled using an irradiance model. Chapter 4 provides a study of how to formulate more accurate polymerization and irradiance models than are found in the research literature.

The theoretical models developed in Chapter 4 are used to formulate a process planning method for an ECPL system in chapter 5. Multiple experiments are conducted to validate the process planning method. Chapter 6 offers a summary of the thesis and an

evaluation of the research questions. Future work after this research is also discussed in the end.

CHAPTER 1

Introduction & Motivation

Exposure Controlled Projection Lithography (ECPL) is developed based on Mask Projection Micro Stereolithography (MP μ SLA), which is a type of Stereolithography (SLA) based rapid prototyping process. The ECPL system is desired for rapidly fabricating precise microstructures for micro-optics applications. The dimensional error of the cured part resulting from using the existing ECPL process planning method was reported to be around 25%. The motivation for this study is to improve the system fabrication accuracy and precision. The following section will provide an introduction and background to stereolithography, micro-stereolithography, and mask projection micro-stereolithography, which leads to the ECPL system. The motivation for the study will be further explained in Section 1.3. The research objective is investigated in Section 1.4. Section 1.5 will present the organization of the thesis.

1.1 Introduction

Making a prototype has traditionally involved a flexible manufacturing process using a variety of tools and machines, and usually taking several weeks or months. An important advance in manufacturing operations is rapid prototyping, a process by which a solid physical model of a part is made directly from a three-dimensional CAD. The stereolithography (SLA) process is one part of that operation. It is based on the principle of curing (hardening) a liquid photopolymer into a specific shape. Micro stereolithography (μ SLA) is the application for SLA fabrication of microstructures at a finer resolution. At present, mask projection micro stereolithography is considered to be a

most effective way to produce microstructures. The Exposure Controlled Projection Lithography (ECPL) process reported in literature was developed based on the (MP μ SLA), which is a new method to fabricate precise microstructures for micro-optics applications. The following sections will provide an overview of these stereolithography processes.

1.1.1 Stereolithography (SLA)

Stereolithography is a type of additive manufacturing process used to create prototypes, production parts, models, and patterns. The technology was researched during the 1970s. Japanese researcher Dr. Hideo Kodama first invented the modern layered approach to stereolithography by using ultraviolet light to cure photosensitive polymers. In 1986, the term “stereolithography” was coined by Chuck Hull. He patented stereolithography as a method to fabricate 3D objects by “scanning” thin layers, which are cured by ultraviolet light from bottom to top. The first 3D printing company, 3D system Inc., was founded by him based on the patent [1].

The Stereolithography process first needs to transfer a CAD model to an STL file. By analyzing the STL file, the entire object is sliced into layers, and support structures and laser scan patterns are determined. The information is delivered to the SLA machine. Inside the SLA machine, the working box contains a laser, beam shaping optics, an XY scanner, a support platform and a resin bath of liquid photopolymer, as shown in Figure 1. When the machine starts, the laser traces and scans a part’s cross section to cure the resin. Then the support platform is moved down one-layer thickness, and the laser cures another layer on top of the just-created layer. The whole process repeats until the entire part has been built.

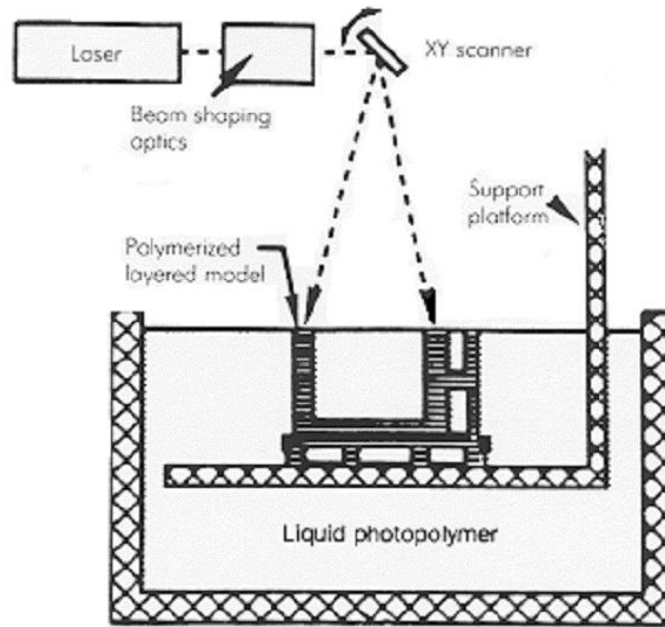


Figure 1: Schematics of SLA machine [1]

Stereolithography is the most mature of the rapid prototyping manufacturing technologies. The advantages of stereolithography are that it is strong, fast and has large size capability. The functional product can be fabricated within one day. The printing speed mainly depends on the geometric complexity of the products. The maximum build envelope can reach to approximately 1500x750x550 mm, and fabricated products are strong enough to be machined. The disadvantage is the cost; resin can cost more than \$2500 per gallon, and the machine can cost more than \$700,000 [2].

1.1.2 Mask Projection Micro Stereolithography (MP μ SLA)

Micro-stereolithography is an application of stereolithography. It was developed to fabricate microstructures in the field of microelectromechanical systems (MEMS), photonics, etc. It has much high resolution than traditional stereolithography. Mask projection micro stereolithography is a type of micro-stereolithography.

The difference between stereolithography and Mask projection stereolithography is that, in the Mask projection stereolithography process, entire cross section layers are cured at the same instant, in contrast to the commonly used translating laser; this eliminates the laser's XY movement, the error caused from the movement is reduced. Figure 2 presents the scheme of the mask projection stereolithography process. The system starts with generating bitmaps from CAD part. The information is then delivered to the computer. Dynamic masking (often DMD) is used in the mask projection stereolithography process to control the projection of bitmaps onto the photopolymer resin. The layer will start to cure the resin by using the first bitmap. After the first layer is cured, the platform moves to cure a second layer, on the top of the first, by using the second bitmap. The process will repeat until the entire part has been built.

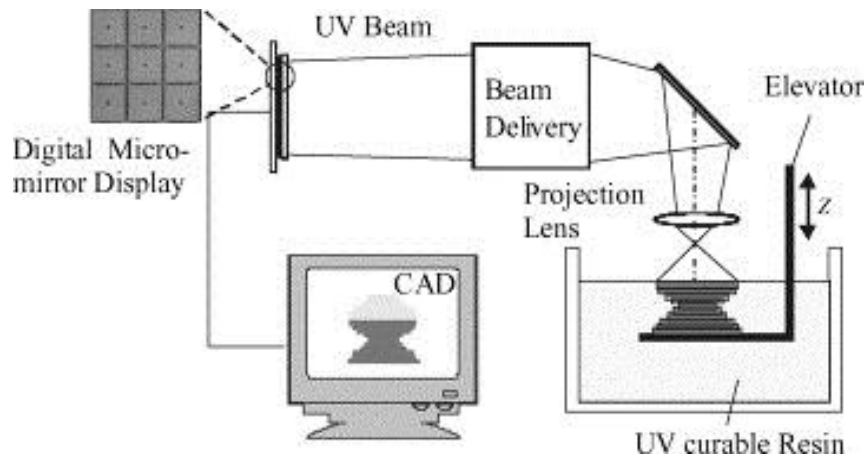


Figure 2: Scheme of the mask projection stereolithography process [3]

There are a few variations of mask projection stereolithography. The dynamic mask can be realized by liquid crystal display (LCD) screens, by spatial light modulators, or by digital micromirror devices (DMD). The resin vat can have a “supply on demand material feed system” rather than a full vat. For the translation stage, Ultraviolet light can

come from above the resin vat, so the stage moves downwards to add layers or ultraviolet light can come from beneath the resin vat, so the stage moves upwards to add layers.

Mask projection stereolithography processes require less time for curing each layer, and they eliminate error from X-Y direction movement. The advantages of Mask projection stereolithography are defined as machine simplicity, cost, and speed. Due to these advantages of mask projection stereolithography, current research of the exposure controlled projection lithography is based on mask projection stereolithography.

Through the literature review, mask projection stereolithography was used to commercialize for applications in industries. Example machines include X30 from Rapidshape, Perfactory 4 DSP from Envision Tec, Projet 1200 from 3D Systems, M1 from Carbon3D etc. Figure 3 shows the photography of X30, Perfactory 4 DSP, Projet 1200 and M1. The building frame for the X30 is 110/62mm. The resolution for the machine is 59 micrometers native voxel. This resolution is high, and it can be used in applications for various industries. One example is used for jewelry. It is also reported that the liquid resins can be obtained in different colors and physical properties provided by Rapidshape. The price for the machine is around 10,000 to 50,000 dollars [4]. The build platform for the Perfactory 4 DSP is 160x100x230mm. The dynamic voxel resolution of the Z-axis is 25 to 150 micrometers. The native pixel size is 83 micrometers. The primary market for the Perfactory 4 DSP is hearing aids. The price for the machine is about 115,000 dollars [5]. The print volume for the Projet 1200 is 43x27x150mm. The native resolution is 56 microns and layer thickness is about 0.03mm. It is a low-cost professional 3D printer. The applications for the Projet 1200 are various. It can be used in electronics, dental and jewelry fabrication operations. The price for the

machine is about 4,900 dollars [6]. The build envelope for the M1 is 144x81x330 mm. It was the first commercial 3D printer from Carbon3D in 2016. Carbon3D suggested that the M1 is ideal for functional prototyping and low-volume manufacturing applications. Moreover, the M1 is offered as an Internet-connected printer to allow Carbon3D to monitor more than 1 million data points per day from each printer. Carbon3D will send update software when issues are detected. They sell the M1 as a machine and software. The whole package for the M1 is priced at \$40,000 per year with a minimum three-year term, since they will provide follow-up support and software [7]. The theory in their machine is based on continuous liquid interface production of 3D objects [8], which is a similar process to the ECPL system.





Figure 3: Photography of X30, Perfactory 4 DSP, Projet 1200 and M1 (from left top to right bottom) [4] [5] [6] [7]

1.2 ECPL Process Overview

The Exposure Controlled Projection Lithography (ECPL) process is similar to the mask projection micro stereolithography process. The difference between the ECPL process and other conventional mask projection micro stereolithography processes is that the stage in the ECPL process is fixed. There is no movement in either the X-Y or the Z direction. Figure 4 shows a block diagram of the ECPL process [9]. As the block diagram indicates, the process model of the ECPL system contains three main parts: apply energy, process, and post-process. To apply energy, light from an ultraviolet source passes through a beam expander to expand the laser beam diameter. Then the light passes through a diffuser to enlarge the diameter and homogenize the beam's intensity, and then through a collimating lens to collimate the light. After that, a UV coated mirror is used to

direct the light on a dynamic mask, which is the DMD projection system. The projection system is used to enlarge or reduce the image presented on the DMD and to project it on the resin chamber. The part is cured in the resin chamber, which consists of two glass slides and a spacer, as shown in Figure 5. The uncured monomer resin is loaded inside. After the curing process is finished, the product will go into a post process, where the uncured resin is washed off, and the final part will be obtained on the substrate [9].

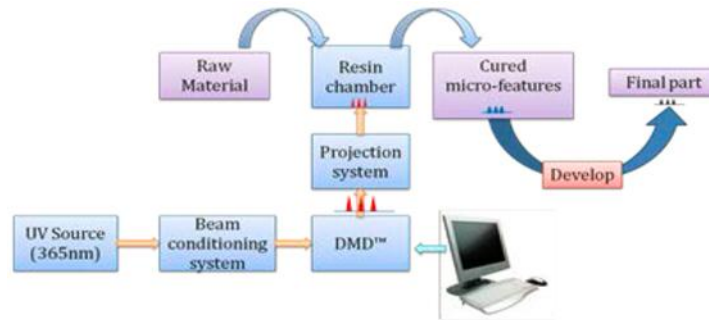


Figure 4: Block diagram of ECPL system [9]

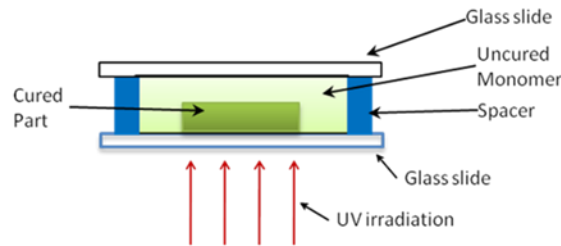


Figure 5: The resin chamber [9]

1.3 Motivation for study

Through the literature, mask projection stereolithography shows its flexibility for fabricating microstructures with high resolution, low cost, and fast printing speed. Due to these advantages, mask projection stereolithography is considered to be a promising process and shows value to be developed further. The motivation for the ECPL process

was to develop a cheap and fast way to produce microstructures with finer resolution. This is considered to be valued since it does not include error from the stage movement. The ECPL process can be even applied for more precise production such as lenses. Recently researchers such as Erdmann et al. [10] and Mizukami et al. [11] have developed techniques similar to the ECPL process. However, the ability to control the process to achieve high accuracy and precision in the final cured shape was not presented. The revised process planning method to control the lateral dimensions of the cured part in the ECPL process with consideration of a ray tracing model and photopolymerization kinetic model was presented by Jariwala et al. [12]. The cured results showed a significant deviation with simulation results in dimensions. Therefore, a hypothesis was developed by Jariwala et.al [13] that the effect of oxygen diffusion and inhibition should be considered during the polymerization process. The revised process planning method provided better control of the curing results. However, accuracy was still not satisfied, and the model was not suitable for all cases. In order to improve accuracy, a similar process planning method, with revised rate constant, was presented by Jariwala et al. [13]. A unique process planning approach was demonstrated which simulated the models in the COMSOL software package and then formulated in MATLAB software to simulate the entire curing process. With the experimentally validated rate constant, the error between simulation and experiments was still around 15%, and the result was not repeatable. This thesis research is thus to conduct a better process planning method model to the ECPL system in order to enable its high flexibility for fabricating microstructures. Due to the current level of research, the application is mainly focused on lens fabrication.

1.4 Research Objective

The primary objective of this research is:

To increase accuracy in obtaining a geometry profile within 5% error of the overall desired geometry profile of the process plan for fabricating lens using the ECPL process.

A process planning method to predict the shape of a part cured by the ECPL process is available in literature and is based on solving the polymerization kinetics and irradiation model. The dimensional error of the cured part resulting from using this process planning method was more than 15%. The goal of this research is to modify the existing process planning method to improve the dimensional accuracy and to reduce the dimensional error within 5%.

In order to reach the research objective, the concept of ECPL system needs to be fully understood. The source, which may cause possible variations and discrepancies, will be identified. By fixing these variations and discrepancies, the revised process planning method is expected to predict the final products within reasonable errors.

1.5 Organization of this thesis

Chapter 1 is intended to provide a brief introduction to this thesis work. The background of stereolithography, mask projection stereolithography and previous work is done for exposure controlled projection lithography process. The motivation of the study and research objective is also indicated.

Chapter 2 presents a literature review of existing process planning methods as well as the chemical aspect of knowledge in order to fulfill the objective. Research limitations and gaps are then analyzed followed by research questions and hypothesis.

Chapter 3 introduces the fabrication of the ECPL system. Existing system design and experimental procedure are explained, followed by pretreatment improvement and a system stability check. The post-processing is described, and fabricated samples are shown in this chapter.

In Chapter 4, the possible reason for causing dimensional error is analyzed. The main process model, polymerization model and irradiance model are discussed and modified to simulate the process better.

In Chapter 5, an empirical process planning method is formulated based on the existing process planning method and revised process models. After that, the devised method was validated by conducting multiple experiments. The error analysis and limitations of the ECPL system are discussed in the following. Chapter 6 concludes the contributions done for the thesis study and revisits all the research questions. Future work is discussed in the end.

CHAPTER 2

LITERATURE REVIEW AND RESEARCH PROBLEM STATEMENT

This chapter presents the literature review about the optical model for the system, the chemical model for photopolymer resin, and the existing process planning method for the ECPL system. The irradiance model with ray-tracing method was explained in the first section. Photopolymerization involved in the process will be fully illustrated with both the empirical modeling approach and the monomer concentration modeling approach. The details of existing process planning methods for ECPL system will be described. Finally, the research question and hypothesis are addressed.

2.1 Irradiance Model

Figure 6 shows the whole fabricating process of the ECPL system. The process inputs are bitmaps and exposure parameters, which are time and intensity. The process modeling includes polymerization modeling and irradiance modeling. The process outputs will be cured parts. The major discussion and research are related to the chemical reaction within the resin chamber, which indicates the process modeling.

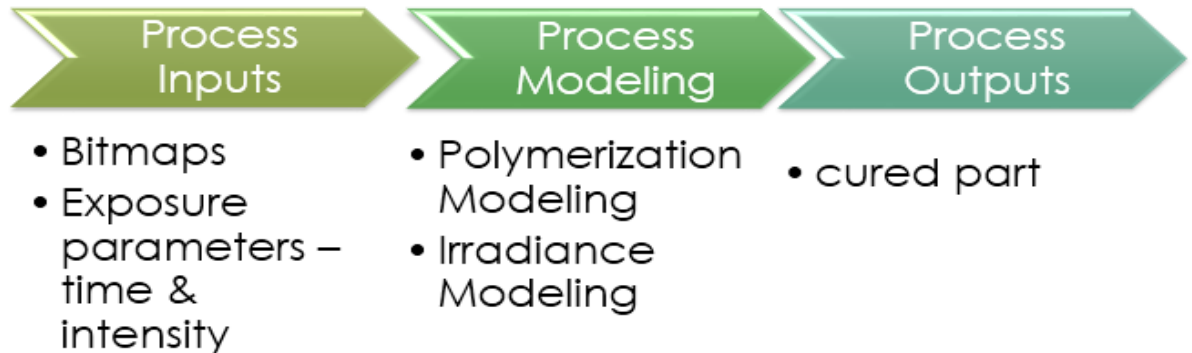


Figure 6: Fabricating process of the ECPL system

The ECPL system is analytically modeled in two phases – an Irradiance Model and a Photopolymerization Model. The irradiance model examines the irradiance received by the resin in terms of the process parameters and is presented in detail in Jariwala et al. [14]. The ray tracing algorithm is adopted from Limaya & Rosen (2007) was used to obtain the irradiance model. It is a method to characterize the optical system in terms of rays. Figure 7 shows a schematic of the ray tracing method [15]. The irradiance distribution on the resin depends upon the power distribution across the light beam incident on the bitmap and upon the optical aberrations caused by the imaging lens, which is shown in Figure 8 [9].

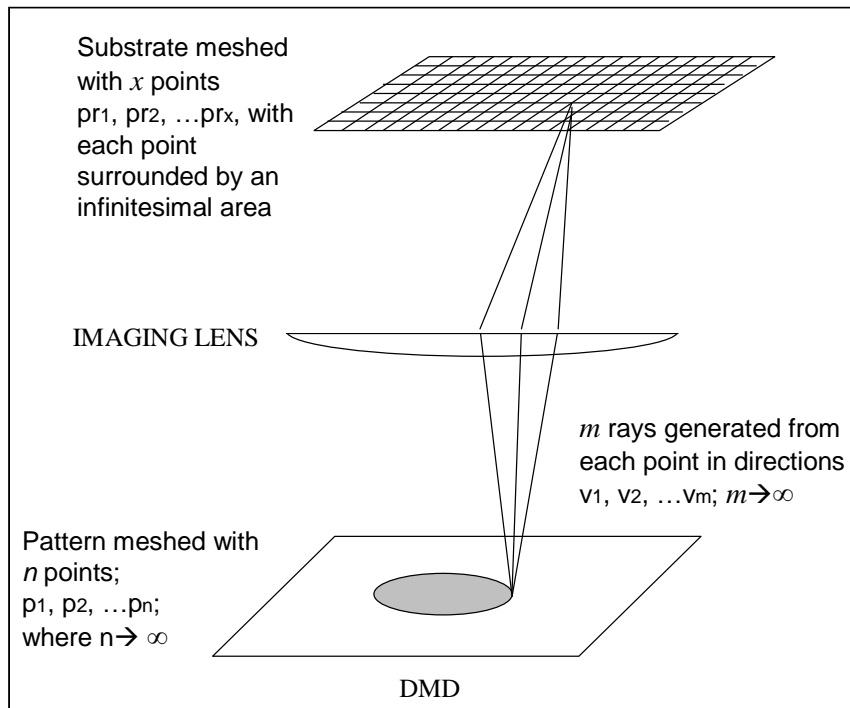


Figure 7: Schematic of the ray tracing method [15]

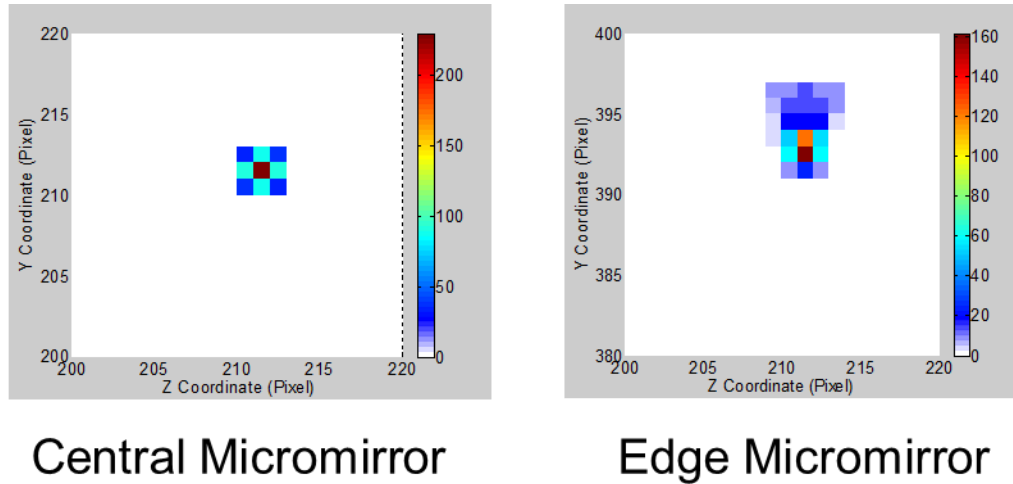


Figure 8: Irradiance distribution [9]

UV Light is the primary energy source in the ECPL system. The total amount of energy is controlled by the exposure time and by the size of the irradiated region, given by the size of the projected bitmaps. The exposure (units of energy/area) is defined as the total amount of UV energy incident per unit area. The total dose of energy provided to the resin is regulated by the distribution of irradiance at the substrate level. The relationship between the irradiance distribution on the DMD chip and the substrate of the resin chamber was investigated as the irradiance model in Jariwala et al. [14]. The irradiance model can be validated by placing a camera at the substrate level. Figure 9 shows the comparison of simulation results from the irradiance model with experimental data (irradiance detected by the camera). The result demonstrates that the irradiance model can estimate the approximate exposure profile on the substrate level, and that there were small deviations.

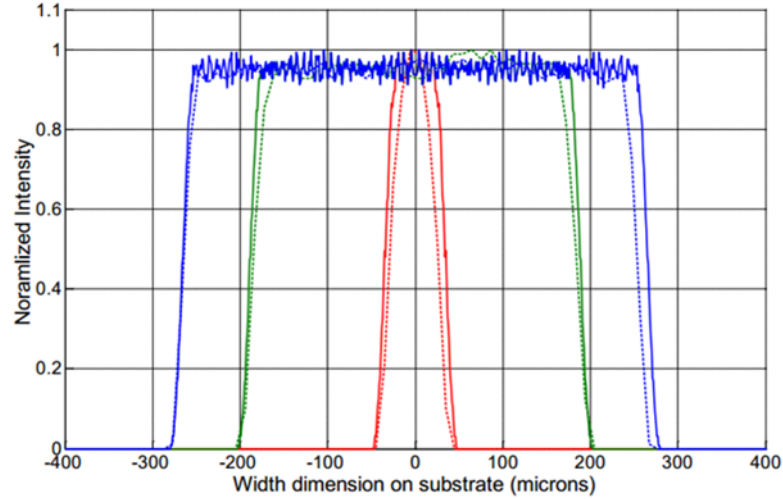


Figure 9: Comparison of simulation results from Irradiance model (solid lines) with data from the camera (dashed lines). Red corresponds to 10 pixels; green to 60 pixels and blue to 90 pixels [9]

2.2 Photopolymerization Model

Photopolymerization is defined as a reaction that bonds monomers or macromers together to form polymer chains or three-dimensional networks by absorbing visible or ultraviolet light [16]. To look inside the polymerization process, there are three primary reaction mechanisms occurring during the polymerization: initiation, propagation, termination and inhibition. The model incorporates the chemical reaction inside the resin with oxygen diffusivity [17-19]. When the photopolymer resin receives light energy, the photoinitiator absorbs it and decomposes into two radicals with first order rate constant of K_d . Then these radicals react with monomers to form polymer chains, and these polymer chains react with monomers again to form more polymer chains as Equations 1, 2 and 3 show [19]

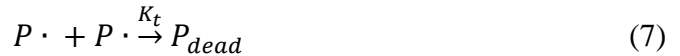




After bonding, the polymer chains can react with radicals and other polymer chains to form longer chains as the propagation process described in equations 4 and 5 [19]



The rate constants used are K_p for propagation rate. Termination will happen as two radicals come together to form a dead radical or as polymer chains react to combine with other polymer chains or radicals to form a dead polymer chain as depicted by the equation 6, 7 and 8 [19].



K_t is the rate for termination. The last reaction occurring during polymerization is inhibition, and oxygen is considered to be an inhibitor in the ECPL process. K_{t,O_2} is the rate for termination of a radical with an oxygen molecule in equations 9 and 10 [19].



Therefore, the polymerization process is that the photoinitiator absorbs the light energy and generates radicals. Those radicals react with monomers to form polymer chains. Polymer chains again combine with other polymer chains and grow. They keep growing until they reach stability, and the final cured structure consists of these polymer chains.

Based on the chemical behavior of polymerization, the estimate of cured shape can be modeled. There are two main approaches: one is the empirical modeling approach, and another one is the monomer concentration modeling approach [9].

2.2.1 Empirical modeling approach

According to Beer Lambert's law of absorption, the light exposure at depth z can be obtained by Equation 11 [1]

$$E(z) = E_{max} e^{\frac{-z}{D_p}} \quad (11)$$

where E_{max} is the exposure at the surface which is $z = 0$, and D_p is the resin "penetration depth" at the given wavelength, which is a resin parameter. It is suggested that curing will only occur when the exposure energy will be greater than or equal to the critical energy (E_c), and the cure depth can be given by Equation 12 [1]

$$z = D_p \ln\left(\frac{E}{E_c}\right) \quad (12)$$

However, the model in Equation 11 and 12 is assumed that the attenuation of radiation through a cured layer is the same as the uncured resin. The radiation effects are not considered. Limaye & Rosen [15] have observed that attenuation through a cured part is much less than that through uncured resin. They conclude that the penetration depth in

cured part is different from the penetration depth of uncured resin. Therefore, the equation to find the cure depth is modified to be [20]

$$z \approx D_{pL} \ln \left(\frac{D_{pL}}{D_{pS}} * \frac{E}{E_c} + 1 - \frac{D_{pL}}{D_{pS}} \right) \quad (13)$$

where D_{pS} is the penetration depth in a solid and D_{pL} is the penetration depth in a liquid. To find the value of the critical exposure and penetration depth for both solids and liquids, a working curve can be found by fitting the curve to multiple experimental results. Based on a fitted working curve, all these parameters can be obtained so that the cured height for the particular resin can be modeled.

2.2.2 Monomer concentration modeling approach

The empirical modeling approach proved that it could accurately predict the height of the cured part. However, the geometry profile of the cured part cannot be obtained by that approach. Carothers and Flory [21-23] described a gel as an infinitely large molecule that is insoluble. Flory used this definition to estimate the degree of cure necessary for the onset of gelation based on the functionality of the reacting monomers [23]. The degree of cure, which is also called the concentration of the monomer, can be computed as Equation 14

$$Conversion = \frac{[M] - [M_0]}{[M_0]} \quad (14)$$

M represents the monomer concentration after polymerization, and M_0 represents the initial monomer concentration. The shape of the cured part can be estimated by finding the track within the resin where the conversion has reached the critical conversion limit. The critical conversion limit is the value where the resin starts to gel.

Past research showed that conversion cut-off value between 10-30% was predicted for gelation [19]. It was suggested that for a constant intensity, the conversion curves could be created to estimate the time required to cure at the certain depth. For the ECPL system, the critical conversion limit was found by Dr. Jariwala to be 20%. In his Ph.D. dissertation, the one-dimension COMSOL simulation results at a depth of 8 μm for the resin used in ECPL system was shown in Figure 10 [9]. The red line indicated fractional monomer conversion and the blue line shows the normalized concentration of oxygen. It is suggested by Boddapati et al. [19] that the resin at the height of 8 μm must start to gel at around 3.8s. As the Figure 10 shows, the monomer conversion of 20% is enough to start the gel. Furthermore, the simulation results from 10% to 30% conversion value of 5s curing time were obtained by the COMSOL and shown in Figure 11. Comparing to the experimental results, 20% was proved to be the best value of the critical value of conversion for gelation in the ECPL system. As a clarification, 20% is not the real conversion rate. It is the value found in the COMSOL simulation by comparing to the experimental geometry profile to the simulation with different conversion number, and 20% was found to be the best case. The real conversion rate can be converted as a function of the value found in COMSOL. Moreover, the real conversion rate is usually around 80% after the sample parts are fabricated, and the conversion rate will be close to 100% after the post processing method, which is washing and flood curing. In the future, the real conversion rates of samples before and after post processing can be measured by using phot-DSC (differential scanning calorimetry)

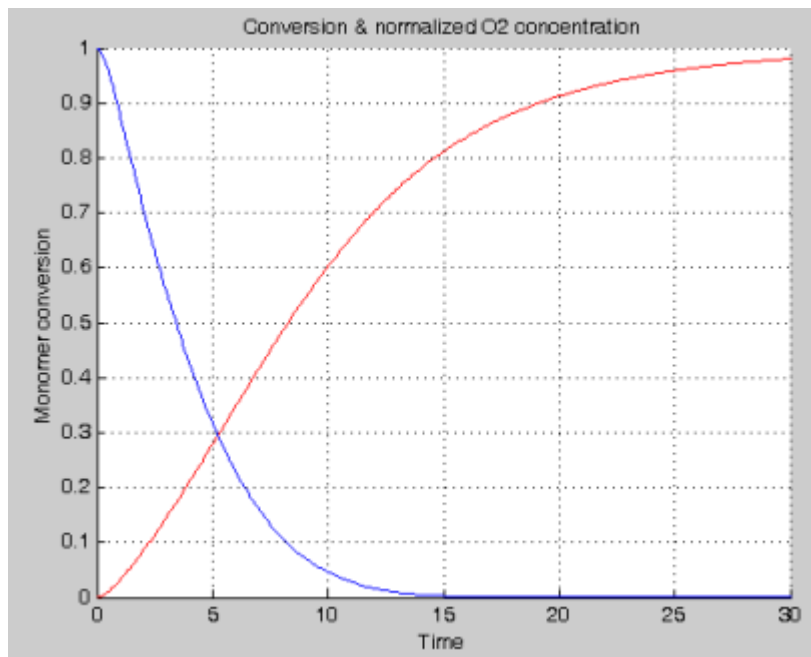


Figure 10: Simulation results from 1D COMSOL® simulation (Red curve shows

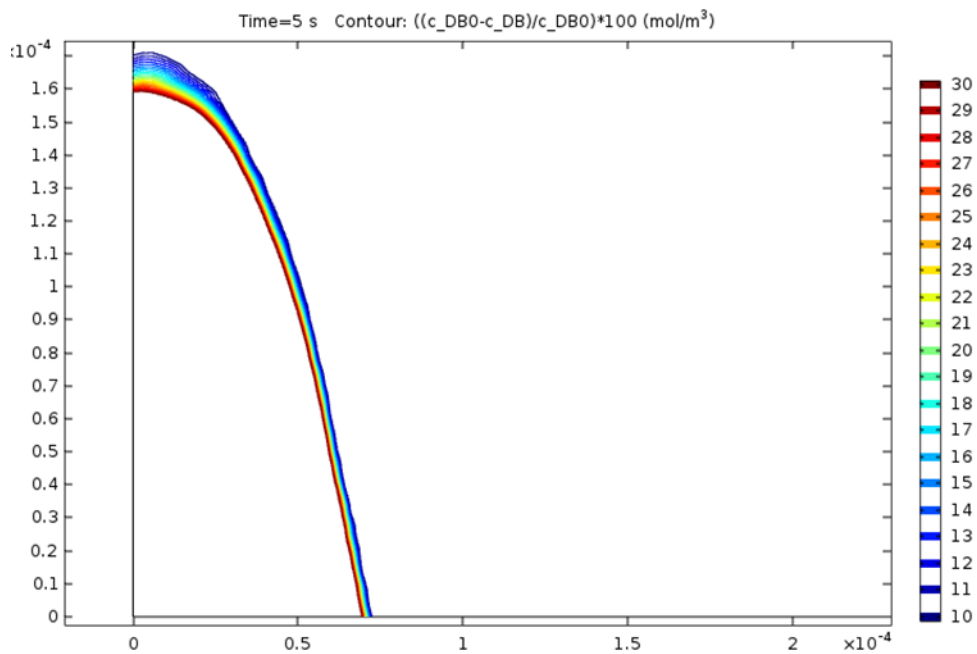


Figure 11: Experimental results from different conversion value

2.3 Existing process planning method for Mask Projection System

Since the objective of this study is to fabricate a lens using the ECPL process, it is necessary to formulate a process planning method that can estimate the inputs for making structures. A process plan can estimate the process parameters required to manufacture a product with the desired specifications. A process plan will require the primary input, and the specifications about the raw materials and the system that will eventually fabricate the final product.

In the literature, several researchers have conducted a study on the process planning method for Mask Projection System. In the literature, several researchers have conducted a study on the Mask Projection System. Monneret et al. [24] developed a mask projection microstereolithography apparatus to obtain 3D objects in 1999. It was reported that they successfully achieved a resolution of 2 micrometers on lateral dimension and some examples of high aspect ratio micro-objects are demonstrated in their work. Another research group of Bertsch, Jiguet and Renaud [25] applied microstereolithography technology to manufacture small and complex ceramic components. They stated that the material available in the microstereolithography process was usually limited to plastic. A new polymer/composite photosensitive resin was introduced in their study to fabricate micro-parts. Their final products showed a good quality with no deformations and no cracks on the components. In 2002, research group of Qinjun Peng [26] developed a novel real-time gray-scale photolithography method to fabricate continuous microstructures. The techniques they used were a digital LCD system and a projection photolithography system. It was reported that the minimal feature size of the fabricated parts could reach 1.6 microns in their experiments.

Dr. Limaye and Dr. Rosen [15] have developed a process planning method for mask projection micro-stereolithography to cure accurate micro parts. The process of curing a single layer was modelled as a layer cure model as shown in Figure 12. The layer cure model was formulated in terms of the process parameters to cure the layer. The layer cure model contains two models: an irradiance model and a cure model. The irradiance model models the light profile received by the resin surface, and the cure model computes the lateral dimensions of the cured layer based on the Beer-Lambert model. The process planning method used by Dr. Limaye and Dr. Rosen [27] used the layer cure model as a database to find process inputs such as pixel size and exposure time based on the desired lateral dimensions. The results from their process planning method concluded about 3% error for most of the features and 10% for very small parts ($< 250 \mu\text{m}$).

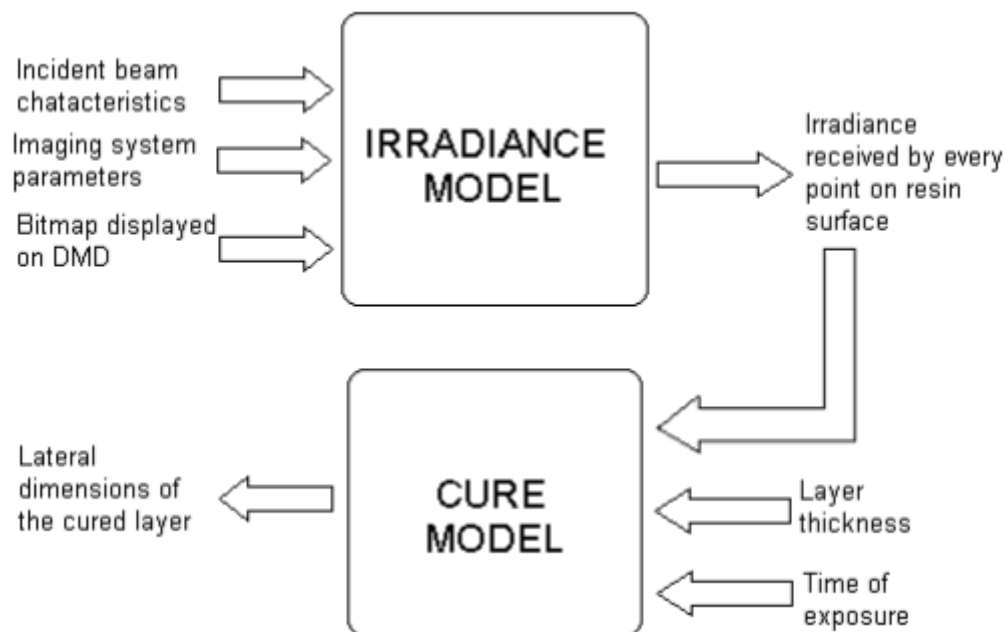


Figure 12: Schematic of the layer cure model from Limaye [27]

In another research group, Dr. Zhou and Dr. Chen [28] has developed a process planning method for mask projection large-area stereolithography to improve the accuracy and resolution of the fabricated parts. Different from the traditional method of curing each layer of the parts, a set of mask images, instead of a single mask, is used in their method. Moreover, due to various optical effects such as aberration and distortion, the energy distribution of a pixel is modeled as a Gaussian distribution. In order to get a uniform and consistent pixel, the grayscale level was applied to the light for each pixel. An optimized pixel blending method combined with the consideration of multiple mask images and the grayscale level was thus developed. The results from their method conclude with about 6% error. Dr. Tumbleston group in 2015 developed the continuous generation of monolithic polymeric parts with feature resolution under 100 micrometers [8]. The theory from their research is similar to the ECPL system, but with larger scale. The commercialized machine M1 from 3D carbon is developed based on their study. Dr. Fang and his group [29] recently begun to investigate potential application in nanoscale imaging and information processing and in 2015, a mask projection micro stereolithography system, which is similar to ECPL system, but with moveable stage was patented by their lab as well. It was reported that their system has a resolution of 10 μ m. Moreover, the process time for their system was about 30 minutes for typical microstructures, which is relatively slow. The ECPL system is target to a more accurate and fast method to fabricate microstructures.

2.4 Existing process planning method for ECPL system

In the ECPL system, the primary input is the desired geometry. The raw material is the photopolymer resin, and the system corresponds to the ECPL optical system

design. The process parameters needed to manufacture a product are bitmaps and exposure time. Amit S. Jariwala in 2013 [30] presented a unique approach to process planning method for an ECPL system. In his work, process planning is used to estimate exposure times and corresponding bitmaps for the desired part shape and dimensions. His model mainly comprises three parts: an irradiance model, a polymerization model, and optimization. The irradiance model would relate to the light profile received on the resin surface by adopting ray tracing. The polymerization model mainly used the monomer concentration modeling approach described in section 2.2.2. He simulated the entire chemical reaction within the resin chamber and found the predicted geometry profile by using a certain value of the degree of cure. MATLAB and COMSOL software were used in the process planning. Part shape and dimensions were provided as inputs. The process planner first estimated the bitmap and exposure time for the first layer. Then, the program connected with COMSOL to modify the time by simulating effects such as oxygen inhibition and diffusion. After that, it calculated the exposure time for the next layers in the same method. The flowcharts for estimating the first set of process inputs and the subsequent set of process inputs is shown in Figures 13 and 14, respectively. In Figure 13, the first bitmap and exposure time were estimated by optimizing the cured part edge. It is to be noted that the primary function of the first bitmap is not to cure the entire part geometry, but to cure the base and the corresponding edge of the desired part. For the subsequent layer process, shown in Figure 14, the inputs are the bitmap for the first “layer” and the corresponding exposure time and the desired cured part geometry. The dotted lines show the simultaneous dependence of the optimization module on the system module and the material module. The dashed lines show the iterative nature of the loop;

the process stops when the entire desired part geometry is cured completely (within a pre-set threshold).

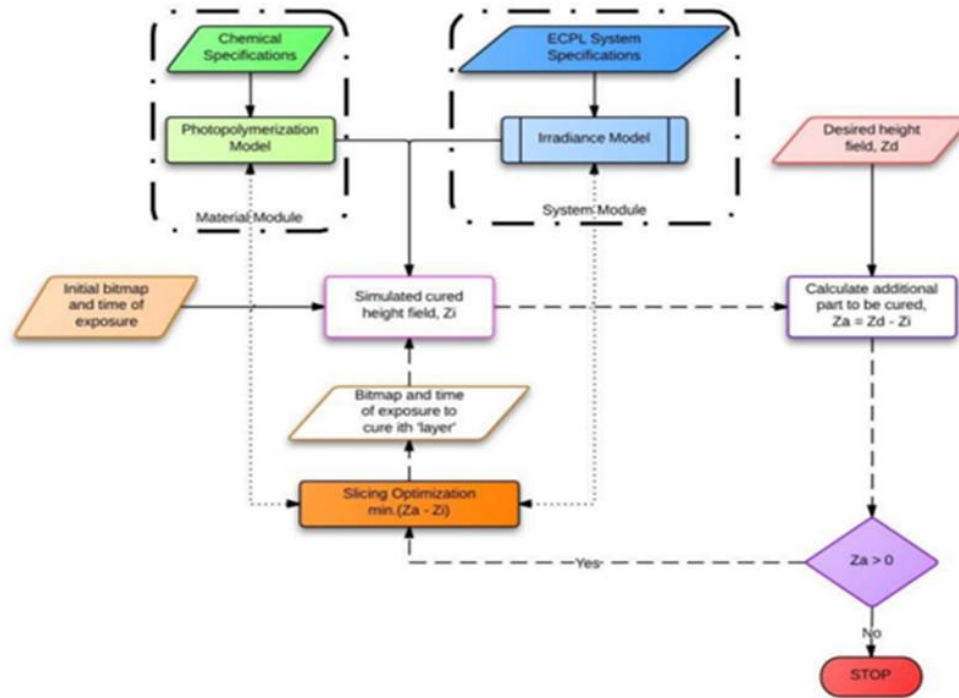


Figure 13: The flow chart for first “layer.” [30]

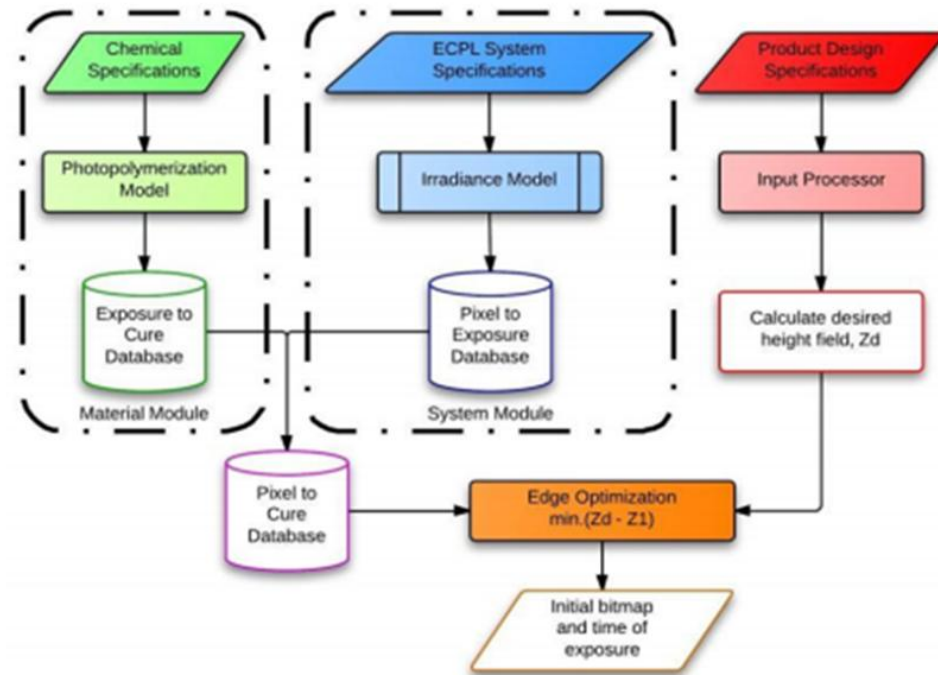


Figure 14: The flowchart for subsequent “layer.” [30]

To validate his process planning method, three samples were conducted [9]. All the results clearly showed that the samples were under-cured. One of the samples in the paper is shown below. The desired diameter was $200\mu\text{m}$; the conic constant was -1 and the sag height was $120\mu\text{m}$. The desired geometry is shown in Figure 15.

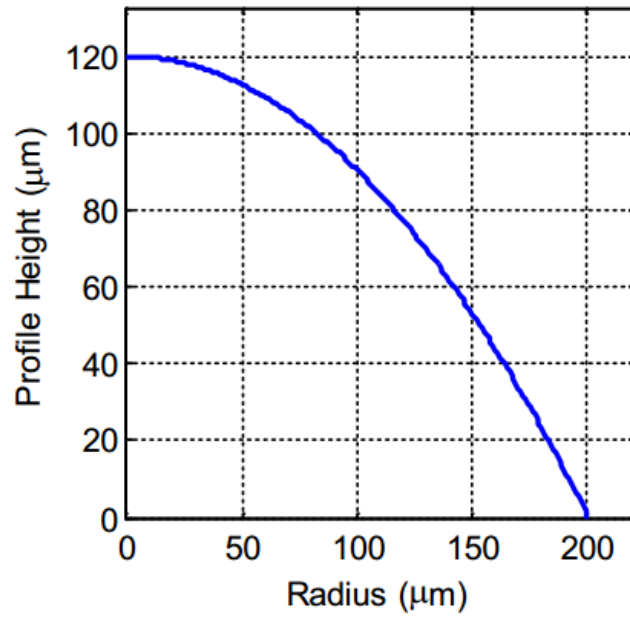


Figure 15: Half cross section geometry of the desired sample [9]

A series of bitmaps and corresponding times was generated by using his process planning method, as shown in Figure 16.

 1.5s	 0.4s	 0.5s	 0.6s	 0.7s
 0.8s	 0.9s	 1.2s	 1.2s	 1.4s
 1.3s	 1.5s	 1.5s	 1.8s	 1.7s
 1.9s	 2s	 2s	 2s	 2s
 2s	X	X	X	X

Figure 16: Bitmaps generated from the process planning method [9]

Figure 17 shows a comparison of the experimental result and the desired geometry. It was stated that the error between the desired geometry and the experimental geometry was more than 15%. The accuracy of the process planning method needs to be improved. Moreover, only three samples with relatively large error were used to validate the process planning method, which is not sufficient. The system was found not to be repeatable and stable.

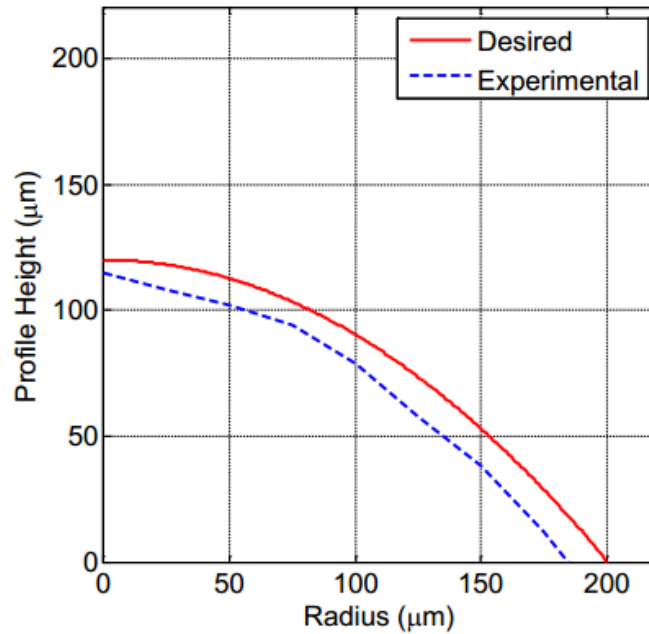


Figure 17: Comparison of desired geometry and experimental geometry [9]

Compared to an even earlier process planning method, which was proposed by Dr. Limaye, the process planning method from Dr. Jariwala modeled the polymerization process by using critical monomer concentration modeling instead of the empirical modeling approach. He took the advantage of the estimation of the entire geometry profile, but also underwent the disadvantage of disconnection from the experimental data. Therefore, in order to improve the accuracy of estimating the entire fabricated geometry profile, the experimental results will be considered to model the process planning method. The research objective can thus be abstracted as following:

To formulate an empirical process planning for the ECPL process in order to better estimate the shape of the fabricated geometry

2.5 Research questions and hypotheses

In order to accomplish the research objective, possible variations in the existing process planning method need to be identified. The system design and assembly of the ECPL process must be checked to have a more stable and repeatable system. The existing theoretical model used to simulate the ECPL process in the process planning method needs to be revalidated by the experimental results. Finally, a refined process planning algorithm is required in order to estimate the process inputs to fabricate samples in the desired dimension. Therefore, two research questions are formulated as below.

Research Question 1: How to refine the polymerization model to better predict the sample geometry profile?

Hypothesis: The polymerization model can be improved if the chemical reaction rates are modified as a function of the irradiation area.

Explanation: The Beer-lambert law suggested that the height of the cured parts depends on the exposure time for the resin. However, the experiments found that a smaller irradiation area, which is less than 200 microns in width, could not reach the same height with the same exposure time. The research on the micro applications in the literature is limited. Therefore, the polymerization model is expected to be modified for the smaller irradiation area.

Research Question 2: How to estimate the bitmaps and exposure times used in order to obtain the desired geometry?

Hypothesis: A more accurate process planning method can be created by controlling the layer width of the entire cured part.

Explanation: The existing process planning method considered minimizing the height difference between the simulation results and desired geometry, but it did not consider the width difference for each curing “layer” between the simulation results and the desired geometry.

2.6 Chapter Summary

This chapter introduced background knowledge related to the ECPL system. The irradiance model and the polymerization model were presented in order to be better explaining the principle of the ECPL system. The drawbacks of the existing process planning method were analyzed as well. The existing process planning method presented the capability to estimate the desired bitmaps and the exposure time needed to fabricate the desired geometry with a high percentage of error. The research objective was made in order to improve the system and process planning method to better estimate the process inputs for ECPL system. The research questions and hypothesis were formulated to accomplish the goal.

CHAPTER 3

ECPL Fabrication System Design Improvement

This chapter will introduce the Exposure Controlled Projection lithography (ECPL) fabrication system design improvement. The existing system design and experimental procedure will be firstly introduced. Due to some drawbacks for the existing system, a few system improvements are developed, and the experimental procedure is modified in order to make the process more repeatable and stable. A procedure for checking the intensity and system stability will be implemented before doing the experiments. Pretreatment improvement is introduced in the following section. Finally, the samples fabricated by the ECPL system will be shown at the end of this chapter.

3.1 Introduction

The existing ECPL process was found not to be stable and repeatable. Even by using the same settings, bitmaps and exposure time as the previous experiment, the dimensions of final products can be different. Another problem is that when we apply a washing process in order to clean samples, samples are easy to wash off. Since the experimental setup is not industrialized, there might be an error caused by small changes or movement of the equipment. Therefore, the existing system design and experimental procedure are considered for improvement.

3.2 Existing System Design and Experimental Procedure

The existing system design and experimental procedure were introduced and explained by Dr. Jariwala [9] in his dissertation. The entire process of ECPL contains three main parts:

1, energy application: UV light source => beam conditioning => projection system

2, process: resin chamber

3, post-process: washing, removal and flat curing.

3.2.1 Energy Apply

Figure 18 shows the schematic of the ECPL system. To apply energy, the ultraviolet light source shines through the beam expander to expand the laser beam diameter. Then the light goes through the diffuser to enlarge the diameter and homogenize the beam's intensity and through the collimating lens to collimate the light. After that, the UV coated mirror is used to direct the light on a dynamic mask, which is a DMD projection system. The projection system is used to enlarge or reduce the image presented on the DMD and to project it on the resin chamber. Entire structures will be formed by a series of bitmap projections.

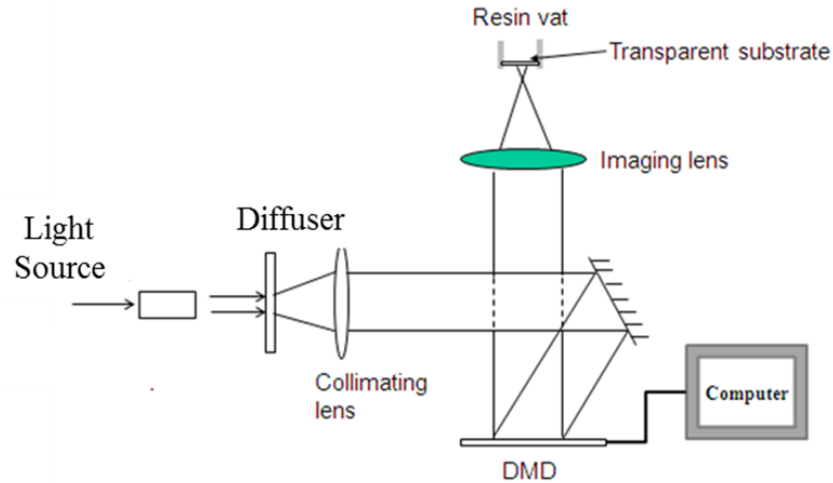


Figure 18: Schematic of the ECPL system [9]

UV light source: The light source used in the ECPL system is an Omnicure® S2000 UV spot curing system from Lumen Dynamics. It is a commercial high-power mercury arc lamp with integral feedback control over the total irradiation intensity. It uses a high pressure 200-watt mercury vapor short arc, and the light is delivered by a 5mm light guide. The light spectrum is in the range of 320-500nm [9].

Beam conditioning: The primary function of the beam conditioning system is to homogenize the light beam and project it on the chip. The beam conditioning system contains a beam expander to expand the laser beam diameter, a diffuser to enlarge the diameter and homogenize the beam's intensity, a collimating lens to collimate the light and a UV coated mirror to direct the light on a dynamic mask, which is a DMD projection system.

Projection System: The primary function of the projection system is to enlarge or reduce the image size presented on the DMD chip and to project it on the resin chamber. DMD stands for digital micromirror device. It is a product of Texas Instruments. The DMD

chip used in the lab was obtained from a ViewSonic PJD 6221 projector [9]. The DMD chip consists of micro-mirrors. These micromirrors are used to display bitmaps that are used to fabricate samples. Furthermore, a single plano-convex lens is used to achieve a magnification of 0.47X between the bitmap size and the size on the chamber. An aperture is placed after the lens in order to block any transverse rays. Figure 19 shows a photograph taken in the lab for the projection system [9]. The blue dashed line indicates the light path through the system.

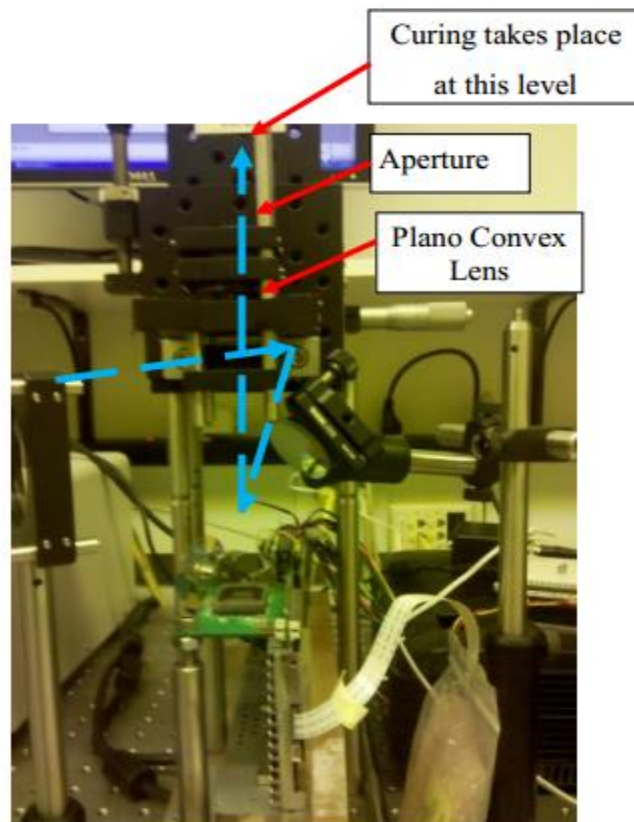


Figure 19: Photograph of projection system [9]

3.2.2 Process – Resin chamber

The major fabricating process takes place in the resin chamber. The existing resin chamber contains two glass slides and two spacers. The uncured resin was loaded inside. Figure 20 shows the schematic of the resin chamber. The procedure to create a resin chamber was introduced in Jariwala [9]. Two frosted glass slides were obtained from the box and cleaned. One was used as the bottom glass slide, and the other was used as the top glass slide. Secondly, sticky tapes were attached in order to put spacers. Thirdly, two cover slides, which are spacers, were attached to the top. Then sticky tapes were used again to the spacers in order to attach the top glass slides. Finally, the top glass slides were placed on the top. Figure 21 presents the steps in constructing the resin chamber.

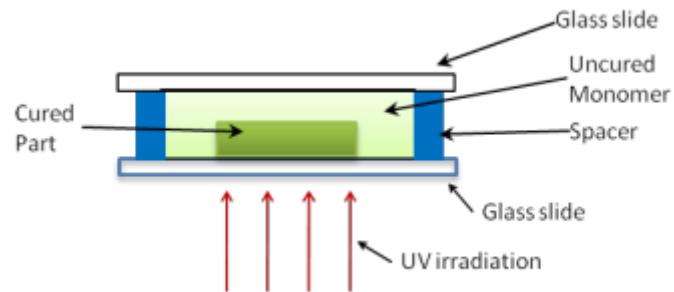


Figure 20: Schematic of the resin chamber [9]

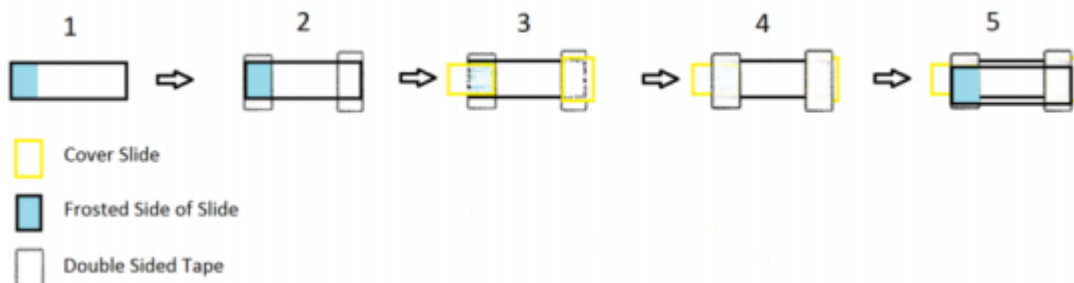


Figure 21: Steps in constructing the resin chamber [9]

Figure 22 shows a photograph of the entire lab setup. It includes the UV light source and light guide as the energy apply, the entire beam conditioning system covered by an aluminum foil sheet, projection systems with DMD chip, projector and lens, and the sample stage where the resin chamber was located. Table 1 shows the specification of the components used in ECPL system; it was provided in Jariwala [9].

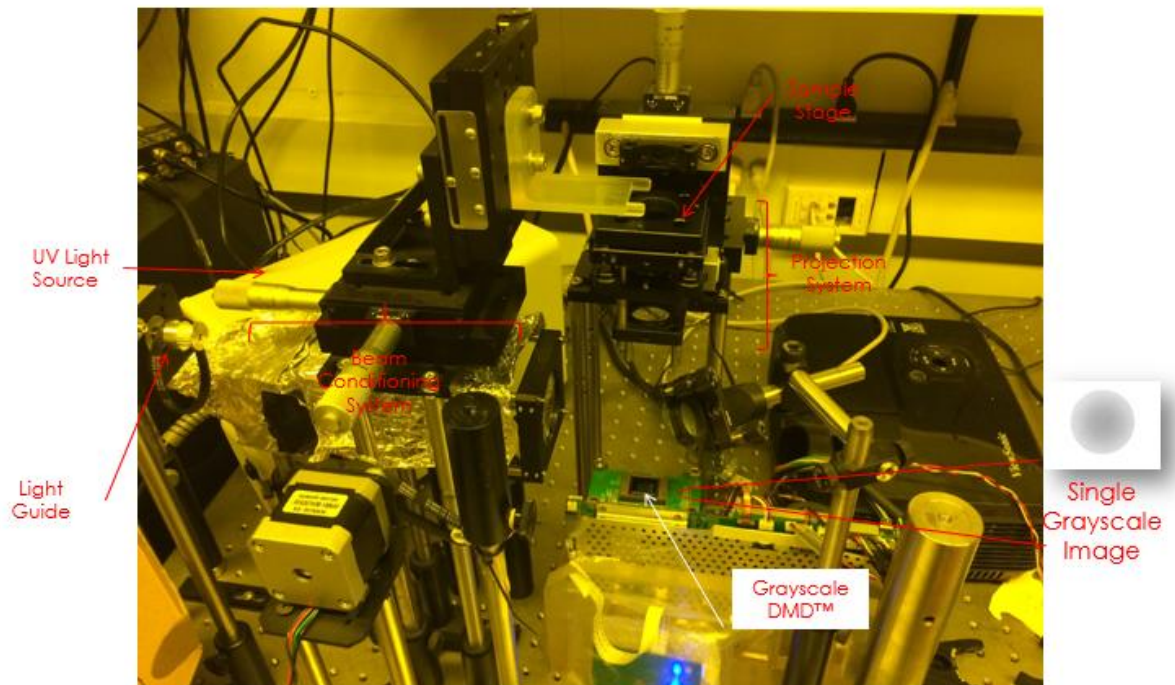


Figure 22: Photograph of the entire lab setup

Table 1: Specification of the components [9]

Component	Description	Model/Manufacturer
UV Lamp source	High pressure 200W Mercury Vapor Lamp Broadband: 320-500nm Light guide diameter = 5 mm	Omnigore S2000 / Lumen Dynamics
Collimating lens	Fused silica Plano convex lens Effective focal length = 150.0mm Diameter = 50.8mm	Thorlabs Catalog # LA4904-UV
Mirror	Round UV Aluminum mirror Diameter = 25.4mm	Thorlabs Catalog # PF10-03-F01
DMD	1024 X 768 array of micromirrors	Obtained from ViewSonic DLP PJD 6221 projector
Imaging lens	Fused silica Plano convex lens Effective focal length = 50.0mm Diameter = 25.4mm	Thorlabs Catalog # LA4148-UV

3.2.3 Post Process

Post processing is used to transform the cured part into a finished product. After the cured part is fabricated, the cured sample is still submerged in the uncured resin in the resin chamber. The uncured part must be removed by gently washed. Inappropriate washing can damage the cured gel boundary and also the surface of the sample. The washing method developed in the ECPL system is to use a solution of water and Triton-X to gently remove all traces of uncured monomer, and then to apply water to clear the surface. The various solvents such as acetonitrile, hexane, a solution of water and soap were also tried. The solution of water and Triton-X is found to be the most effective and repeatable way to clean the samples. After the sample is clearly washed, nitrogen gas was

used to remove extra water in order to get a clean and clear surface. The flat curing will be applied to the end in order to harden the sample [9].

3.2.4 Experimental Procedure

The chemical used in the research is a combination of tri-functional acrylate monomer-trimethylolpropane (TMPTA, SR-351) obtained from Sartomer and the photoinitiator 2, 2-dimethoxy-1, 2-diphenylethan-1-one (DMPA, IRGRACURE-651) obtained from Ciba Specialty Chemicals. The ratio of the photoinitiator and monomer is 1:4 in mass [9]. The resin solution will be prepared in advance in order to make samples. To fabricate samples, a resin chamber was first assembled by following the steps introduced above, and the chemical solution was loaded into the chamber. After that, the resin chamber was placed on the sample stage. Then, the PowerPoint with all bitmaps and corresponding exposure time was loaded on the computer to control the projector. The software provided by Omnicure was used to control the UV light source. By opening the shutter of the UV light source and processing the PowerPoint image, the sample was cured in the resin chamber. Finally, post processing was applied.

Based on existing experimental procedure, there was no system check before doing any experiment. Since the equipment was set up personally by graduate students in the lab, and not all mirrors, lens, and supports are fixed, some discrepancies may have occurred. Hence, a light intensity check, a system stability check, and pretreatment were done before the experiment.

3.3 Intensity and System Stability Check

The ECPL system was found to be very unstable. It was not possible to get the same samples' dimensions by using the same experimental settings, exposure time and bitmaps. However, we found that the shape of experimental samples was fairly stable, although the dimensions were not. While analyzing the ECPL system, it was found that the intensity of the UV light had never been monitored, and it was always assumed that the intensity of the UV light was constant and stable. Therefore, an intensity check was considered to be necessary before fabricating samples. To do this, a power meter was used to measure the intensity. The procedure to check the intensity is listed in the following:

1. Plug in the power supply and sensor connector to the Optical Power and Energy Meter.

The power meter (with red cover) used in the lab is shown in Figure 23.

2. Take the cover off the sensor and place the sensor in the working place as shown in Figure 24

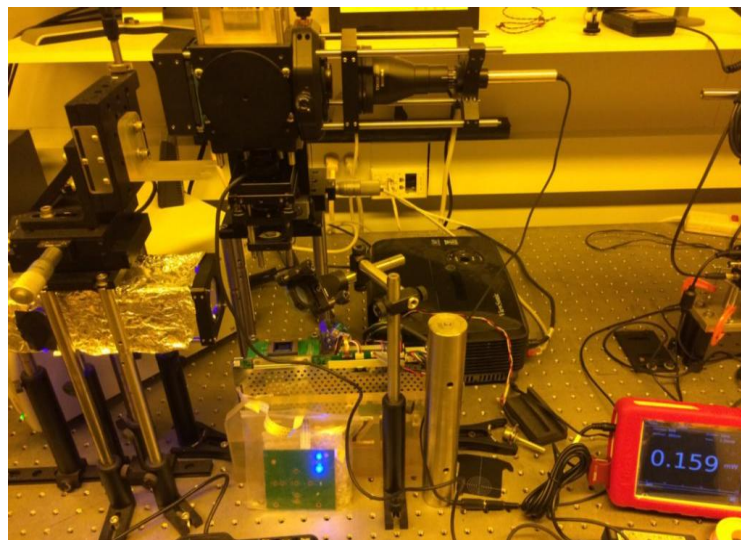


Figure 23: Power meter used in the lab

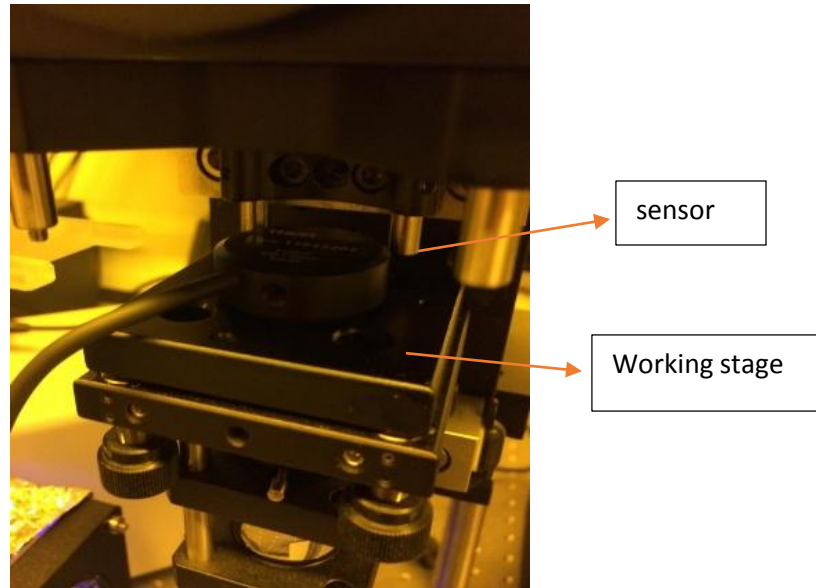


Figure 24: Sensor placing in the working space

3. Turn on the Optical Power and Energy Meter
4. Balance the Meter
5. Project the entire black square bitmap in PowerPoint
6. Set the iris level to 22
7. Open the shutter control
8. Take the measurements. (Example in Figure 25)



Figure 25: Example power meter measurements

For the UV light source used in this study, the power for entire bitmap was measured to be 0.160mW. The intensity was calculated as Power over the area: Intensity = Power/Area. The bitmap was measured to be 4.65*3.64 mm by caliper, so the area is 16.926 mm². Therefore, the intensity was calculated to be 9.5×10^{-3} mW/mm². The intensity check was added to the experimental procedure as the first step of ensuring the stability of the system.

Another problem was found during the discovery of the light intensity check. The existing system setup used aluminum foil as the cover of the beam conditioning system in order to reflect all the lights. However, it was found that the aluminum foil was easy to touch during every experiment, and the intensity changed if the aluminum foil moved. Therefore, a better solution was required as a replacement for the aluminum foil. The replacement needed to be stable and not easily touchable. Black Microfiber cloth with black cardboard was considered to be used to solve the problem. Microfiber cloth was cut to the certain shape and attached to the black cardboard. It offered the same function as aluminum foil but with more stable structure. Figure 26 shows a photograph of the current cover of the beam conditioning system.

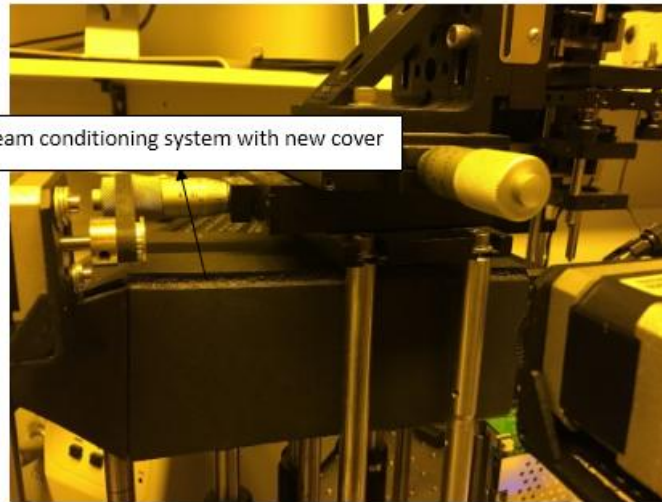


Figure 26: Beam conditioning system with black fiber cloth and black cardboard

3.4 Pretreatment Improvement

For a thorough system, samples are considered to be stored for a long time. Samples that are fabricated through the ECPL system are expected to stay in the glass slides for at least two days. Furthermore, when the post-processing process, especially the washing process, was applied to the samples, samples were expected to stay in the bottom glass slides to avoid any damage and loss. However, it was found that samples were easy to wash off in post processing. These two concerns led to the conclusion that the adhesion between the bottom glass slide and the samples needs to be improved. In order to increase the adhesion, the pretreatment for bottom glass slides was conducted. The procedure for the pretreatment is listed below.

1. Solution Prep:

- Saline Solution (only prepare this if there is no existing bottle of this solution in lab.)

- Remove the methacryloxypropyl-trimethoxysilane (MAPTMS) bottle from the refrigerator and let it come to room temperature.
 - Make sure the bottle is at room temperature before opening it!
 - Mix one part MAPTMS with 49 parts ethanol to obtain a 2% by vol. solution to be used to treat the slides.
 - Place the original saline bottle back in the refrigerator.
 - Store this solution in a bottle with green cap and label it.
- KOH Solution
 - Fill a small basin/petri dish with purified water, and add KOH pellets while stirring to obtain a concentrated solution for slide pre-treatment.

2. Pre-treatment:

- Submerge the slides in the KOH solution, and occasionally agitate, to ensure uniform distribution over the surface area.
- Slides must be submerged in the KOH solution for a minimum of 2 hours.

3. Treatment:

- Remove slides from the KOH solution and place face-up (frosted side up) on a wipe on the hot plate (turned off). Gently wipe down each slide to remove the excess chemical, while avoiding streak marks.
- Using a micropipette, coat each slide with the 2% MAPTMS solution prepared. Ensure that the entire surface of the slide is covered by the chemical.
- Wait ~10-15 mins, and then re-coat the slides with the 2% solution.
- Turn on the hot plate, and set the temperature to 100°C. Ensure that the slides are located in the center of the plate, to provide optimal heat distribution.

- Wait 5-7 mins, and then apply a final coat of the 2% solution.
- Wait an additional 20 minutes to allow the slides to finish drying, then turn off the hot plate and store the slides.

In addition, it is important to clean the slide with alcohol swabs/tissue prior to using it for the experiments. The saline should be chemically bonded to the glass slides and should retain a mono-layer even after cleaning with alcohol swab/tissue. Moreover, the final coated slides are expected to be completely clear. No cloudiness (likely caused by a build-up of salts from the KOH bath or increased acrylate crosslinking outward from the slide surface) is allowed in the slides.

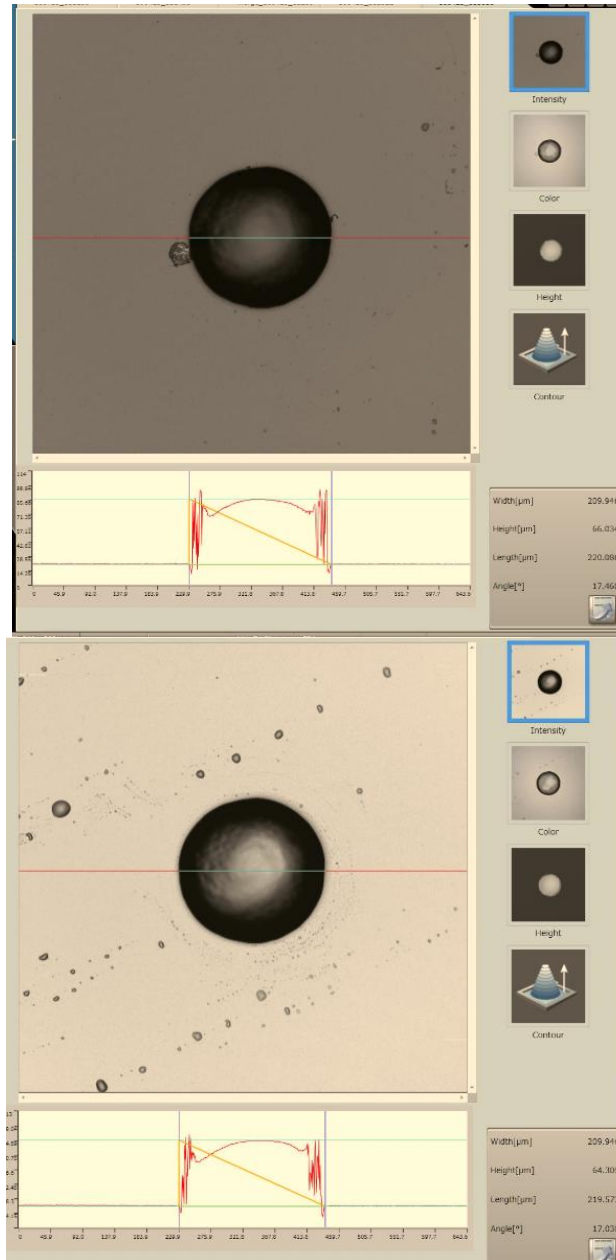
3.5 Experimental Results

In order to see the quality of products for the ECPL system, two sets of experiments were conducted. The first experiment was performed by three students. Each of them made a star-shape cured part by using the same bitmaps and exposure times. The second experiment was made by the same students. The students made the second sample, using the same setting as the first, one week later after the first sample to compare results. These samples were made by following the existing experimental procedure with the pretreatment and system design improvement. A confocal laser microscope (3D LEXT Confocal microscope from Olympus, accessed from the Georgia Tech Marcus Organic Nanotechnology Cleanroom) was used to measure the three-dimensional profiles of the cured parts. Figure 27 shows the comparison of these two experiments. It is clearly seen that the samples are well fabricated and repeatable. The dimensional error between the samples, which use the same settings, bitmaps and exposure time but made were made on different days, are less than 1%. Therefore, the

ECPL system with the improvement introduced in this chapter is proven to be a repeatable, quality and high precision system, and it is valid to research further on the ECPL system. The sample height range for those products which can be fabricated from the ECPL system is about $40\ \mu\text{m}$ to $150\ \mu\text{m}$. It may take about 5 seconds to 1 minute. It is workable for ECPL system to fabricate much larger parts, but it would take much longer time to do it, which is not our goal in this case.



(a)



(b)

Figure 27: (a) comparison of the products made by three different students (b) comparison of the products made at different times

3.6 Chapter Summary

This chapter presented the design of the existing ECPL system. The system setup was discovered to find the unstable factors that affect the ECPL system. The system was improved along with setup modification, experimental procedure modification and pretreatment on the experimental slides. Due to these improvements, the ECPL system was modified to improve stability, and the products of the ECPL system were found to be clean, clear, smooth and repeatable.

CHAPTER 4

THEORETICAL MODELLING REVISION

This chapter will introduce the existing ECPL process planning method with possible reasons causing the error. In order to improve the ECPL process planning method to better estimate the fabricated geometry shapes, the foundation of the process planning method—the irradiance model and the polymerization model—is considered for modification. Research question 1 with its hypothesis is discussed and validated in this chapter. More details will be explained in the following.

4.1 Introduction to the ECPL process planning method

The existing process planning methods for the ECPL system are discussed in Jariwala et al. [30] In this work, process planning is used to estimate the exposure times and corresponding bitmaps for the desired part shape and dimensions. MATLAB and COMSOL software are used in the process planning. Part shape and dimensions are provided as inputs. The process planner first estimates the bitmap and exposure time for the first layer. Then, the program connects with COMSOL to modify the time by simulating effects such as oxygen inhibition and diffusion. After that it calculates the exposure time for next layers by using the same method. The flowchart for estimating the first set of process inputs and the subsequent set of process inputs is shown in Figures 28 and 29, respectively. With reference to Figure 28, the first bitmap and exposure time were estimated by optimizing the cured part edge. It is to be noted that the primary function of the first bitmap is not to cure the entire part geometry, but to cure the base and the corresponding edge of the desired part. For the subsequent layer process shown in Figure 29, the inputs are the bitmap for the first “layer” and the corresponding exposure

time and the desired cured part geometry. The dotted lines show the simultaneous dependence of the optimization module on the system module and the material module. The dashed lines show the iterative nature of the loop and the process stops when the entire desired part geometry is cured completely (within a pre-set threshold).

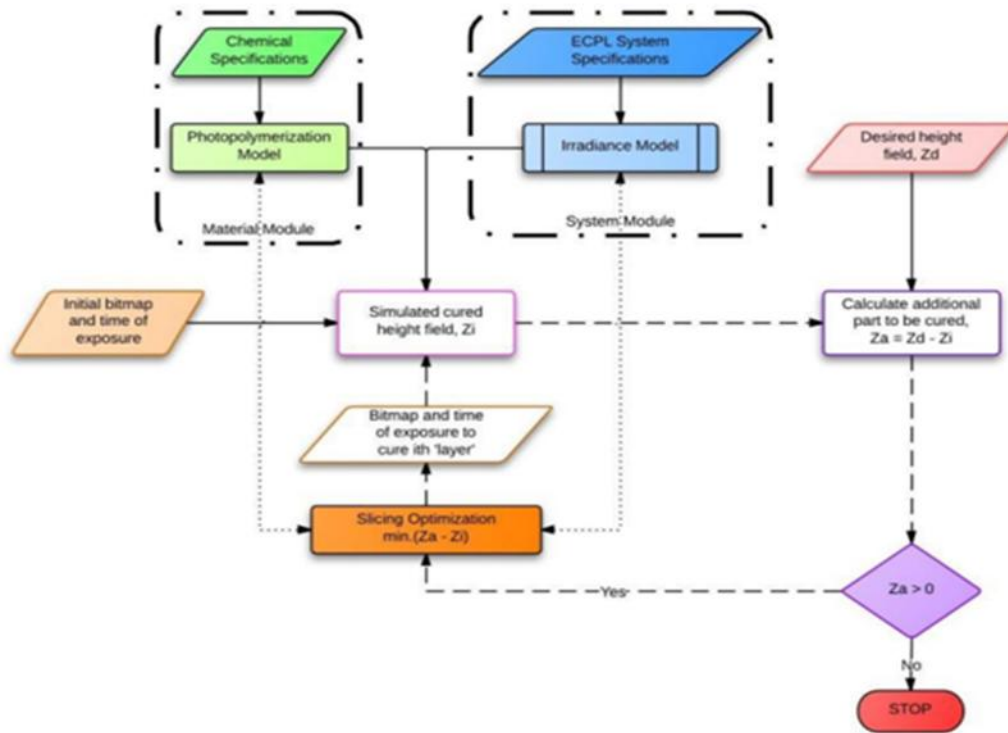


Figure 28: Flowchart for first “layer.” [30]

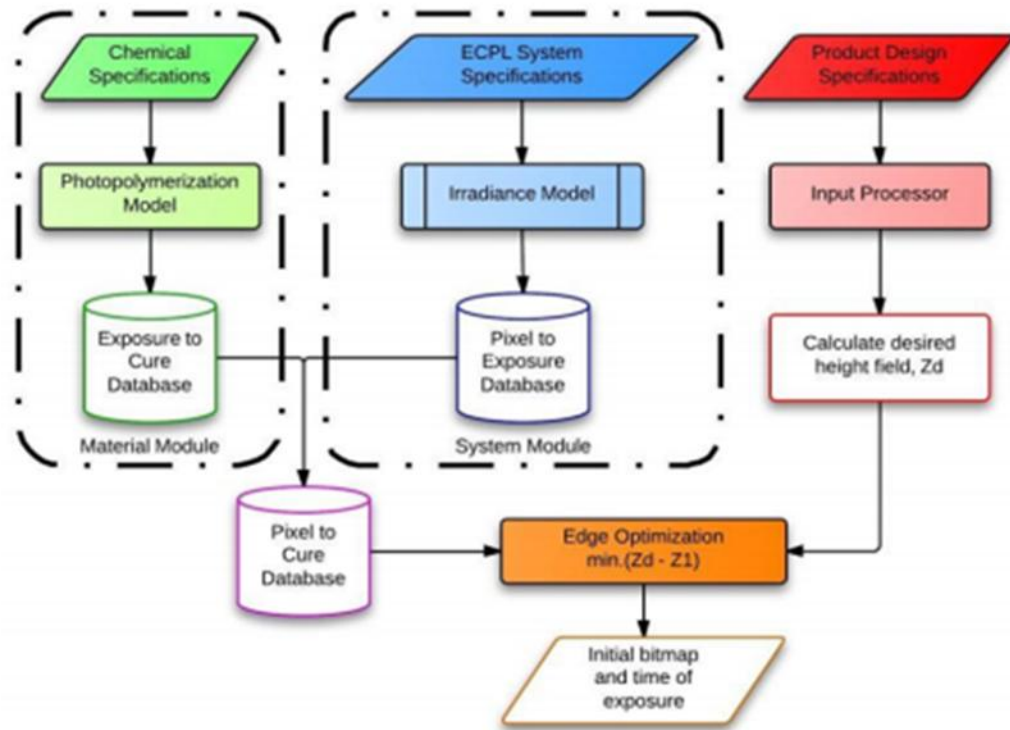


Figure 29: Flowchart for subsequent “layers.” [30]

Analyzing the existing process planning method reveals that the causes of a large error between simulation and the experimental result may depend on three parts: the photopolymerization model, the irradiance model, and the process planning algorithm. Discussion of the polymerization model and irradiance model will be performed in this chapter, and the improvement of the algorithm will be introduced in next chapter.

4.2 Revised Irradiance Model

The existing irradiance model has been demonstrated to be able to predict the exposure profile on the substrate level very well. Experimental validation was also reported in Jariwala et al. [9]. A detailed explanation for finding the irradiance model was illustrated in Chapter 2. Dr. Jariwala et al. shows the comparison of simulation results

from the irradiance model with data from the camera, which can be seen in Figure 30. As Figure 30 shows, compared to the solid line, the dashed lines become much narrower on the top. The top region of the irradiance model has much more variation between the solid lines and dashed lines than the bottom region of the irradiance model, which means that for a small amount of curing time, the irradiance model cannot estimate the exposure profile to a high degree of accuracy. Since the objective of this study is to decrease the dimensional error within 5% of the process planning method, it is necessary to modify the simulation irradiance model to better fit the experimental results.

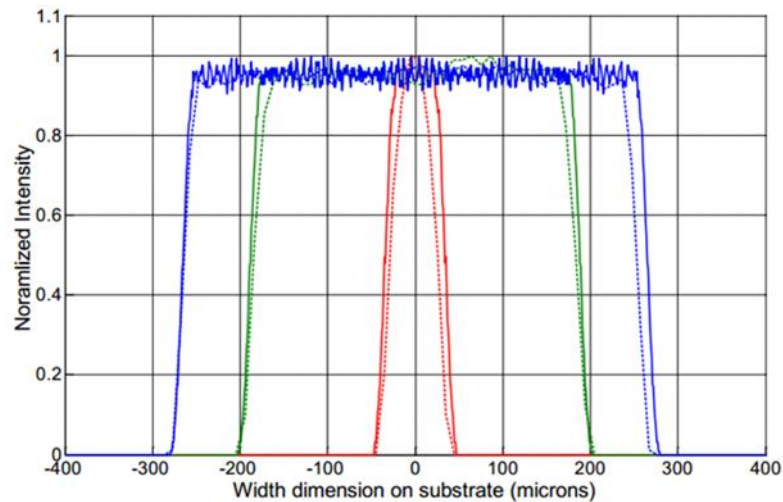


Figure 30: Comparison of simulation results from Irradiance model (solid lines) with data from the camera (dashed lines). Red corresponds to 10 pixels; green to 60 pixels and blue to 90 pixels [9]

4.2.1 Investigation on Effects of Irradiance Model

In order to investigate the sample dimensional effect caused by the irradiance model, several experiments were done by fabricating multiple aspheric lenses with different geometry specifications. Since the irradiance model was found not to have

significant effects on the cured parts' height, only the diameters of cured parts were considered. In the experiment, the same bitmap is used to project with different exposure times, which means the irradiation areas are kept the same and sample heights are varied. In the meantime, simulations were run by using the same irradiation area and exposure times through the existing model. Figure 31 shows the plot between dimensional error and sample height. The dimensional error means the difference in diameter between the simulation results and the experimental results. Sample heights mean the desired height for the final products. As the graph shows, the dimensional error shows an inverse linear relationship to the desired height, which means longer exposure time leads to a less dimensional discrepancy between the models in the experiment. The discrepancy found in this experiment well proves that the variation in the top region of the existing irradiance model may directly raise the dimensional error in diameter.

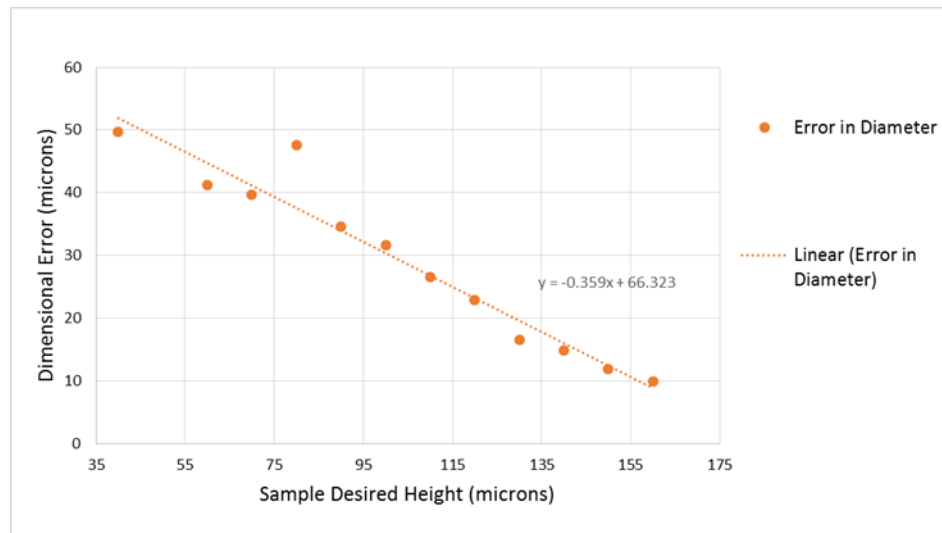


Figure 31: Dimensional Error vs. Sample Desired Height

4.2.2 Irradiance Model Revision

To modify the mismatch between the model and experimental results, the irradiance model was revised by manually fitting the model to experimental results, since the experimental result on the top region is generally narrower than the model for all sizes of irradiation area. We can generate the entire model to be narrowed in the top region by changing the slope of the sides. The existing irradiance models created by Dr. Jariwala were obtained. They were used as the incident light profile in the COMSOL simulation. To revise the entire irradiance model, the profiles for the size of 10 pixels, 60 pixels, and 90 pixels were obtained, to be generated to fit the experimental results, and then the linear regression method was applied to the rest. Figure 32 shows the comparison between the old irradiance model (blue line) and the new irradiance model (red line). What has applied for the new irradiance model is to narrow the top region of the irradiance model. The left top graph shows the light profile of curing 10 pixel-size bitmap based on old irradiance model (blue line) and new irradiance model (red line). The right top graph shows the same comparison for curing 60 pixel-size bitmap and the bottom graph is for curing 90 pixel-size bitmap.

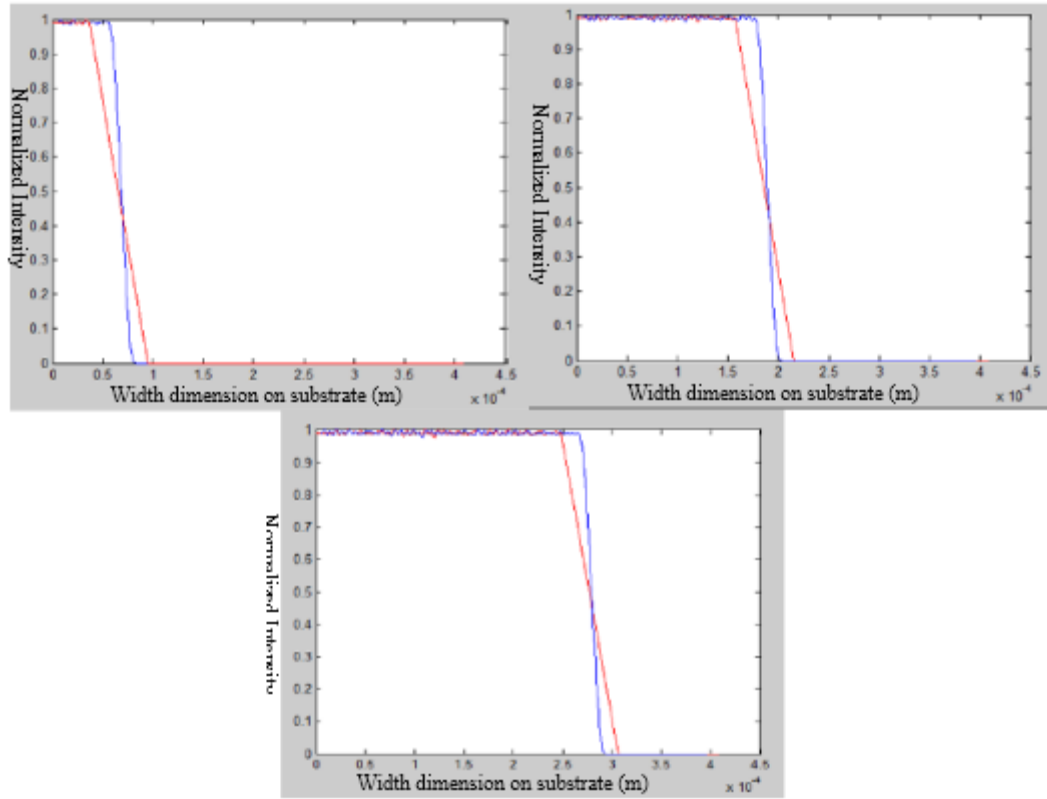


Figure 32: Examples of revised irradiance model. 10 pixels (left top); 60 pixels (right top); 90 pixels (bottom)

4.3 Revised Polymerization Model

The polymerization model describes the chemical reaction in the resin chamber in the ECPL process. The polymerization process of oxygen inhibition in the ECPL process was formulated by Dr. Jariwala [9] and explained in chapter 2 as well. The model incorporates the chemical reaction inside the resin with oxygen diffusivity. The polymerization kinetic model is presented briefly as follows. The concentrations of photoinitiator [In], radicals [$R\cdot$], unreacted double bonds [DB], and oxygen [O_2] were modeled in the kinetic model. The reactions considered by them were as follows [18].

When the photopolymer resin receives light energy, the photoinitiator absorbs it and decomposes into two radicals with first order rate constant of K_d ,



The initiator decomposition rate, K_d , is well known in literature and is modeled as a function of the local intensity, which varies with depth (following the Beer-Lambert Law) [18]

$$K_d = \frac{2.3\Phi\epsilon\lambda}{N_Ahc} I_0 e^{(-2.3\epsilon[In]z)} \quad (16)$$

where $0 < \phi < 1$ is the quantum efficiency of the photoinitiator, N_A is Avagadro's number, h is Planck's constant, and c is the speed of light. The molar absorptivity of the resin, ϵ , depends upon the source wavelength λ . The depth inside the resin is z . The kinetic equation of the initiator can then be given as,

$$\frac{d[In]}{dt} = -K_d[In] \quad (17)$$

The radicals can then react with the double bonds to form longer chains, to form a dead radical or to be quenched with dissolved oxygen as depicted by the following three equations.



R_{dead} is a species produced that destroys one or more radicals. The rate constants used are K_p for the propagation of a radical through an acrylate double bond, K_t for termination between two radicals, and K_{t,O_2} for termination of a radical with an oxygen molecule. R^* represents non-propagating radicals.

The overall rate of initiator decomposition, R_i , is modeled by multiplying the constant rate K_d by the initiator concentration $[In]$

$$R_i = K_d[In] \quad (21)$$

The kinetic equations for the double bond $[DB]$, live radicals $[R\cdot]$ and oxygen $[O_2]$ can be given as follows:

$$\frac{d[R\cdot]}{dt} = 2k_d I(z)[In] - 2k_d [R\cdot]^2 - k_{t,O_2} [R\cdot][O_2] \quad (22)$$

$$\frac{d[DB]}{dt} = -k_p [R\cdot][DB] \quad (23)$$

$$\frac{\partial [O_2]}{\partial t} = -k_{t,O_2} [R\cdot][O_2] + D_{O_2} \frac{\partial^2 [O_2]}{\partial z^2} \quad (24)$$

The effect of oxygen inhibition and diffusion is explicitly modeled in Eq. 24. Due to the high diffusivity of dissolved oxygen in the photopolymer resin, it was assumed that the oxygen would primarily diffuse from uncured top layers of the sample chamber down to the curing front, compete with double bonds for radicals and significantly slow down the rate at which the double bonds are converted, thus increasing the gel time. Equation 24 described the one-dimensional model of the effect of oxygen inhibition and diffusion. To transfer to the two-dimensional model, this equation was modified to account for oxygen diffusion in two dimensions as shown in Eq. 25. Since we are looking for the profile of the cross section, only the x-direction and the z-direction are considered.

$$\frac{\partial [O_2]}{\partial t} = -k_{t,O_2} [R \cdot] [O_2] + D_{O_2} \frac{\partial^2 [O_2]}{\partial x^2} + D_{O_2} \frac{\partial^2 [O_2]}{\partial z^2} \quad (25)$$

The researchers estimated the rate constants, K_t , K_p & K_{t,O_2} by fitting the simulation results with the experimental data from Fourier-transform infrared (FTIR) experiments [9]. They had suggested that the individual rate constants are not unique and may vary. Since the FTIR experiments were conducted at 100 times the intensity of the light used in the ECPL system, it is possible that the effect of oxygen inhibition and diffusion was not adequately captured using the presented rate constants. Hence, these constants were varied to suit the ECPL experimental conditions. The reaction rates used in the existing ECPL simulation are listed in Table 2.

Table 2: Existing reaction rates for ECPL system

Parameter	Value	Units	Source
Quantum efficiency of radical, Φ	0.6	-	[17]
Molar absorptivity of photons at 365nm wavelength, ϵ	15	m ² /mol	[17,31]
UV light Intensity, I_0	8	W/m ²	experimental
Molecular weight of Monomer, TMPTA	296	g/mol	Sartomer
Molecular weight of Photoinitiator, DMPA	256	g/mol	Ciba
Rate constant for propagation reaction, K_p	1.66	m ³ /mol-s	Modified from [19]
Rate constant for termination reaction, K_t	1.31	m ³ /mol-s	Modified from [19]
Rate constant for termination via oxygen quenching, K_{t,O_2}	125	m ³ /mol-s	Modified from [19]
Diffusion coefficient of Oxygen, D_{O_2}	1.00E-10	m ² /s	[32]
Initial concentration of Oxygen, $[O_2]_0$	1.05	mol/m ³	[33]

Polymerization is the major section of the entire ECPL process. It will cause a lot of dimensional error if the polymerization model is not able to perfectly predict the chemical reaction within the chamber. It directs to the research question 1.

Research Question #1: *How does polymerization model affect the sample dimension?*

4.3.1 COMSOL Simulation Model

To simulate the polymerization process, all the equations from 15 to 25 are used in COMSOL software with 2D conditions. The simulation will provide the concentration of each molecule. To estimate the part height, degree of cure introduced by Flory is used. The degree of cure, which is also called monomer conversion, is computed using the following equation:

$$Conversion = \frac{[M]-[M_0]}{[M_0]} \quad (26)$$

M represents the monomer concentration after polymerization and M_0 represents the initial monomer concentration. As polymerization occurs, monomer molecules combine to form polymer chains, so as time goes on, less and less unreacted monomer is in the resin. Thus, [M] will always be less than [M₀] after polymerization starts. Therefore the conversion value will always be positive. The shape of the cured part can be estimated by finding the track within the sample where the conversion has reached the critical conversion limit. The degree of cure in the ECPL system was found to be 20% from the simulation as introduced before in Section 2.2.2.

COMSOL simulations were used to predict the height, diameter and geometry profile of the fabricated samples. The irradiance model that represents the incident light profile was used as the input. The whole resin chamber in the actual experimental setup

was created as a rectangle in the COMSOL model. The entire process was considered to be symmetric. Therefore, only half of the chamber was created. The width of the model was 500 μm , and the height of the model was 400 μm . The simulated finite element geometry is shown in Figure 33. The entire geometry was meshed by using 3095 triangular elements, and the size of the finest mesh was 0.15 μm . The entire meshed domain was assumed to be filled with chemical resin. The left side of the boundary was considered to be symmetric, and the others were considered to be insulated, which is close to the real experimental setup.

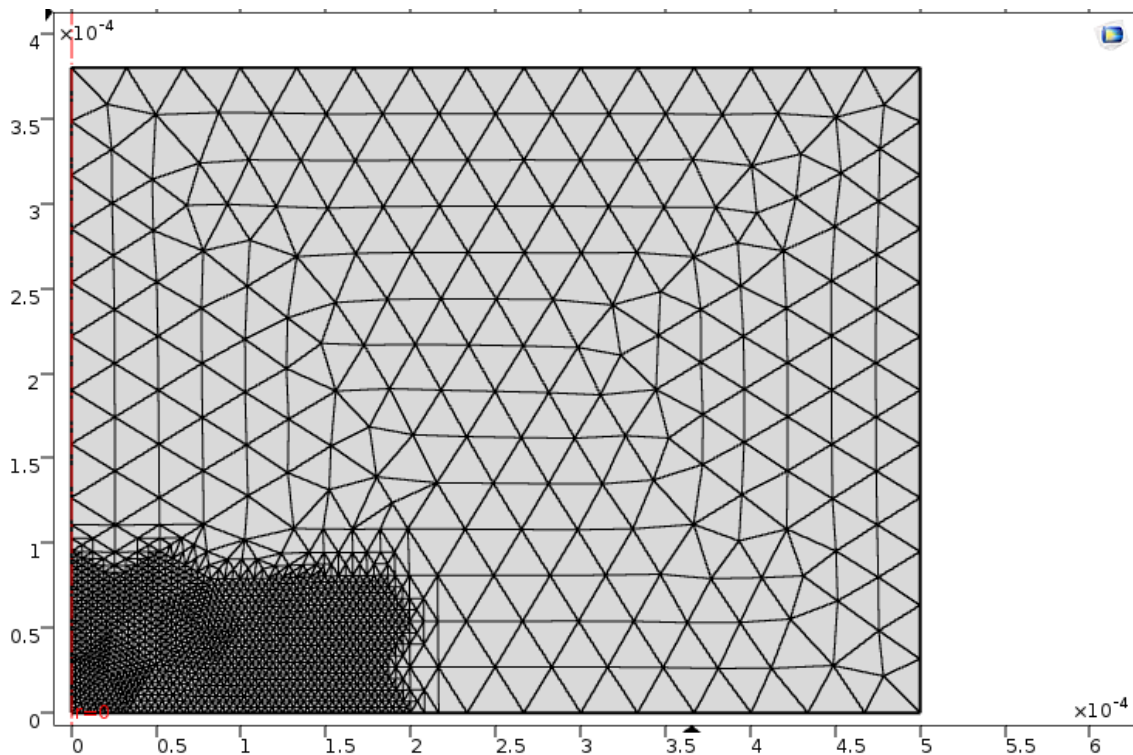


Figure 33: Schematic of FE model used in COMSOL

4.3.2 Analysis of the existing polymerization model

By analysis of the existing polymerization model, three groups were found to cause the discrepancy between the simulation and experimental results.

Group1: variation from the existing polymerization model

Figure 34 shows the experimental validation from Dr. Jariwala's Ph.D. thesis. Dr. Jariwala [9] concludes that the existing polymerization model with revised rate constant can closely predict the height and width of the cured parts. However, some variations can be still found in Figure 34. Since the objective of this study is to decrease the error between the simulation and experimental results within 5%, the existing polymerization model is not accurate enough to fulfill the task.

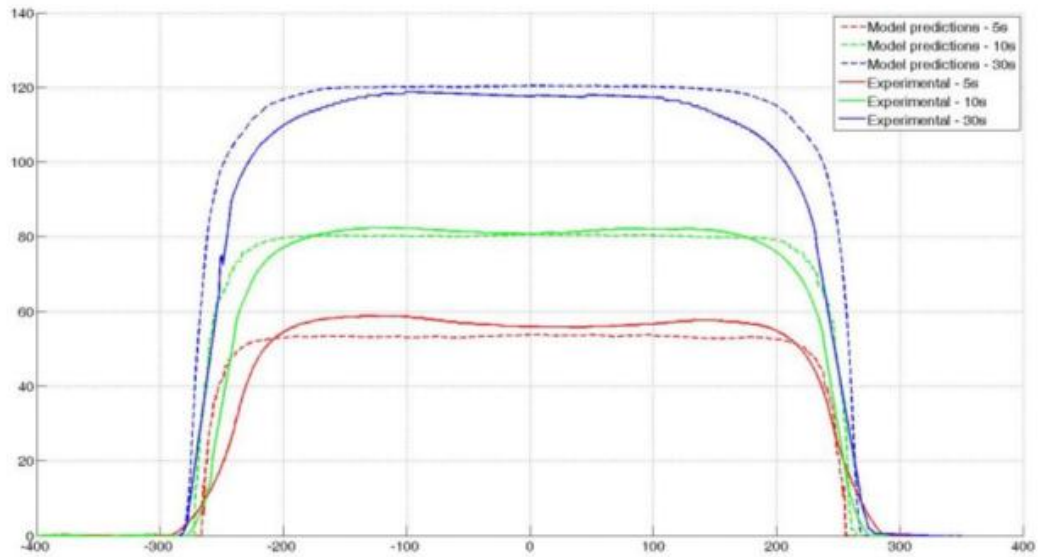


Figure 34: Comparison of experimental profiles (solid lines) with simulated profiles (dashed lines) Red for 5s exposure time; Green for 10s; Blue for 30s [9]

Group 2: variation from changing the system design and chemicals

Since the current system design was improved to be more repeatable and stable, the reaction rates might be changed due to the changing of system design and the chemical resin. Multiple experiments and simulations were run to compare the existing

polymerization model prediction of the chemical reaction with the current system design. A group of experiments was conducted. A circle bitmap with 28-pixel size in radius was used to perform experiments and simulations. The same bitmap was used for exposure in different times. The theoretical working curve for 28 pixels in radius is listed in Figure 35 as the blue line. It is the simulation result obtained from COMSOL software by using the existing reaction rates. The red X marks represent the experimental data points from the latest system for exposure time 5.1 s, 15.8 s and 28.1 s. A much larger error is shown in Figure 35 than in Figure 34. Compared to Figure 35, the Figure 34 does not show much error in height, but Figure 35 shows a huge difference, which means the reaction rates need to be calibrated again to allow the polymerization model to match the experimental results.

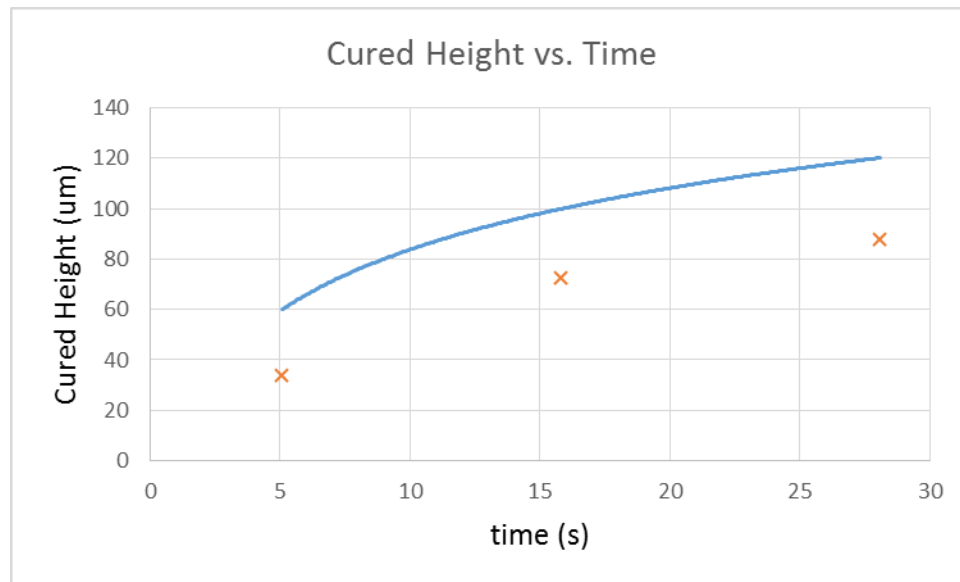
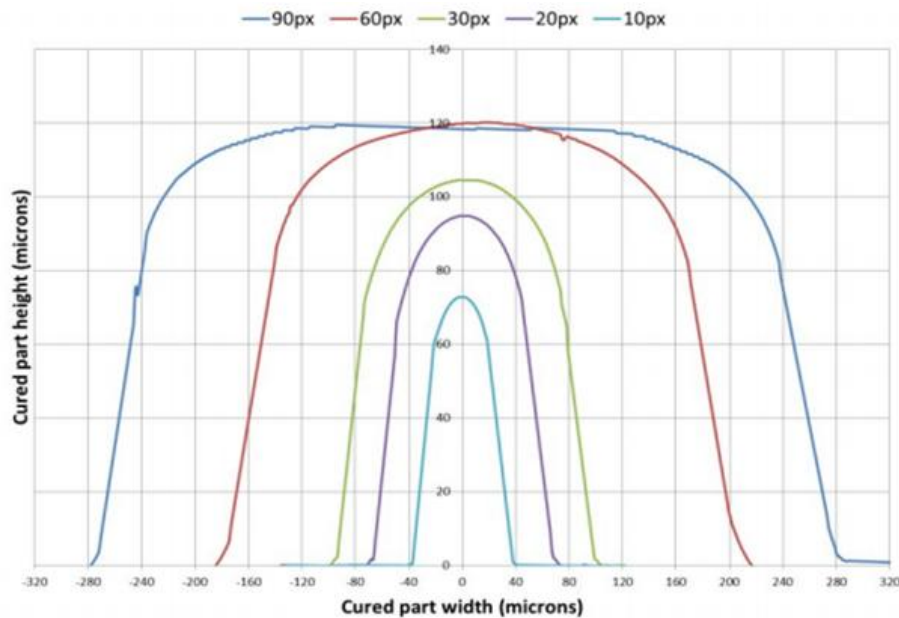


Figure 35: Cured Height vs. Time (blue for simulation results and red X for experimental data)

Group 3: variation in smaller irradiation area

Figure 36 was obtained in Dr. Jariwala's Ph.D. thesis. It shows the cross-sectional profile of the cured samples by using 3D confocal microscopy [9]. Different irradiation area for 10 pixels, 20 pixels, 30 pixels, 60 pixels and 90 pixels in diameter were used to expose. All samples were cured by the same intensity and the same exposure time, which is 30 seconds. The Figure 35 demonstrates that the samples reach the same height in larger pixel size such as 90 and 60 pixels and then gradually decreases for the smaller pixel size such as 30, 20 and 10 pixels. However, according to the Beer-Lambert Law and the simulation from COMSOL, all samples will reach the same height after being exposed the same amount of time if the reaction rates are kept the same. The Lambert Law and other literature reviews mainly focus on relatively larger samples, but the ECPL is focusing on the micro scale, which is a research gap in the mask projection stereolithography process. Therefore, the COMSOL simulation and the existing polymerization model fail to simulate the reaction for that smaller irradiation area.



**Figure 36: Cross-section profile obtained from 90px, 60px, 30px, 20px and 10px
through ECPL system**

To sum up all the three aspects, which cause discrepancies between the simulation model and experimental results, the refined research question 1, along with its hypothesis was made below. It is suggested that kinetic model needs to be modified to explain the phenomena driving the photopolymerization reaction.

Refined Research Question 1: How to refine the polymerization model to better predict the sample geometry profile

Hypothesis for research question 1: The polymerization model can be improved if the chemical reaction rates are modified as a function of the irradiation area.

4.3.3 Empirical model of chemical reaction rates

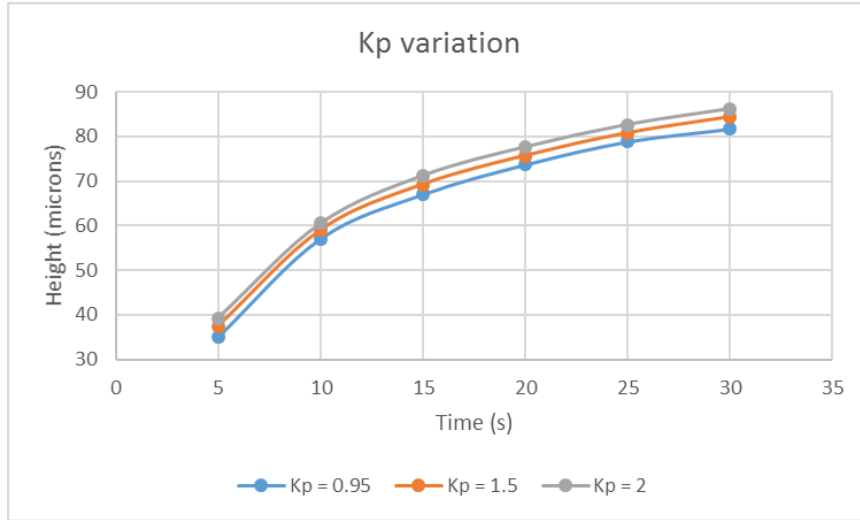
To empirically revise the chemical reaction rates, multiple experiments were performed. Since the polymerization model will mainly affect the height of the cured parts, only the height of the cured sample was considered and measured. There are two steps to revise the chemical reaction rates.

Step one: revise reaction rates for the larger irradiation area

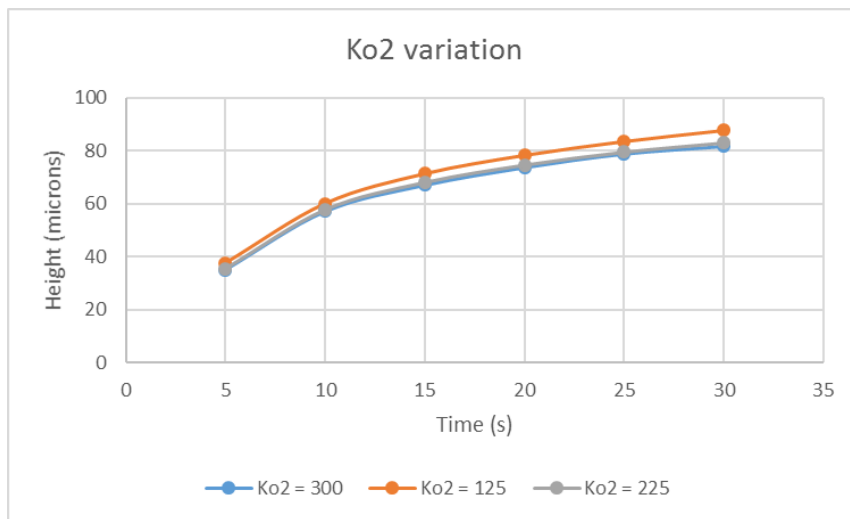
This step is to fix the error causing from group 1 and group 2 discussed in the above section. New reaction rates were obtained by fitting the simulation results to the experimental results. The author, Boddapati et al. [19] did specify that the rate constants may vary over a significant range as long as the ratio of $K_p/\sqrt{K_t}$ is kept constant, and the ratio was found to be 1.45 in ECPL system in Dr. Jariwala's Ph.D. thesis. Hence, the

ratio of $K_p/\sqrt{K_t}$ will keep the same in this study. K_p , K_t , K_{t,O_2} and oxygen diffusion rate will be revised to fit the experimental working curve.

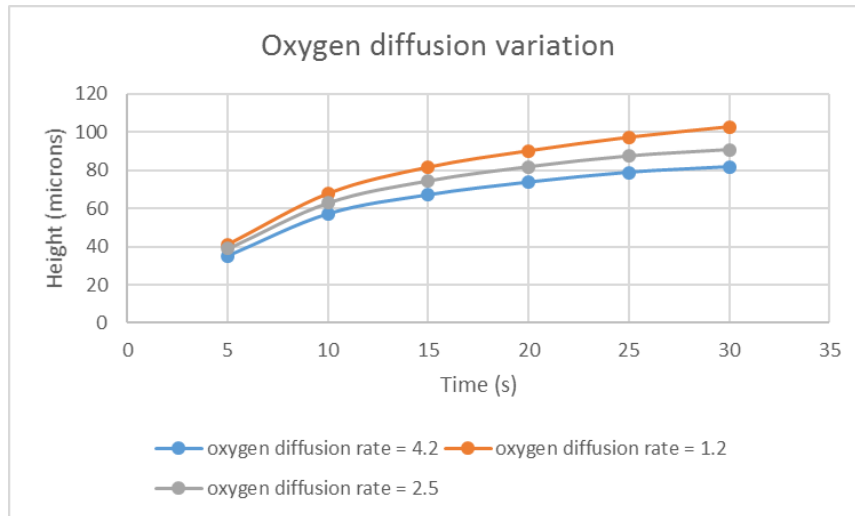
To determine the value of these rates, it will be necessary first to find the effects on working curve by changing these values. To do that, a parameter study was conducted. One parameter was changed for study and other rates were kept the same. Figure 37 shows the results of the working curve by changing these values. As the graph shows, changing of K_p and K_t will move the entire working curve up or down. The difference between each exposure time seems to be constant. Larger K_p values result in a larger dimensional part. Changing K_{t,O_2} was found not have significant influence on the working curve. Moreover, the working curve was almost the same for the values of 225 and 300. The oxygen diffusion rate shown in the following figure has no effect on the curvature of the working curve. Based on those findings, the steps to revise reaction rates will be first to find the value of oxygen diffusion rate to get the curvature of the simulation working curve to fit the experimental working curve. Then to find the appropriate K_p value that fits the entire simulation working curve to the experimental working curve. Finally, the K_{t,O_2} value can be changed to get the best fit. A manual iteration method was used for finding these values to fit the simulation results to the experimental results.



(a)



(b)



(c)

Figure 37: Parameter study for (a) K_p (b) $K_{(t,O_2)}$ & (c) oxygen diffusion rate

By using above method, the values of K_p , K_t , K_{O_2} and oxygen diffusion rate were determined to be $0.95 \text{ m}^3/\text{mol}\cdot\text{s}$, $0.43 \text{ m}^3/\text{mol}\cdot\text{s}$, $300 \text{ m}^3/\text{mol}\cdot\text{s}$ and $4.2\text{e-}10 \text{ m}^2/\text{s}$. The intensity was experimentally modified to be $9.5 \text{ W}/\text{m}^2$. Figure 38 shows the comparison of the simulation result prior to changing the rate constants and the simulation result after using the new rate constants. The X marks shows the experimental data.

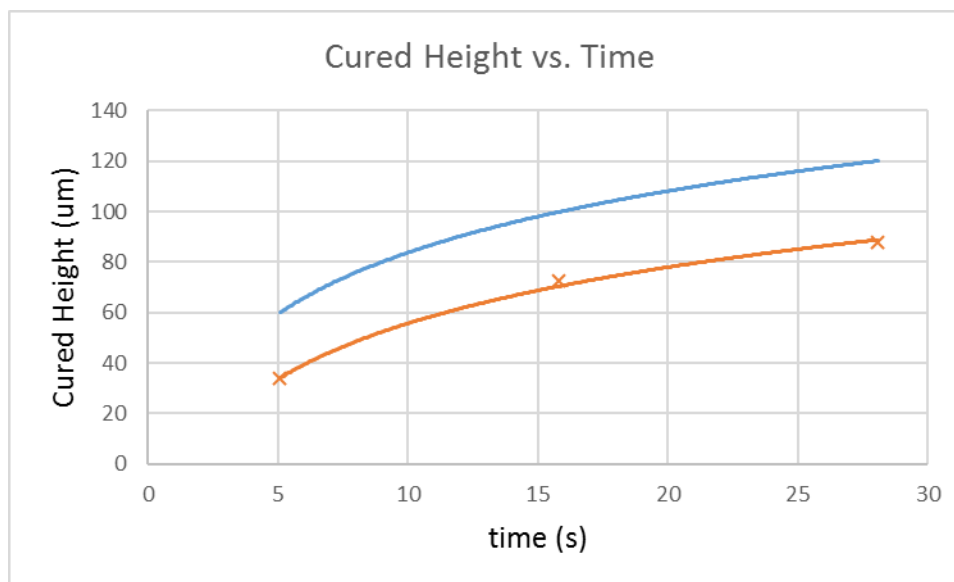


Figure 38: Comparison between the simulation result before changing the rate constants (blue line) and the simulation result after using the new rate constants (red line)

Step two: revise reaction rates for the smaller irradiation area

This step fixes the error caused from group 3. The cause of height deduction for smaller irradiation areas is still unknown at the current stage. Further study can be performed to find the reason. However, it is found that for the smaller irradiation area, the results still follow the working curve drawn from the Beer-Lambert Law. In order to refine the polymerization model to better predict the cured part geometry, the chemical reaction rates are considered for revision. In order to do this, multiple experiments were done to find the relationship between reaction rates and irradiation area. A single bitmap with 8 pixels in radius was exposed for 10s, 20s, and 30s separately. The confocal microscope was used to measure the height of the resulting samples. The same procedure was done for the bitmaps with 10 pixels, 12 pixels, 14 pixels and 20 pixels in radius. The

results were listed in Table 3. Figure 39 shows a plot of all these results, and it suggests that the cured height for the same amount of time gradually decreased as the irradiation area was reduced, and the reduction seems to be even.

Table 3: Height dimension for 8px, 10px, 12px, 14px, 16px and 20px for 10s, 20s and 30s respectively

pixels	8	10	12	14	16	20
Height for 10 s (um)	30.24	38.91	45.43	51.46	55.37	68.04
Height for 20 s (um)	44.73	49.35	60.95	66.93	70.36	80.95
Height for 30 s (um)	49.53	55.90	68.62	74.95	79.95	90.07

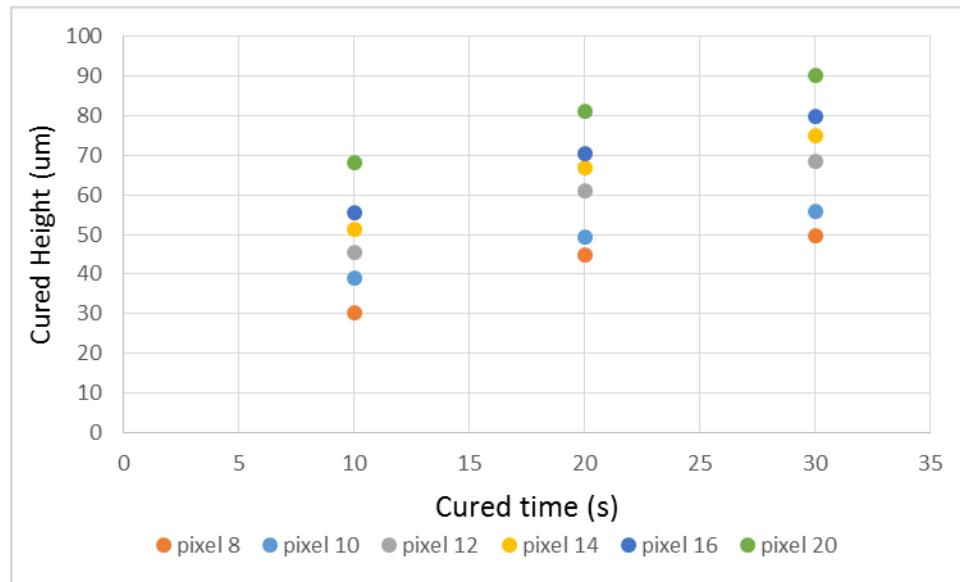


Figure 39: Plot of Table 3

After the experimental result was analyzed, the reaction rates revised to allow the simulation fit the experimental result. The light intensity and oxygen diffusion rate were not considered for change, since these are system parameters. Changing the oxygen termination rate did not significantly affect the entire working curve, so it was kept the same. Therefore, radical termination and propagation rates were considered for change. A

manual iteration method was used to find the best fit of simulation data to the experimental results. By fitting the experimental results, K_p and K_t for pixel size of 8, 10, 12, 14 and 16 were determined and listed in the Table 4. The size of 20 pixels was found to reach the similar height as the larger irradiation did, so that the size of 20 pixels was determined to be the critical point for distinguishing a relatively large irradiation area from a relatively small irradiation area. To plot K_p value as a function of pixel size, a linear relationship was found between K_p and pixel size. The equation of the trend line was obtained to estimate the K_p and K_t values of other smaller irradiation areas. In the case of calculating value of K_t , equation $\frac{K_p}{\sqrt{K_t}} = 1.45$, mentioned previously, was used.

Table 4: K_p and K_t value for pixel 8, 10, 12, 14 and 16 from simulation

Pixel size in Radius	K_p value ($\text{m}^3/\text{mol-s}$)	K_t value ($\text{m}^3/\text{mol-s}$)
8	0.65	0.20
10	0.71	0.24
12	0.74	0.26
14	0.79	0.30
16	0.82	0.32

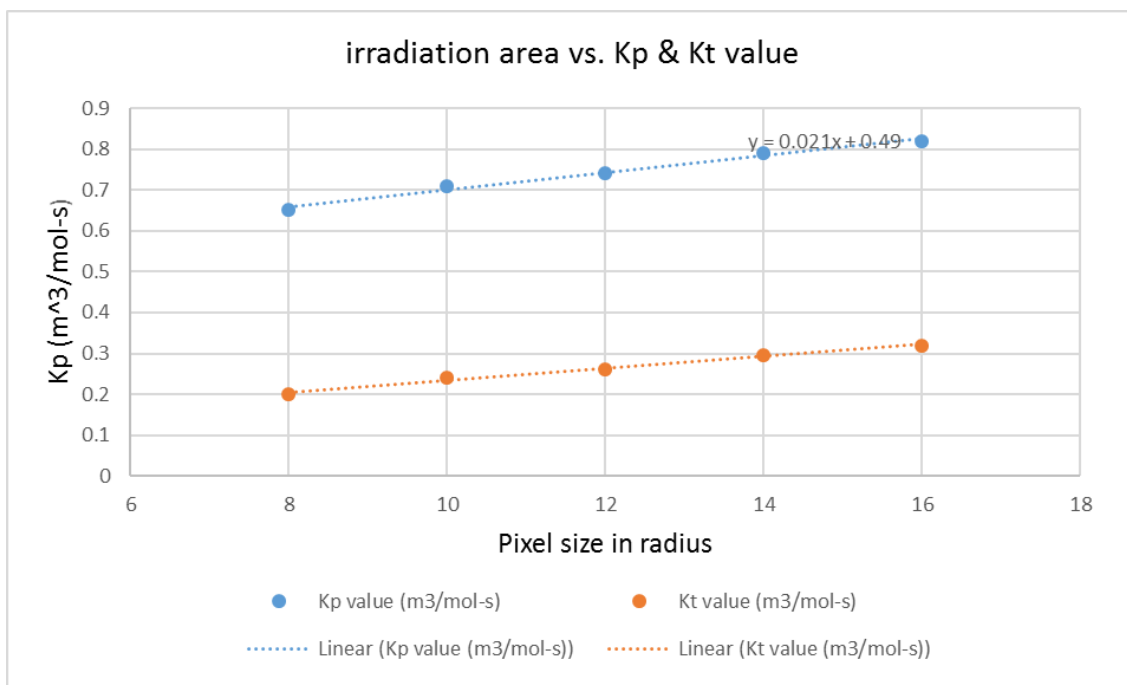


Figure 40: Plot of Table 4 with fitted line and equation

As noticed, the revised reaction rates in both smaller irradiation area and larger irradiation area are from the simulation by empirically fit the experimental data. The real reaction rates can be determined theoretically in the future to see if the revised reaction rates in the simulation are reasonable or not. Moreover, the reason for the reaction rates vary up to 200 μm bitmap size and then become constant is still under the investigation. It may be because that the radicals in smaller irradiation area are not as active as in larger irradiation area or, some other factors are missing in the model. Also, it is not certified if changing with other parameters such as power intensity and chemicals used in the resin will have any effect on changing 200 μm to other values. 200 μm might be the value that the light profile is getting stable. All the values under 200 μm might have more light aberrations. Further study needs to be conducted in the future.

4.4 Experimental Validation with Revised Model

To validate the revised irradiance model and polymerization model, which is also summed as research question 1, multiple experiments were conducted to compare the geometry profile from the fabricated samples with simulation results. A single bitmap with 10 pixels in radius was used to expose for 10s, 20s and 30s. The geometry profile was obtained from the 3D confocal microscope with 20X magnification. The same procedure was repeated for bitmaps with 20pixels and 30pixels in radius. The same curing process was simulated in the COMSOL software as well. Figures 41, 42 and 43 show the comparison of the experiments and the simulations.

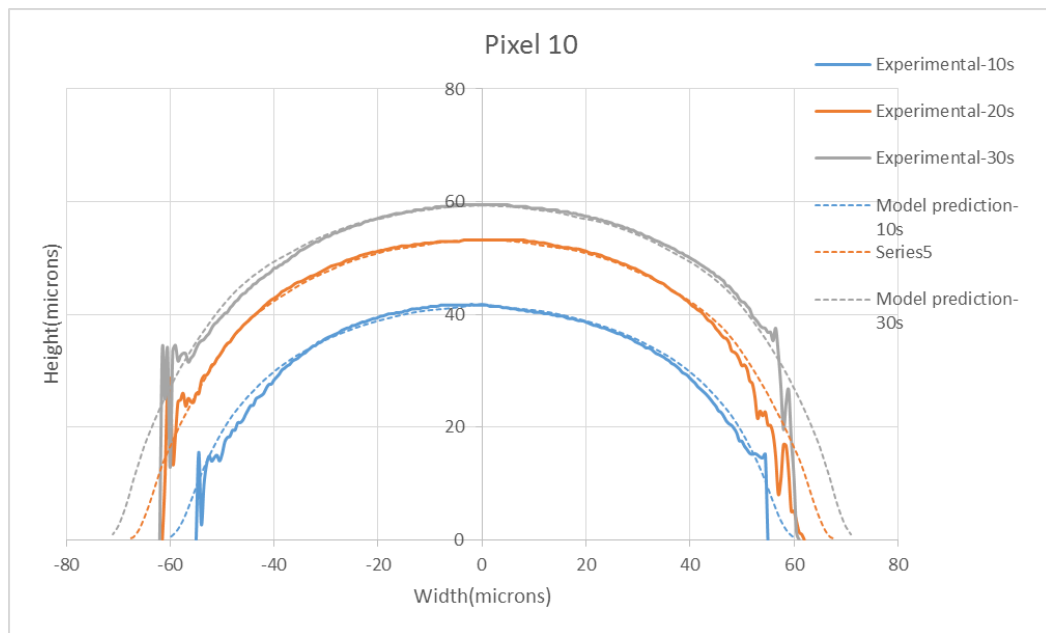


Figure 41: Comparison between experimental results and simulation results of geometry profile for 10px bitmap with exposure time of 10s, 20s and 30s

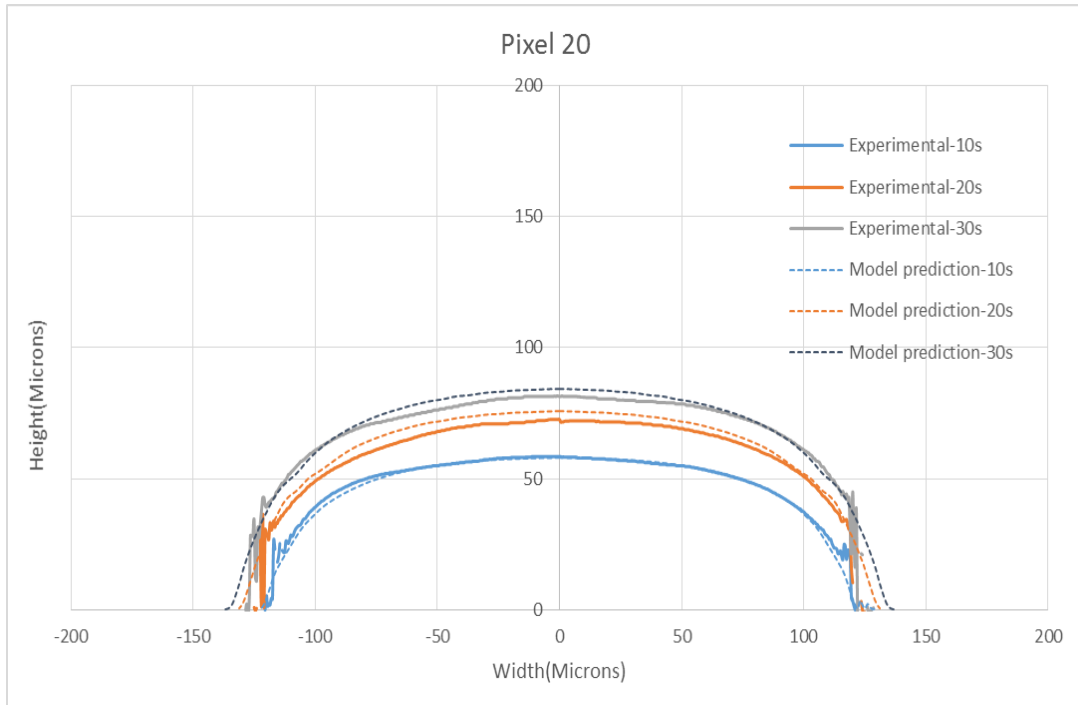


Figure 42: Comparison between experimental results and simulation results of geometry profile for 20px bitmap with exposure time of 10s, 20s and 30s

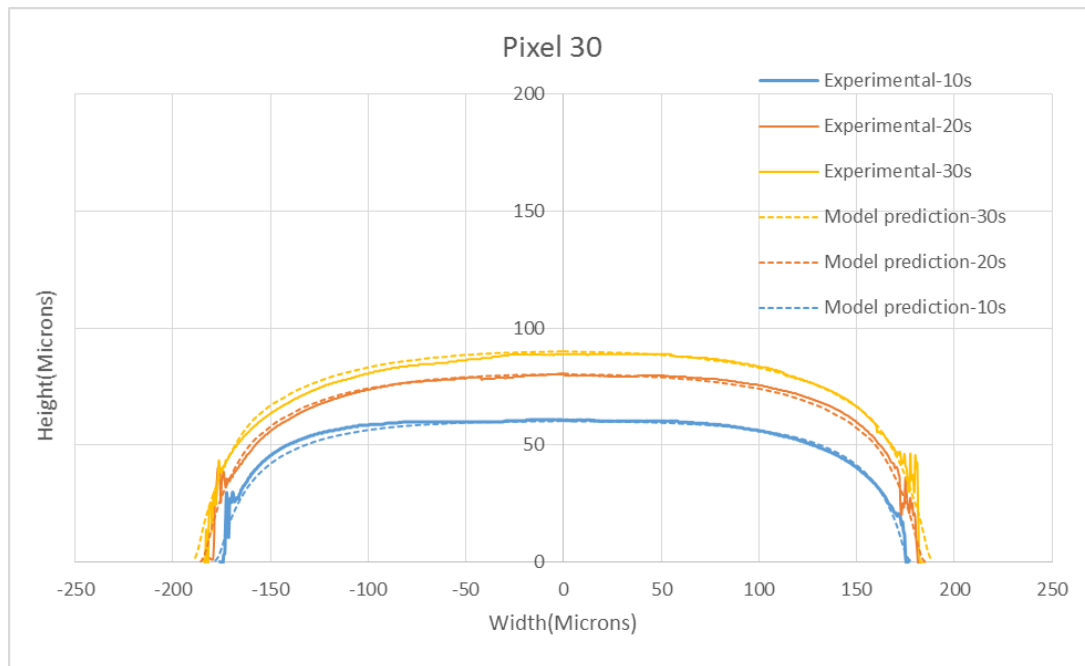


Figure 43: Comparison between experimental results and simulation results of geometry profile for 30px bitmap with exposure time of 10s, 20s and 30s

The simulation closely predicts the height and width of the cured parts. Moreover, the entire geometry profiles from the simulation closely match the experimental results from the confocal microscope. It can be seen that for pixel size of 10, there was some variation in the edge profile. A potential explanation for the discrepancy will be the microscope limitation. For the case of pixel size of 10, the diameter was only 120 microns. The edge of the samples is very thin and sharp. When measuring samples, the laser for the confocal microscope will pass through the scanning mirrors and microscopes to provide the excitation light in order to get very high intensity. Then the emitted light from the samples will pass through a path similar to that of a detector. The final geometry of the measured sample will be analyzed by those emitted lights. Since the edge of the cured parts fabricated by the ECPL system is very thin, the emitted light in the edge region may not be able to go back to the detector, which will cause the mismatch and noise in the sample edges. Despite the small variations, the COMSOL simulations successfully demonstrate the generation for cured parts. The Hypothesis for the research question 1 is well validated.

4.5 Chapter Summary

This chapter first presented the discrepancy of the existing theoretical models of the ECPL system: the irradiance model and the polymerization model. The irradiance model was modified to better match the experimental results. The existing polymerization model was found to be insufficient to describe the chemical reaction inside the resin. Hence, research question 1 was addressed to get a better polymerization model. The

existing kinetic model with oxygen diffusion and inhibition was used in this study. The software COMSOL was used to simulate the reaction within the resin. The research showed that the reaction rates in the literature should be modified based on the ECPL system in order to simulate the entire reaction inside the resin. Furthermore, the research demonstrated that the reaction rates for smaller irradiation areas, where the diameter was less than 200 microns, should be varied, depending on the irradiation area, in order to get a more accurate polymerization model. The experimental results and simulated results presented that the reaction rates had a linear relationship with the irradiation area for those where the diameter was less than 200 microns and the reaction rates became constant for larger irradiation areas. Based on the finding, the reaction rates were modified in the COMSOL simulation model. Finally, multiple experiments were conducted to validate that the new polymerization model had a much better estimate of the geometry profile of the fabricated parts.

CHAPTER 5

PROCESS PLAN FORMULATION AND VALIDATION

Chapter 4 discussed the revisions made on the theoretical model for the ECPL system, which is the irradiance model and the polymerization model. In this chapter, an empirical process planning method will be formulated based on the theoretical models and revised process plan algorithm. The shape limitation was addressed based on the current assumptions of the ECPL system. Multiple experiments were performed to validate the new process planning method. Error analysis and limitation are concluded from these experiments. Research question 2 along with its hypothesis will be addressed in this chapter as well.

5.1 Formulation of the empirical process planning method

In the last chapter, the foundation of the process planning method was discussed and modified. In order to fabricate samples through ECPL system, the process inputs of bitmaps and exposure times are needed. Therefore, the method to estimate the bitmaps and exposure times need to be discovered which relates to our second research question.

Research Question #2:

How to estimate the bitmaps and exposure times used in order to obtain the desired geometry?

5.1.1 Empirical process planning method

The same process planning method algorithm proposed by Dr. Jariwala [9] is used to form an empirical process planning method. For convenience, Figures 44 and 45 are shown again to demonstrate the flow chart for the empirical process planning method for

both first “layer” and subsequent “layers.” ECPL system specifications and irradiance model were revised. The photopolymerization model was modified by empirical revision of the chemical specifications.

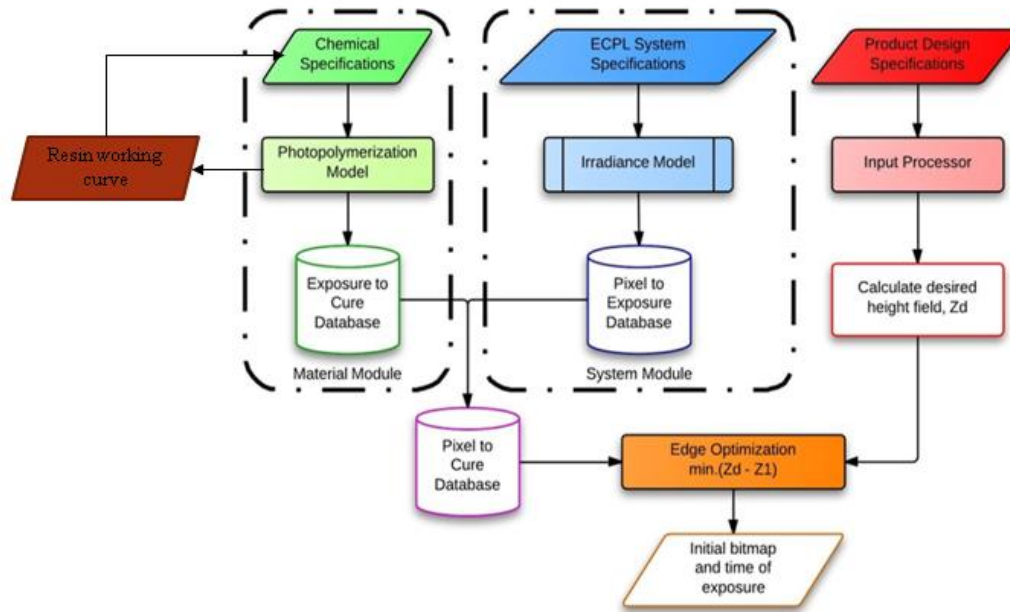


Figure 44: Flowchart for first “layer.” [9]

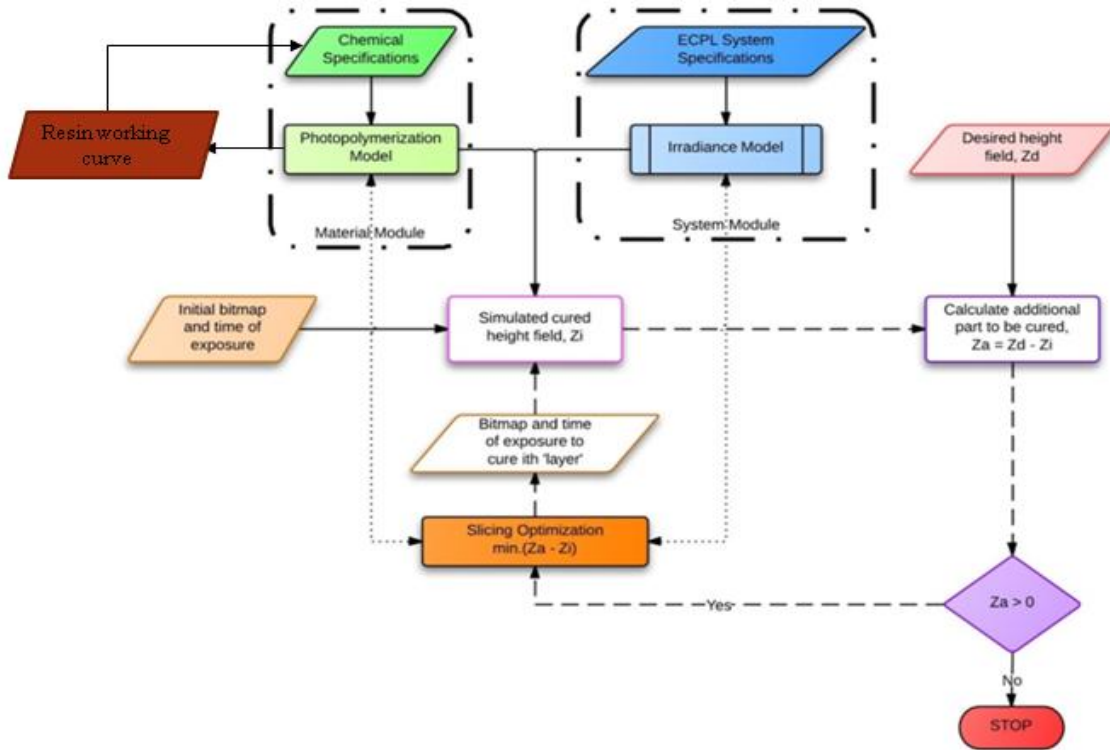


Figure 45: Flowchart for subsequent “layer.” [9]

The input of the first “layer” is the desired cured part geometry. The output is expected to be the initial bitmap and corresponding exposure time. The goal for the first “layer” is to minimize the difference between the cured part geometry profile from the simulation model and the desired shape. As figure 46 shows, B_i indicates the bitmap used to cure the i^{th} “layer”, and T_i represents the corresponding exposure time. The resolution for the bitmap is 1-pixel size, and the resolution for exposure time is 0.1 second. Z is considered as the geometry profile. r refers to the radial distance from the center, and k is the coordinate of the intersection between the curves Z_k and Z_r . The algorithm for subsequent “layers” is similar to the first “layer”. The input will be the desired geometry, the initial bitmap and the exposure time. The output is designed as the bitmaps and

exposure times to cure the entire desired cured part. The objective is the same as the first “layer”.

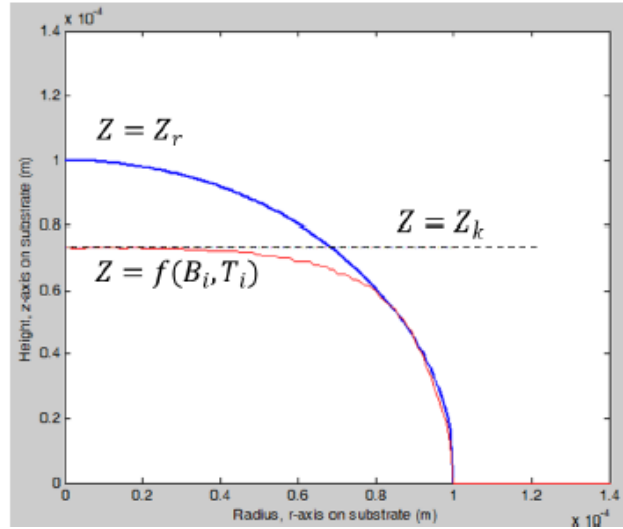


Figure 46: Plots illustration for the optimization [9]

5.1.2 Simulation results

Since the research objective of this thesis is to fabricate lens-shaped structures, the following discussion will be limited to fabricating axisymmetric shapes only, which means only circle-shaped bitmaps will be used. Applying the process planning method, two cases were simulated.

Case 1: aspherical lens with 0 conic constant

An aspherical lens is a lens that has a spherical front surface. The curvature gradually changes from the center of the lens to the edge. To determine the curvature, the conic constant was used here as a parameter. Smith [34] addressed that the conic section through the origin can be applied as the equation as following

$$y^2 - 2Rx + (K + 1)x^2 = 0 \quad (27)$$

where R is the radius of curvature at $x = 0$ and K is the conic constant.

Figure 47 shows the 3-dimensional view of an aspherical lens. Figure 48 shows the desired half cross section of an aspherical lens. The desired diameter was $150\ \mu\text{m}$, and the desired height was $60\ \mu\text{m}$. The conic constant was set to be 0.

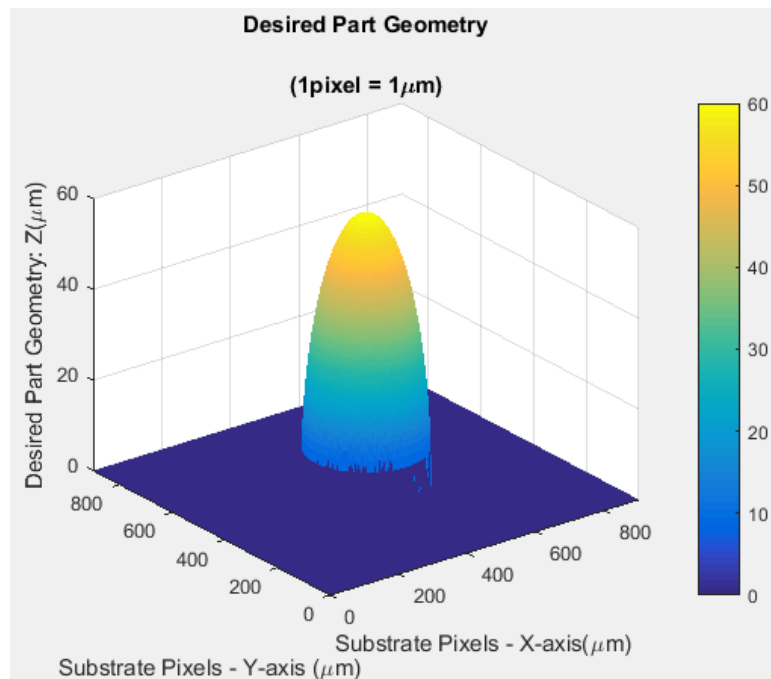


Figure 47: 3-dimensional view of an aspherical lens

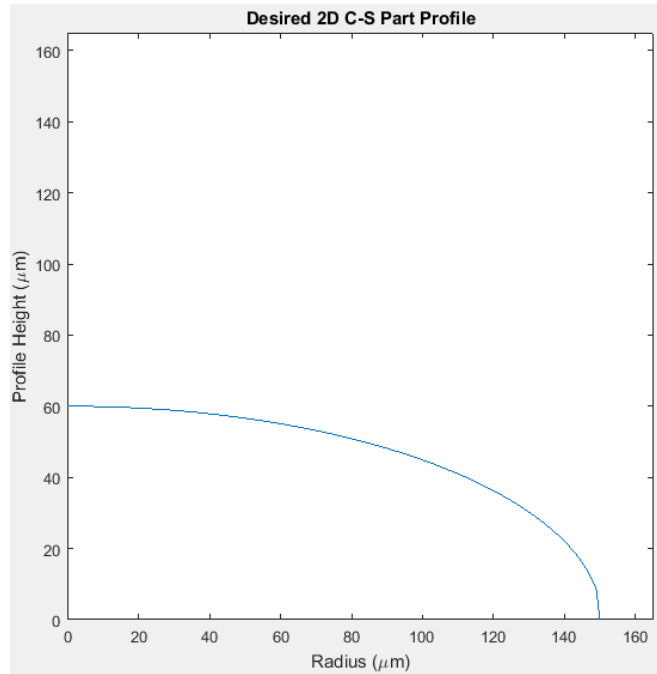


Figure 48: Desired half cross section of the aspherical lens with 0 conic constant

The process planning method provided 20 cured “layers”, and the simulation process is shown in Figure 49. Although there is some variation in the final simulated shape, the simulation process is proven to be able to plan this case.

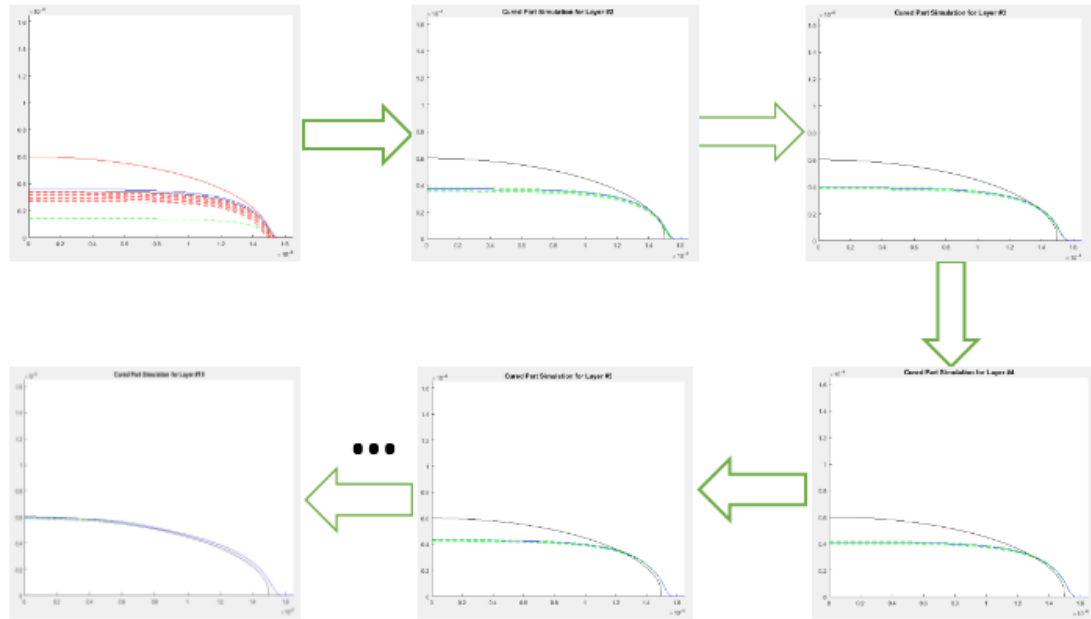


Figure 49: Simulation process for case 1

Case 2: aspherical lens with -1 conic constant

Figure 50 shows the desired half cross section of an aspherical lens with a conic constant of -1. The desired diameter was 150 μm and the height was 60 μm .

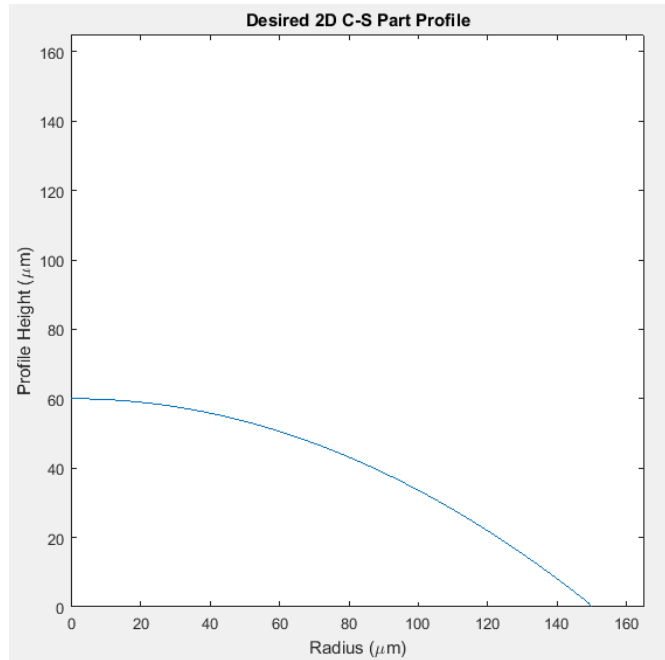


Figure 50: Desired half cross section of the aspherical lens with -1 conic constant

The process planning method provided 20 cured “layers”, and the simulation process was shown in Figure 51. As the figure shows, the simulated profile was much larger than the desired geometry, especially in the diameter. The process planning method failed to provide the bitmaps and exposure times to cure this case.

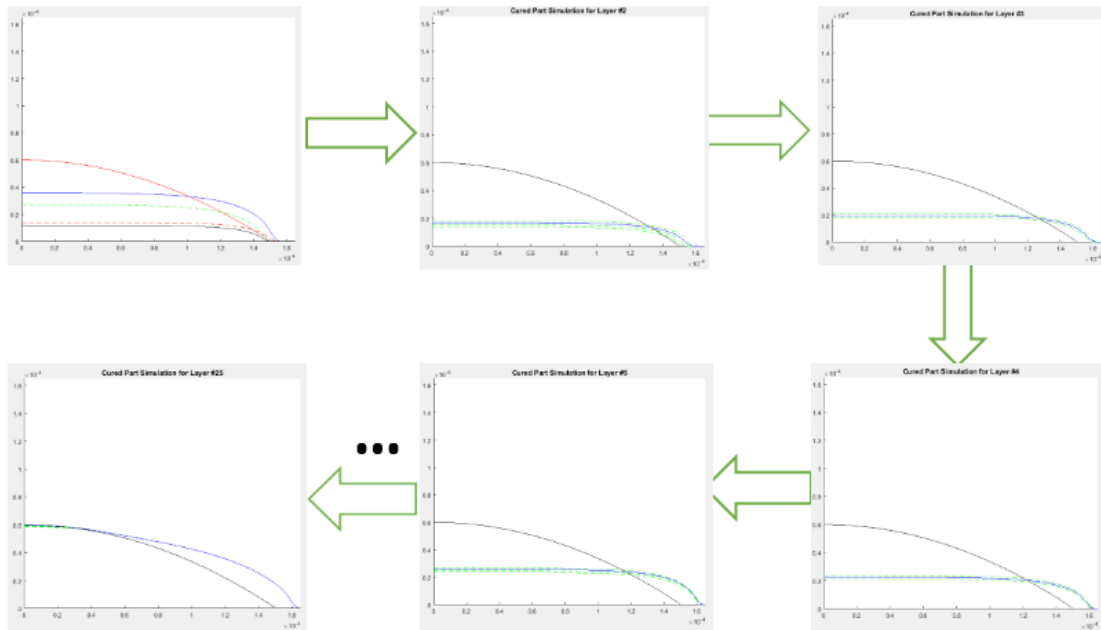


Figure 51: Simulation process for case 2

Case 1 with a conic constant of 0 was successfully simulated and Case 2 with -1 conic constant was failed, which shows that the current process planning method is only able to simulate some cases. Moreover, it is found that the difference between the case 1 and case 2 is the conic constant, which relates to the edge slope of the desired geometry. For case 2, the first three “layers” keep expanding even though the bitmap size is decreasing. The existing process planning algorithm only considers minimizing the error between the previous “layer” and the current “layer”. It did not consider the entire geometry and it failed to control the width of the cured part. Therefore, the hypothesis for research question 2 is addressed as follows:

Hypothesis for research question 2:

A more accurate process planning method can be created by controlling the layer width of the entire cured part.

5.2 Revised process planning method

5.2.1 Revised process plan algorithm

The algorithm for the existing process planning method is to minimize the sum of the height difference between the simulated height and the desired height from the previous layer to current layer. but it did not consider the error from the earlier layer. That leads to the failure to simulate case 2. To better illustrate the problem, Figure 52 presents the cured profile for pixel 30 in radius from 3s exposure time to 30s. The profiles for 2s and 1s are not shown. The reason is that the curing will start at approximately the third second to pass the critical exposure. As shown in the figure, the radius of the cured part will increase at the beginning and then reach stability later. Therefore, for case 2, since the exposure time for the first “layer” is short, the radius will keep increasing when curing subsequent “layers”.

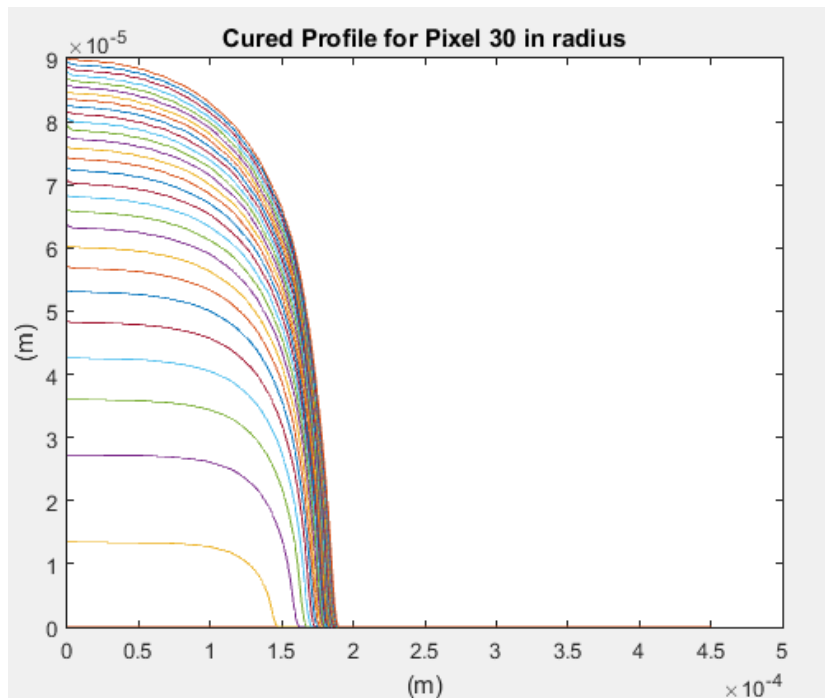


Figure 52: Cured profile for pixel 30 in radius

To solve the problem, the overall diameter needs to be monitored when curing subsequent “layers”. If the overall diameter is increasing when curing the subsequent “layer”, the bitmap size using for the first “layer” needs to be reduced. Since the first bitmap is the largest bitmap and has the longest exposure time in our case, it will be easier to change the first bitmap instead of changing the subsequent bitmaps. Therefore, the algorithm for curing subsequent “layers” should be changed. Pseudocode algorithm for curing the subsequent “layer” was developed in the following.

PSEUDOCODE FOR CURING SUBSEQUENT “LAYER”

Input: Initial bitmap, B(1); initial exposure time T(1); desired geometry

Output: Estimated required bitmaps, B, and corresponding exposure time, T

FUNCTION CURING_SUBLAYER

- 1, Input B(1), T(1) & desired geometry
- 2, Get desired radius, R_d from desired geometry
- 3, Get desired height, Z_d from desired geometry
- 4, Run COMSOL simulation with bitmap, B(1) & time, T(1)
- 5, Get the simulated cured height field for first layer, Z
- 6, Calculate additional part to be cured, $Z_a = Z_d - \max(Z)$
- 7, Get the radius of the simulation & name it as $R_{\max}(1)$
- 8, Set Layer =2
- 9, Set flag_radius = 0
- 10, **WHILE** $Z_a \geq 1e-6$ **DO**
 - Set Bitmap = B(1)-1 & Time = 0.1
 - Run COMSOL simulation with all bitmaps, B & times, T
 - Get the simulated cured height field, Z
 - Calculate overcure error

```

WHILE overcure error <=3e-6 DO
    Time = Time + 0.1
    Run COMSOL simulation with all bitmaps, B & times, T
    Get simulated cured height field, Z
    Calculate overcure error
ENDWHILE
Store Bitmap as B(Layer) & Time as T(Layer)
B(Layer) = Bitmap & T(Layer) = Time
Find the maximum radius on the Layer & name it as Rmax(Layer)
IF Rmax(Layer) > Rmax(Layer-1)
    Set flag_radius = 1
ELSE
    IF flag_radius =1
        Calculate difference between desired radius and cured radius, Rdiff
        = Rmax(Layer) - Rd
        WHILE Rdiff >=3e-6 Do
            B(1) = B(1) - 1;
            Run COMSOL simulation with all bitmaps, B & times, T
            Get the maximum radius as Rmax(Layer)
            Rdiff = Rmax(Layer) - Rd
        ENDWHILE
        flag_radius = 0
    ENDIF
ENDIF
Get the simulated cured height field, Z
Calculate additional part to be cured, Za = Zd-max(Z)
Layer = Layer +1
ENDWHILE
11, Output all the bitmaps, B, and times, T

```

END FUNCTION

When the first “layer” is created, the bitmap and corresponding exposure time will be provided to the subsequent “layer” curing process. The program will reduce one pixel size and increase exposure time by 0.1s increments to enlarge the part. The process will keep increasing exposure time until the sample is over cured within a range. The over cured error is referred as $\sum(Z_i(r) - Z_d(r))|r \geq \textit{intersection}$. Z_i is cured profile height field on current layer and Z_d is the desired profile height field. r refers to the sampling period, and intersection means the intersection point between the desired profile and current cured profile. It was coded in the second while loop in step 10. To achieve that goal, a threshold was set up to stop curing the current “layer”. Since we cannot always get the exact profile of the desired geometry, we consider that it is acceptable if over curing error is less than 3 microns. It can be set as a smaller number, but that will cause the entire program run for a very long time, which is not necessary.

As an output of the subsequent “layers”, exposure time and pixel size will be obtained. In contrast to the other process planning method, at the meantime of curing the subsequent “layer”, the radius of the entire curing part will be monitored. For each “layer”, the maximum width of the existing curing part will be found and stored as the radius of the current “layer”. If the value is greater than that of the previous “layer”, it means that though the pixel size is decreased for the subsequent “layer”, the width of the curing part keeps expanding which is not we want. If this situation happens, the flag will be recorded as 1 instead of 0. The program will monitor the radius until the radius becomes stable. Then the program will modify the pixel size for the first “layer” in order to get the right width of the desired geometry. When the next “layer” is proceed, the first

bitmap, B(1), will be adjusted by decreasing the first bitmap size to minimize the difference between the desired radius and simulated radius, which indicates the third while loop in step 10. The entire program will stop when the height difference between the desired geometry and simulation is less than 1 micron.

The reason for only changing the first bitmap to reduce the width of the sample can be referred to Figure 52 again. The width of the sample expands significantly in the first 4 to 5 seconds and after that, the changing of the width is only 1 micron or even less, which can be negligible. Since when curing a sample, the first “layer” takes the longest time and the largest bitmap size, changing the size of the first bitmap will allow us easily achieve the desired geometry. Moreover, the revised process planning method is only working for convex geometry parts. Future work can be done for fabricating concave lens.

5.2.2 Shape limitation of the ECPL system

By applying the new process plan algorithm, the case 2 was rerun. Figure 53 shows the final simulation profile after building 24 layers. The blue line indicates the simulated geometry profile and the black line indicates the desired geometry profile. The simulation result is much better than the previously obtained result. The simulated profile reached the desired the height and radius, but the entire geometry profile still had some discrepancy on that. That leads to the question of whether the ECPL process is able to fabricate a sample with a negative conic constant?

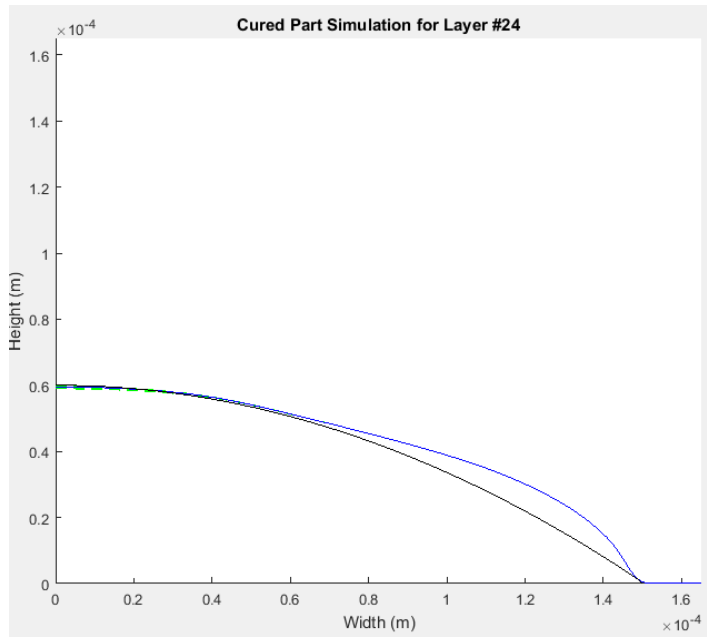


**Figure 53: Geometry profile for case 2 from the revised process planning algorithm
(Blue line: simulated geometry profile; Black line: desired geometry profile)**

To investigate this problem, Figure 53 can be used again for illustration. In order to discover the curvature easily, the idea of a tangent line was introduced. If we apply a tangent line to demonstrate the curvature, the slope of the tangent line can be used as a characteristic parameter. As Figure 54 shows, the slope of the tangent line of the cured profile gets sharper with increasing time, and then reaches stability in some points. This shows the limitation of the ECPL process. By analyzing that, the capability to reach the certain slope in the edge in ECPL process is limited. The range of the slope of the tangent line in the edge is suggested to be -1.475 to -3.671 by analyzing Figure 54. Therefore, the ECPL system is not able to fabricate the entire geometry for samples with slope out of the range. This problem can be fixed by using grayscale bitmaps, which can be discovered in the future. The slope of the tangent line in the edge for case 2 is calculated to be -0.73

which is out of the range. Hence, the case 2 is not expected to be fabricated precisely in the ECPL system in the current stage.

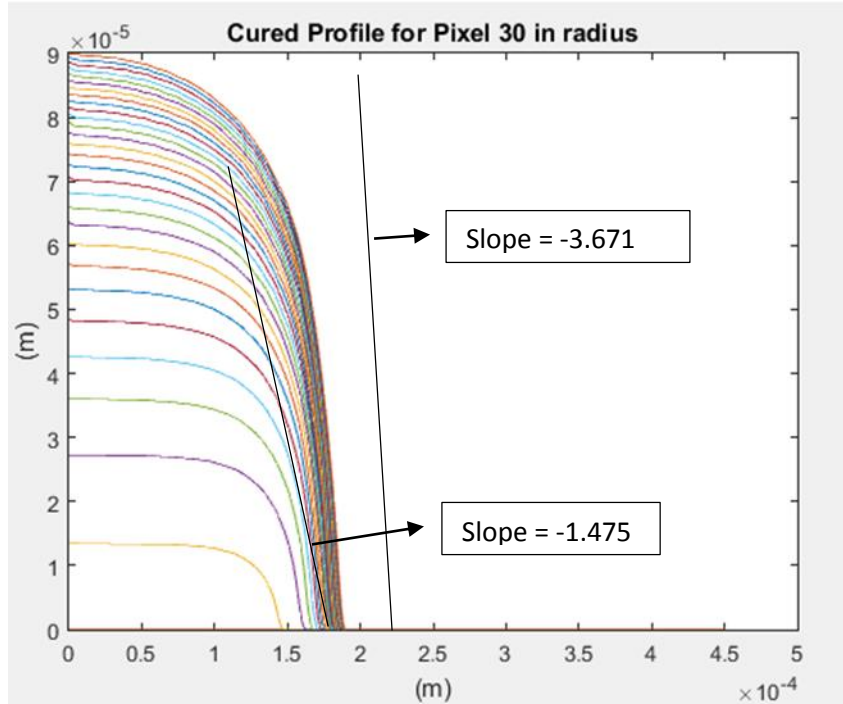


Figure 54: Slope analysis

5.3 Experimental Validation

To validate the refined hypothesis 2, three cases were conducted.

Case 1: The desired geometry was an aspheric lens of 200 micrometers in diameter and 50 micrometers in height. The conic constant was 0. After running the process planner on this geometry, the bitmaps and exposure times were computed, as shown in Figure 55. The experimental results are shown in Figure 56. A 20X microscope objective was used to obtain the dimensional height and diameter, but measured points along the profile had significant noise. Therefore, the 50X microscope objective was used to get the geometry

profiles. The figure shows the comparison of desired geometry and experimental result in half-sectional view.

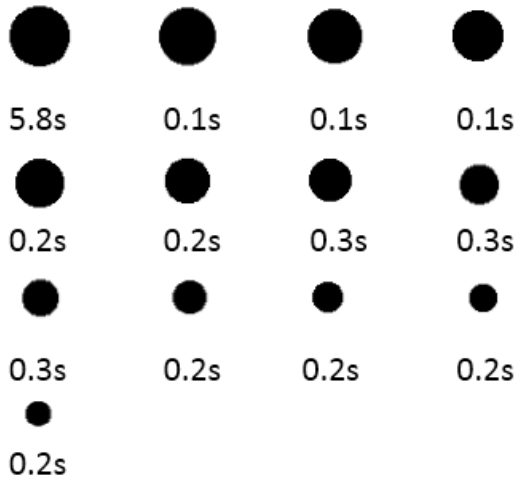


Figure 55: Bitmaps and exposure times used to fabricate the sample

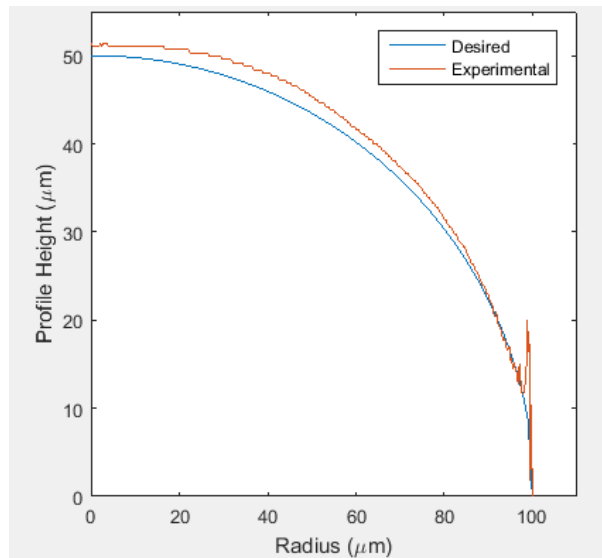


Figure 56: Comparison of the desired geometry and experimental result for case 1

Case 2: The desired geometry was an aspheric lens of 300 micrometers in diameter and 60 micrometers in height. The conic constant was 0. The same procedure was applied as

was used in case 1. Figure 57 shows the process inputs used in case 2: bitmaps and exposure times. Figure 58 presents the comparison of the desired geometry and the experimental result in half-sectional view.

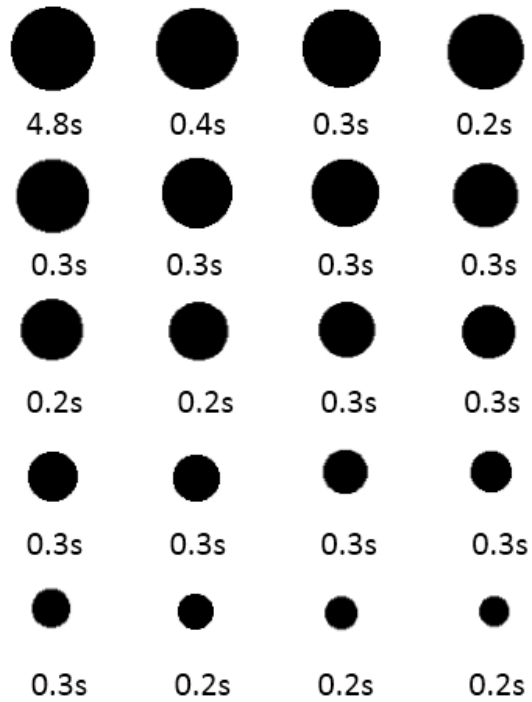


Figure 57: Bitmaps and exposure times used to fabricate the sample for case 2

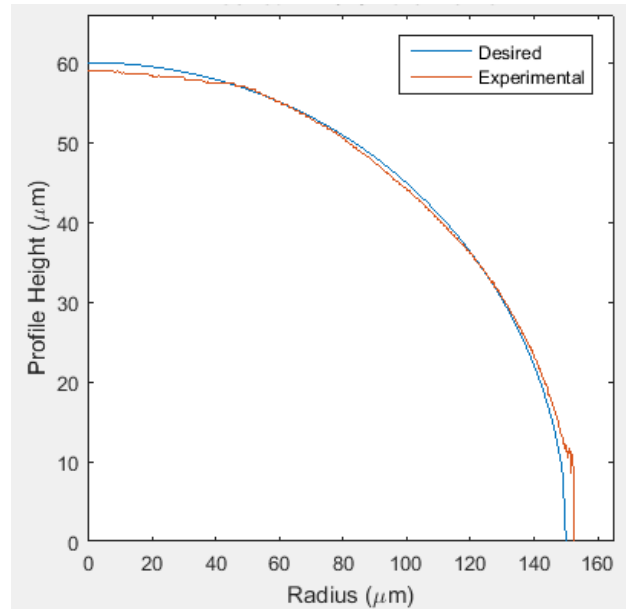


Figure 58: Comparison of the desired geometry and experimental result (right) for case 2

Case 3: The desired geometry was an aspheric lens of 400 micrometers in diameter and 80 micrometers in height. The conic constant was 0. The same procedure was applied as was used in case 1. Figure 59 shows the process inputs used in case 3: bitmaps and exposure times. Figure 60 presents the comparison of the desired geometry and the experimental result in half-sectional view.

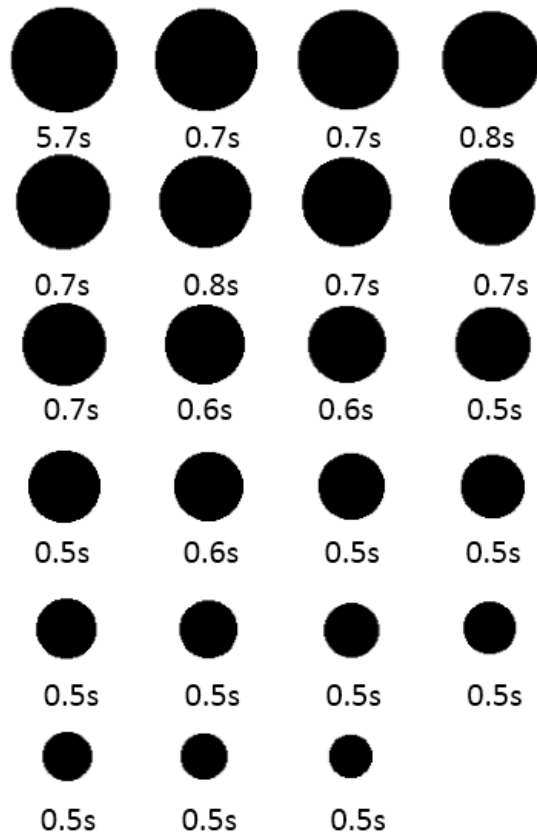


Figure 59: Bitmaps and exposure times used to fabricate the sample for case 3

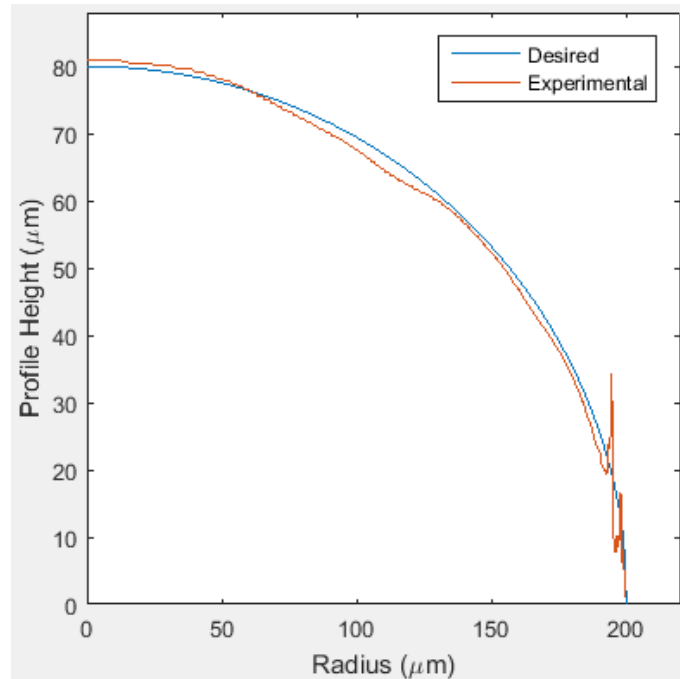


Figure 59: Comparison of the desired geometry and experimental result for case 3

Case 4: This is a special case. The desired geometry was an aspheric lens of 300 micrometers in diameter and 60 micrometers in height. The conic constant was -1. This case was discussed above in the section 5.1.2. The same procedure was applied as was used in case 1. Figure 61 shows the process inputs used in case 4: bitmaps and exposure times. Figure 62 presents a comparison of the desired geometry in black line and the experimental result in red in half-sectional view. The simulated geometry profile is also provided in the blue line. The experimental result fit the simulated geometry profile extremely well. As a conclusion, the results prove that the process model created in this study is highly accurate.

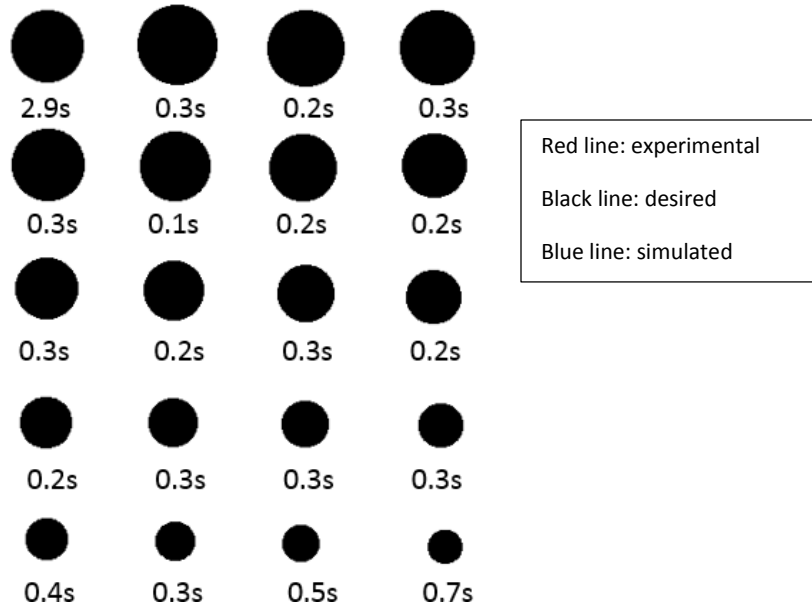


Figure 60: Bitmaps and exposure times used to fabricate the sample for case 4

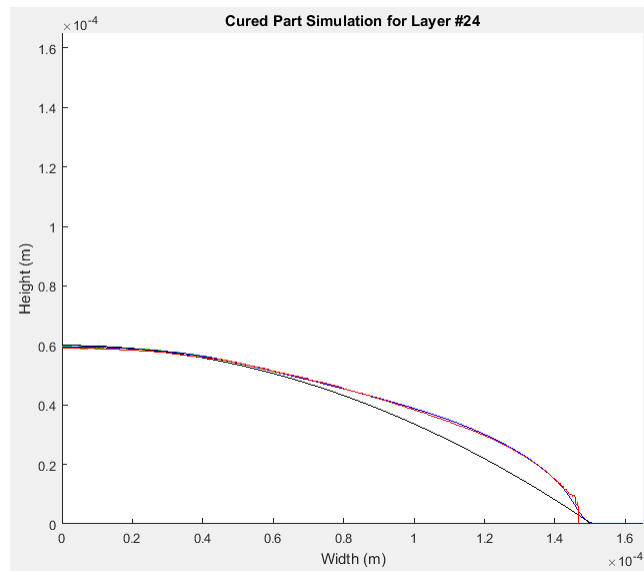


Figure 61: Comparison of the desired geometry and experimental result for case 4

5.4 Error Analysis

Overall, these three cases show that the experimental results matched the desired geometry very well. Table 5 shows the error percentage in height and the error

percentage in diameter. The error percentage was calculated as (experimental value – desired value) / desired value. It was noted that three samples were fabricated for each case, and the result shown in the table is the average.

Table 5: Error percentage in height and diameter for case 1, 2 and 3

Case	Error in Diameter	Error in Height
Case 1: D = 200 μm H = 50 μm	1.43% or 2.85 μm	4.95% or 2.475 μm
Case 2: D = 300 μm H = 60 μm	1.96% or 5.87 μm	1.72% or 1.032 μm
Case 3: D = 400 μm H = 80 μm	-0.4% or 0.8 μm	0.76% or 0.608 μm

The table demonstrates that the deviation between the experimental result and the simulation result is less than 5% in all three cases. To account for the possible error in the process planning method, there are three aspects that may cause the discrepancy listed in Table 6.

The first possible error is the threshold for simulation when we run the Matlab program to obtain the desired geometry. The exposure time for each layer will be increasing until the simulation result is larger than the desired profile within 3 microns cumulative error, as we discussed above. The condition to stop curing the entire sample is when the maximum height within ± 1 microns to the desired height and as well as

satisfying the condition to stop for each layer. Therefore, there will be a maximum of 3 microns over cure for entire profile and maximum 1-micron difference in the sample height.

The second possible error is the deviation in polymerization model. The estimate of the reaction rate can match the experimental model to the simulation model within ± 2 microns, which can be shown in Figure 41, 42 and 43. Although the new polymerization model can accurately predict the entire profile, there is still some mismatch between the reality and the model. ± 2 microns are considered reasonable to accept.

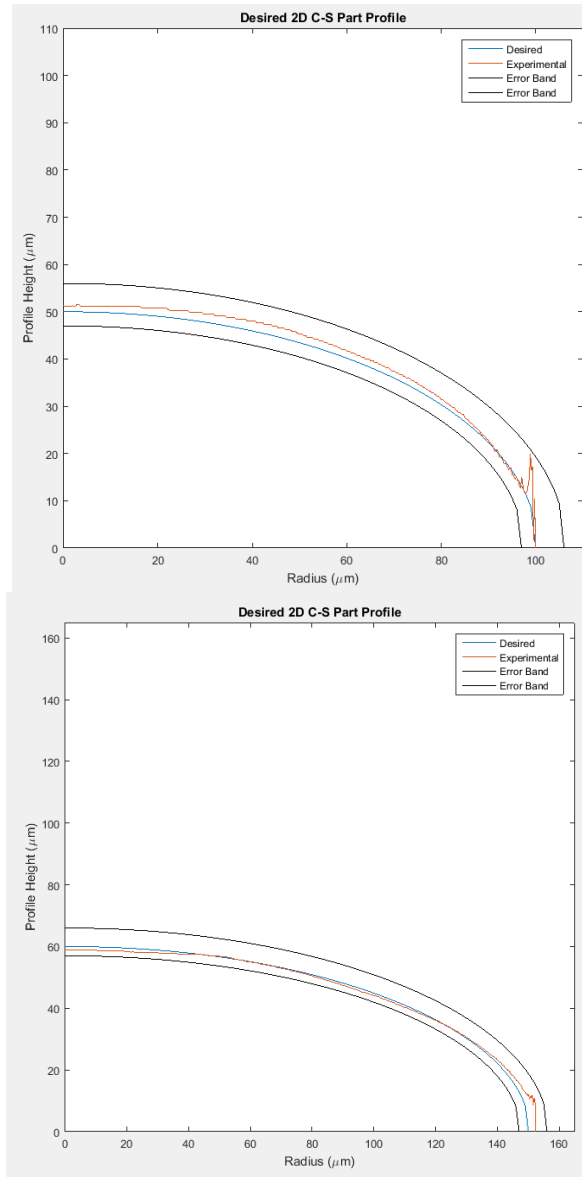
The third possible error is the minimum difference between times and pixels. That is the limitation for pixel step size and time step size. Since the minimum size changing for the bitmap is 1, and the minimum time changing for exposure time is 0.1s, due to the system limitation, it will cause 1 micron discrepancy in width.

Table 6: Allowable discrepancy for process planning method

Threshold for simulation	+3 microns overall; ± 1 microns in height
Deviation in polymerization model	± 2 microns overall
Minimum difference between times and pixels	± 1 microns in width
Overall	-3 to +6 microns

To add on all these possible errors, the tolerance for the empirical process planning method is -3 to +6 microns. Compared to Table 5, all the values are within this

tolerance. Figure 63 shows error bands for cases 1, 2, and 3 with the desired profile and experimental profile for a better demonstration.



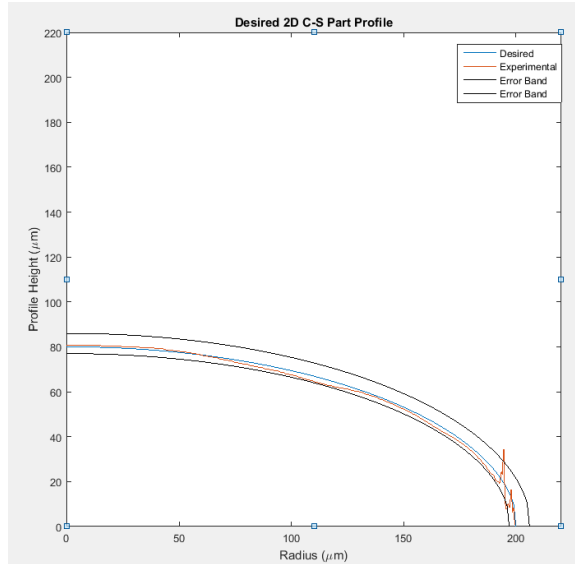


Figure 62: Comparison of the desired geometry and experimental result with error band for case 1, 2 and 3

The ability for the process planning method to achieve the diameter and height is proved above. The research goal is not only to increase the accuracy in obtaining the diameter and height, but also to improve the geometry profile as well. Therefore, error in the geometry profile is considered in the following. To calculate the error percentage in the geometry profile, Equation 28 was used:

$$Error = \frac{\sum(Z-Z_r)}{\sum Z_r} * 100\% \quad (28)$$

Z presents the experimental height for the corresponding x value and Z_r presents the desired height for the corresponding x value. Adding them together will provide an approximate area difference between the experimental profile and the desired profile. The sampling period, which is the delta-r (change in radius) between the Z and Z_r measurements, depends on the number of values that are exported from the confocal microscope. 441, 672, 862 and 647 are used in cases 1, 2, 3 and 4 respectively. Based on

that, the profile error for case 1 is 3.95%, 1.5% for case 2, 2.21% for case 3 and 7.63% for case 4. Although 7.63% is larger than our 5% goal, it is due to the limitation of the constant intensity, which is still expected. Hence, the research question #2 is validated and the research objective is successfully achieved.

5.5 Chapter Summary

This chapter presented the failure of the existing process planning method and proposed the second research question on how to get a better process planning method in order to get the correct process inputs. The new polymerization model and irradiance model, which were described in the last chapter, were applied to the new empirical process planning method. The algorithm of the existing process planning method was used at first. The software Matlab along with COMSOL was used to formulate the process planning method. The simulated results showed that the old algorithm was insufficient to get the accurate process inputs. The old algorithm did not consider the vertical radius of cured profile for each “layer”. It only considered the error between the simulated profile and the desired profile on the current “layer” and the previous “layer”. However, the research showed that the first several “layers” might keep expanding in a certain condition. Therefore, a better process planning method was formulated by controlling the vertical radius of the cured profile. Multiple experiments were conducted to validate the new process planning method. Error analysis was performed as well. The error on simple dimensions such as height and width, or entire geometry profile were both less than 5%, which was set as the goal of the research at the beginning of the thesis.

Moreover, the simulation results demonstrated the limitations of the current process planning method. Since it was assumed that the intensity was constant and flat,

the new empirical process planning method can be used only for the certain shapes of lenses. A more complete process planning method, which can be used for more complex geometry, is expected to be discovered in the future.

CHAPTER 6

CLOSURE AND RECOMMENDATIONS

This chapter summarizes the concepts and findings through the entire document. In Section 6.1, a summary of the thesis will be conducted to get an overall understanding of the research. Section 6.2 readdresses all the research questions and hypotheses. An evaluation of hypotheses will be performed in the following. In Section 6.3, the value and the contributions of this work will be presented. The scope of future work will be suggested at the end of this chapter.

6.1 Summary of the thesis

Overall, the objective of this thesis is to formulate an empirical process planning method in order to get a better estimate of the process inputs for the desired geometry. Compared to the process planning methods reported in the literature, the goal of the new empirical process planning method is to decrease the profile error between desired geometry and simulated geometry within 5%. Due to the application of the ECPL system and current level of research, the target geometry discovered in this thesis is focused on the symmetrical lens. In this thesis, the background of the ECPL system was fully illustrated in Chapter 1 and 2. In order to fulfill the objective of this research, knowledge of stereolithography and mask projection micro-stereolithography were necessary. The existing theoretical models for the ECPL system—the polymerization model and the irradiance model--were discussed in Chapter 2, and the existing process planning method for ECPL system was discussed as well. The research gap and motivation of this study were introduced, and the research questions, and hypotheses for this thesis were addressed.

In Chapter 3, the design of the ECPL system was improved to get a more stable and valuable system. The basic setup for the ECPL system was available in the literature. The existing ECPL system was found not to be stable and repeatable for fabricating samples. After discovery, the beam conditioning system, which was used to homogenize and collimate the light, was improved to get a more stable and constant light. The UV light was found to be unstable after a number of years' assumption to the contrary. Hence, the intensity of the light was expected to be checked every time before the experiments. Furthermore, in order to enhance the adhesion between the experimental slides and samples, a designed pretreatment method was applied to the glass slides. The samples from ECPL system were found to be acceptably smooth, clean and clear, which showed that the discovery of the ECPL system is reasonable and valuable.

The research conducted in this thesis focused on how to formulate a more accurate process model of the ECPL system. The existing polymerization model could not be directly applied to the ECPL system. The reaction rates and system coefficients needed to be modified. Moreover, it was experimentally found that the polymerization model could be accurately modeled if the reaction rates for smaller irradiation area were set linearly. The details of empirically modeling the polymerization model and the irradiance model were described in Chapter 4. COMSOL software was used to simulate the process, and multiple experiments were conducted to validate the theoretical models.

Chapter 5 presented an empirical process planning method based on the new polymerization model and irradiance model. The software Matlab was used to formulate the process planning method. The new process planning method showed the ability to estimate the process inputs for the desired geometry by comparing the simulated part

geometry with the experimental results. This research finally showed a more accurate process planning method than was found in the literature for the ECPL system. The polymerization model and irradiance model created in this thesis can be used by other researchers to get the predictions of the shape from stereolithography process, especially for micro-applications.

6.2 Evaluation of hypothesis

This section provides evaluation of the research questions and hypotheses. The objective of this research presented at the beginning of the paper is readdressed here:

To increase accuracy in obtaining geometry profile within 5% error of overall desired geometry profile of the process plan for fabricating lenses using the ECPL process.

In order to achieve this research goal, the research questions were identified, and the corresponding hypotheses were performed. The validation of the hypotheses will be discussed in the following:

Research Question 1: How to refine the polymerization model to better predict the sample geometry profile?

Hypothesis: The polymerization model can be improved if the chemical reaction rates are modified as a function of the irradiation area.

Explanation: The Beer-lambert law suggested that the height of the cured parts depends on the exposure time for the resin. However, the experiments found that smaller irradiation areas, less than 200 microns in width, cannot reach the same height with the same exposure time. The research on the micro applications in the literature is limited.

Therefore, the polymerization model is expected to be modified for the smaller irradiation area.

Validation of Hypothesis 1: An existing kinetic model from the literature, with oxygen inhibition and diffusion was used in this study. The entire model was modeled in the COMSOL software to simulate the chemical reaction and estimate the geometry profile of the cured parts. The working curves for both larger irradiation samples and smaller irradiation samples were created based on the Beer-Lambert Law. The chemical reaction rates were modified to fit the working curve to the experimental data. Moreover, the chemical reaction rates were found to be the same for larger irradiation areas and in an inverse linear relationship to smaller irradiation areas. Possible reasons were listed and analyzed for future work. Finally, the hypothesis was experimentally validated that the combination of revised irradiance model and revised polymerization model are able to estimate the shape of a cured part within $\pm 2 \mu\text{m}$.

Research Question 2: How to estimate the bitmaps and exposure times used in order to obtain the desired geometry?

Hypothesis: A more accurate process planning method can be created by controlling the layer width of the entire cured part.

Explanation: The existing process planning method considered minimizing the height difference between the simulation results and the desired geometry, but it did not consider the width difference for each curing “layer” between the simulation results and desired geometry.

Validation of Hypothesis 2: MATLAB and COMSOL software were used to apply the empirical process planning method with the revised polymerization model, irradiance model, and process plan algorithm. Simulation results showed that the existing process plan algorithm was not able to estimate accurately the process inputs: exposure time and bitmaps. It showed that the existing process planning method did not consider the vertical radius of the cured profile for each “layer”. Therefore, the hypothesis was made that controlling the part’s vertical radius needs to be considered in the process planning method. New algorithm with considering the part width for each “layer” was implemented in the MATLAB software. The new process planning method showed a much better profile prediction to the desired geometry. 4 samples with different geometry specifications were conducted to validate the new process planning method. Through the new process planning method, the process inputs: bitmaps and exposure time were obtained for each case. Samples were fabricated by using these bitmaps and exposure times. The experimental results showed a good match to the desired geometry. The profile error was concluded within 5% of the desired geometry, which successfully fulfill the goal of this research study.

6.3 Contributions

A process planning method for the Exposure Controlled Projection Lithography System was available in the literature. However, the existing process planning method concluded more than a 25% error in estimating the geometry profile of the fabricated samples. For the polymerization model in the literature, there were two approaches. One was to use the Beer-Lamberts model to estimate the height of the cured parts. The model was created experimentally, so that this model was very accurate for estimating the

geometry height. Another approach was to simulate the chemical reaction inside the resin to estimate the profile of the cured parts. Compared to the Beer-Lamberts model, this model was able to provide the part profile, as well as the part height. Since the reaction rates can vary due to the experimental environments and resin properties, the model created by this approach can be hard to control. Due to these advantages and disadvantages of the approaches, an empirical polymerization model, which combined these two approaches together, was created in this research to formulate a better polymerization model. A revised process planning method based on this empirical polymerization model was created for the ECPL system.

The primary contribution of this work is in the accuracy of estimating the geometry profile by using the polymerization model. The contributions of the thesis can be concluded as follows:

1. It has been shown that the empirical process planning method created in this study provides the most accurate estimates of the process inputs for the ECPL system through the literature. The error was more than 25% in the existing process planning method. The new empirical process planning method provides less than 5% error between the estimating profile and the experimental profile. The method can be used for the ECPL system to fabricate the desired lens.
2. The polymerization model created in this thesis can be used for other stereolithography processes, especially for micro-applications. The Beer-lambert model shows that the height of the cured part has a certain relationship with the time, but no relationship with the irradiation area. This research found that smaller irradiation area, which is less than 200 microns in width, cannot reach the same

height as those larger irradiation areas. The new polymerization model in this study included this finding.

3. The exact reason for the height difference between the smaller irradiation area and larger irradiation area was not found in this study. However, the method to modify the polymerization model for the smaller irradiation area was to change the propagation rate and termination rate for the radicals linearly. It was conjectured that the diffusion rate for some species was different in the smaller irradiation area. More discovery can be contributed in the future.
4. This thesis provided a next generation of the ECPL system. The setup of the ECPL system was improved, and the procedure for fabricating lenses through the ECPL system was modified as well, which offered a more mature system.

6.4. Future Work

Future work is expected to mature the ECPL process as a manufacturing process for fabricating micro applications for different shapes of geometry.

For the design of the ECPL system, the UV light source was expected to be real-time monitored so that any decaying of the lights can be found on time. Moreover, the smallest resolution for the system is limited by many factors, such as magnification of the projection system and the minimum step sizes for pixels and time. More precise instruments can be used for better resolution.

The reason for using different reaction rates for smaller irradiation areas in the polymerization model created in this study can be discovered in the future. More chemical aspects of knowledge are needed. Moreover, the reaction rates of the resin and the conversion rates of the samples can be determined experimentally by using photo-

DSC (differential scanning calorimetry) as a comparison to the value used in the simulation.

As Chapter 4 indicates, reaction rates vary up to 200 μ bitmap size and then become constant. 200 μ m is the value which was found in the experiment. However, more investigation can be done to see if 200 μ m is a fixed critical point or not. Will 200 μ m change to other values if changing the system parameters such as power intensity or chemical resin? More experiments and parametric study can be done to see the difference.

The process planning method created in this study is sufficient for fabricating lens shape structures, but not for other more complex geometry such as cones and non-axisymmetric geometries. Improvement can be made by using grayscale bitmaps. By applying grayscale method, instead of determining pixel is black or white, we will use different gray scale levels to describe each pixel in the DMD chip. The total energy in each pixel can be varied in a finer resolution, which led to the fabricated samples with a better resolution, a better accuracy and a wider variety of shapes.

A real-time monitoring system is expected to be developed for estimating the part dimensions. The process planning method studied in this research provided a good estimate, but the model for the process planning method needed to be modified depends on different situations of the system. The system coefficients and chemical reaction rates need to be modified every time if the system is changed or the resin is switched. A real-time monitoring system can be developed to overcome this drawback.

APPENDIX
COMSOL MODEL

Explanation of Matlab Codes:

A.1 `axisymnewfirstlayer` FUNCTION - COMSOL Multiphysics Model M-file for curing first “layer”

A.2 `axisym_growth7` FUNCTION - COMSOL Multiphysics Model M-file for curing subsequent “layer”

Appendix A.1: COMSOL Multiphysics Model M-file for curing first “layer”

```
function [profile] =
axisymnewfirstlayer(time,result_folder,findex,saving,Pix)
tic;
Pix
size_fix = 400e-6;
if Pix>19
    a = 0.95; %Kp value
else
    a = 0.021*Pix+0.49;
end
b = (a/1.45)^2; %Kt value
clear profile;
clear Z;
file_n = strcat(result_folder,'\ ',num2str(findex),'_lightools.txt');
%
%
% Model exported on Feb 3 2016, 17:01 by COMSOL 5.2.0.220.

import com.comsol.model.*
import com.comsol.model.util.*

model = ModelUtil.create('Model');

model.modelPath('E:\dropbox\Dropbox\ECPL_YingZ\comsol');

model.label('axisym_2.2-finalversion.mph');

model.comments(['Axisym 1.10\n\n']);

model.param.set('ep', '15', 'Epsilon (m^2/mol)');
model.param.set('MW', '256', 'Molecular Weight (g/mol) of Initiator');
model.param.set('wt', '20', 'Percentage concentration of PI (%)');
model.param.set('I0', '9.5', 'Peak Irradiation (W/m^2)');
model.param.set('lambd', '365e-9', 'Wavelength (m)');
model.param.set('phi', '0.6');
model.param.set('NA', '6.023e23');
model.param.set('H', '6.626e-34', 'J-s');
model.param.set('c', '3e8', 'Speed of light (m/s)');
model.param.set('Dpi', '0.0624e-10', 'Diffusivity of Initiator');
model.param.set('Dm', '0.054e-10', 'Diffusivity of Monomer');
model.param.set('exposure', '6', 'Exposure Time');
model.param.set('Ktoxy', '300', 'Radical termination rate constant with
oxygen');
model.param.set('Kt', b, 'Termination rate constant');
model.param.set('Kp', a, 'Propogation rate constant');

model.modelNode.create('mod1');

model.geom.create('geom1', 2);

model.modelNode('mod1').defineLocalCoord(false);
```

```

model.file.create('res6');
model.func.create('int6', 'Interpolation');
model.func('int6').set('source', 'file');
model.func('int6').set('filename', file_n);
model.func('int6').importData;
model.func('int6').set('funcname', 'Intensity_profile');
model.geom('geom1').axisymmetric(true);

model.mesh.create('mesh2', 'geom1');

model.geom('geom1').create('R1', 'Rectangle');
model.geom('geom1').feature('R1').set('size', {'5.0E-4' '3.8E-4'});
model.geom('geom1').feature('R1').set('pos', '0.0,0.0');
model.geom('geom1').setGeom('F:\EDUCATION\COMSOL\Matlab_Script_new\currentmodel_geom1.mphbin');

model.selection.create('sell', 'Explicit');
model.selection('sell').set([1]);
model.selection('sell').label('monomer');

model.variable.create('var1');
model.variable('var1').set('In', '(wt) / (MW * 0.0001)', 'Initiator (mol/m3)');
model.variable('var1').set('Kd1', '(2.3 * phi * ep * lambda) / (NA * H * c)', 'Rate of Dissociation');
model.variable('var1').set('c_DB0', '(3*(100-wt)) / (296*0.0001)');
model.variable('var1').set('Kd', 'Kd1 * I0 * exp(-2.3 * ep * In * z)', 'Kd1 * I0 * exp(-2.3 * ep * In * z) [m^3/mol]');
model.variable.create('reactionvar1');
model.variable('reactionvar1').model('mod1');
model.variable('reactionvar1').set('r_1_rxn_chdi', 'Kd*c_I*Intensity_profile(r)');
model.variable('reactionvar1').set('r_2_rxn_chdi', 'Kp*c_R*c_DB');
model.variable('reactionvar1').set('r_3_rxn_chdi', 'Kt*c_R^2');
model.variable('reactionvar1').set('r_4_rxn_chdi', 'Ktoxy*c_R*c_O2');
model.variable('reactionvar1').selection.geom('geom1', 2);
model.variable('reactionvar1').selection.set([1]);

model.physics.create('chdi', 'DilutedSpecies', 'geom1');
model.physics('chdi').identifier('chdi');
model.physics('chdi').field('concentration').field('c_I');
model.physics('chdi').field('concentration').component({'c_I' 'c_R' 'c_DB' 'c_Rdead' 'c_O2'});
model.physics('chdi').create('reac1', 'Reactions', 2);
model.physics('chdi').feature('reac1').selection.named('sell');

model.mesh('mesh2').create('ftril', 'FreeTri');
model.mesh('mesh2').create('ref1', 'Refine');
model.mesh('mesh2').feature('ref1').selection.geom('geom1', 2);
model.mesh('mesh2').feature('ref1').selection.all;

model.view('view1').axis.set('abstractviewxscale', '9.106754532695049E-7');
model.view('view1').axis.set('ymin', '-7.1492027018393856E-6');

```

```

model.view('view1').axis.set('xmax', '5.579602438956499E-4');
model.view('view1').axis.set('abstractviewscale', '9.106754532695049E-7');
model.view('view1').axis.set('abstractviewbratio', '-0.018813690170645714');
model.view('view1').axis.set('abstractviewratio', '0.8178684115409851');
model.view('view1').axis.set('abstractviewrratio', '2.424607276916504');
model.view('view1').axis.set('xmin', '-4.837231244891882E-6');
model.view('view1').axis.set('abstractviewlratio', '-0.20234939455986023');
model.view('view1').axis.set('ymax', '3.8079856312833726E-4');

model.physics('chdi').prop('ShapeProperty').set('order_concentration', '2');
model.physics('chdi').prop('MassConsistentStabilization').set('glim_mas s', '0.1[mol/m^3]/chdi.helem');
model.physics('chdi').prop('MassConsistentStabilization').set('massStre amlineDiffusion', '0');
model.physics('chdi').prop('MassConsistentStabilization').set('massCros swindDiffusion', '0');
model.physics('chdi').prop('TransportMechanism').set('Convection', '0');
model.physics('chdi').feature('cdm1').set('D_c_I', {'1e-20'; '0'; '0'; '0'; '1e-20'; '0'; '0'; '0'; '0'; '1e-20'});
model.physics('chdi').feature('cdm1').set('D_c_R', {'1e-20'; '0'; '0'; '0'; '1e-20'; '0'; '0'; '0'; '0'; '1e-20'});
model.physics('chdi').feature('cdm1').set('D_c_DB', {'1e-20'; '0'; '0'; '0'; '1e-20'; '0'; '0'; '0'; '0'; '1e-20'});
model.physics('chdi').feature('cdm1').set('D_c_Rdead', {'1e-20'; '0'; '0'; '0'; '1e-20'; '0'; '0'; '0'; '0'; '1e-20'});
model.physics('chdi').feature('cdm1').set('D_c_O2', {'4.2e-10'; '0'; '0'; '0'; '4.2e-10'; '0'; '0'; '0'; '0'; '4.2e-10'});
model.physics('chdi').feature('cdm1').label('Diffusion');
model.physics('chdi').feature('init1').set('initc', {'In'; '0'; 'c_DB0'; '0'; '1.05'});
model.physics('chdi').feature('react1').set('R_c_I', '-r_1_rxn_chdi');
model.physics('chdi').feature('react1').set('R_c_R', '2*r_1_rxn_chdi-2*r_3_rxn_chdi-r_4_rxn_chdi');
model.physics('chdi').feature('react1').set('R_c_DB', '-r_2_rxn_chdi');
model.physics('chdi').feature('react1').set('R_c_Rdead', 'r_3_rxn_chdi+r_4_rxn_chdi');
model.physics('chdi').feature('react1').set('R_c_O2', '-r_4_rxn_chdi');

model.mesh('mesh2').feature('ref1').set('numrefine', {'3'});
model.mesh('mesh2').feature('ref1').set('boxcoord', 'on');
model.mesh('mesh2').feature('ref1').set('ymax', '0.0001');
model.mesh('mesh2').feature('ref1').set('xmax', '0.0002');
model.mesh('mesh2').run;

model.study.create('std1');
model.study('std1').create('time', 'Transient');

model.sol.create('soll');

```

```

model.sol('sol1').study('std1');
model.sol('sol1').create('st1', 'StudyStep');
model.sol('sol1').create('v1', 'Variables');
model.sol('sol1').create('t1', 'Time');
model.sol('sol1').feature('t1').create('fc1', 'FullyCoupled');
model.sol('sol1').feature('t1').create('d1', 'Direct');

model.result.create('pg1', 'PlotGroup2D');
model.result('pg1').set('data', 'dset1');
model.result('pg1').create('con1', 'Contour');
model.result('pg1').feature('con1').set('data', 'dset1');

model.study('std1').feature('time').set('tlist', time);
model.study('std1').feature('time').set('rtolactive', true);
model.study('std1').feature('time').set('mesh', {'geom1' 'mesh2'});

model.sol('sol1').attach('std1');
model.sol('sol1').label('Solver 1');
model.sol('sol1').feature('st1').label('Compile Equations: Time
Dependent');
model.sol('sol1').feature('t1').set('solfile', false);
model.sol('sol1').feature('t1').set('storeudot', false);
model.sol('sol1').feature('t1').set('bwinitstepfrac', '1.0');
model.sol('sol1').feature('t1').set('tlist', time);
model.sol('sol1').feature('t1').set('atolglobalmethod', 'unscaled');
model.sol('sol1').feature('t1').set('initialstepbdf', '0.0010');
model.sol('sol1').feature('t1').set('atolglobal', '0.0010');
model.sol('sol1').feature('t1').feature('fc1').active(false);
model.sol('sol1').feature('t1').feature('fc1').set('damp', '1.0');
model.sol('sol1').feature('t1').feature('fc1').set('ratelimitactive',
true);
model.sol('sol1').feature('t1').feature('d1').set('errorchk', 'off');
model.sol('sol1').runAll;

model.result.dataset('dset1').label('Solution 1');
model.result('pg1').label('Concentration (chdi)');
model.result('pg1').feature('con1').set('levelmethod', 'levels');
model.result('pg1').feature('con1').set('smooth', 'everywhere');
model.result('pg1').feature('con1').set('descr', '((c_DB0-
c_DB)/c_DB0)*100');
model.result('pg1').feature('con1').set('resolution', 'extrafine');
model.result('pg1').feature('con1').set('levels', 'range(20,10,20)');
model.result('pg1').feature('con1').set('expr', '((c_DB0-
c_DB)/c_DB0)*100');
model.result('pg1').feature('con1').set('recover', 'ppr');

fig1 =figure;
mphplot(model,'pg1');
if saving ==1
    currentmodel = 'F:\EDUCATION\COMSOL\Matlab_Script_new\currentmodel';
    model.save(currentmodel);
end
data = [];
xdata =[];
ydata = [];

```

```

max_size = 6e-4;
axesObjs = get(fig1, 'Children');
dataObjs = get(axesObjs, 'Children');
objTypes = get(dataObjs, 'Type');
xdata = get(dataObjs, 'XData');
ydata = get(dataObjs, 'YData');
zdata = get(dataObjs, 'ZData');
xcoord = 0:1e-6:(400e-6+50e-6);

profile.x = xcoord;
profile.y = zeros(1,length(xcoord));
[sizexa sizexb] = size(xdata{1});
[sizeya sizeyb] = size(ydata{1});
if sizexa ==2
    data(1,:) = [xdata{1}(1,:) xdata{1}(2,:)];
else
    data(1,:)=xdata{1};
end
if sizeya ==2
    data(2,:) = [ydata{1}(1,:) ydata{1}(2,:)];
else
    data(2,:)=ydata{1};
end
[dummy index] = sort(data(1,:));
sorted_x = data(1,index);
sorted_y = data(2,index);
for k = 1:length(xcoord)
    [min_difference, array_pos]=min(abs(sorted_x(:)-xcoord(k)));
% locate the index where the x-coordinate is xccord
    if (min_difference < 4e-6)
        profile.y(k)=sorted_y(array_pos);
    end
    if ((profile.x(k)>=max_size) || (profile.x(k)<-max_size))
        profile.y(k) = 0.0; % manually clean the edges
    end
end
y = sort(profile.y);
l = length(y);
for z = 0:(l-1)
    newy(z+1)=y(l-z);
end
profile.y = smooth(newy);
% Clear stuff before next loop for incremental time
clear xdata;
clear ydata;
clear zdata;
close(fig1); % Close the COMSOL plot figure

end

```

Appendix A.2: COMSOL Multiphysics Model M-file for curing subsequent “layer”

```
% COMSOL Multiphysics Model M-file
% Generated by COMSOL 3.5a (COMSOL 3.5.0.603, $Date: 2008/12/03
17:02:19 $)
% Some geometry objects are stored in a separate file.
% The name of this file is given by the variable 'flbinaryfile'.
% This function simulates for only one time period only
% Mesh is fixed to assuming 400 microns of curing

function [profile] =
axisym_growth7(time,result_folder,findex,saving,Pix)
tic;
size_fix = 400e-6;
if Pix>19
    a = 0.95;    %Kp value
else
    a = 0.021*Pix+0.49;
end
b = (a/1.45)^2;    %Kt value
% clc;
clear profile;
clear Z;
file_n = strcat(result_folder,'\ ',num2str(findex),'_lightools.txt');

import com.comsol.model.*
import com.comsol.model.util.*
model = mphload('F:\EDUCATION\COMSOL\Matlab_Script_new\currentmodel');
presol = strcat('sol',num2str(findex-1));
currsol = strcat('sol',num2str(findex));
% model.sol(presol).detach;

model.func('int6').set('source', 'file');
model.func('int6').set('filename', file_n);
model.func('int6').importData;
model.func('int6').set('funcname', 'Intensity_profile');
model.param.set('Kt', b, 'Termination rate constant');
model.param.set('Kp', a, 'Propogation rate constant');

model.sol.create(currsol);
model.sol(currsol).study('std1');
model.sol(currsol).create('st1', 'StudyStep');
model.sol(currsol).feature('st1').set('study','std1');
model.sol(currsol).create('v1', 'Variables');
model.sol(currsol).attach('std1');
model.sol(currsol).create('t1', 'Time');
model.sol(currsol).feature('v1').set('initmethod', 'sol');
model.sol(currsol).feature('v1').set('initsol', presol);
model.sol(currsol).feature('v1').set('notsolmethod', 'sol');
model.sol(currsol).feature('v1').set('notsol', presol);
model.sol(currsol).feature('v1').set('solnum', 'auto');
model.sol(currsol).feature('v1').set('notsolnum', 'auto');
model.sol(currsol).feature('t1').set('tlist', time);
```

```

dataset = strcat('dset',num2str(findex));
model.result('pg1').run;
model.result('pg1').set('data', dataset);
model.result('pg1').run;
model.result('pg1').feature('con1').set('data', dataset);

model.sol(currsol).runAll;

model.result('pg1').run;

fig1 =figure;
mphplot(model,'pg1');
if saving ==1
    currentmodel = 'F:\EDUCATION\COMSOL\Matlab_Script_new\currentmodel';
    model.save(currentmodel);
end
data = [];
    xdata =[];
    ydata = [];
    max_size = 6e-4;
    axesObjs = get(fig1, 'Children');
    dataObjs = get(axesObjs, 'Children');
    objTypes = get(dataObjs, 'Type');
    xdata = get(dataObjs, 'XData');
    ydata = get(dataObjs, 'YData');
    zdata = get(dataObjs, 'ZData');
    xcoord = 0:1e-6:(400e-6+50e-6);

    profile.x = xcoord;
    profile.y = zeros(1,length(xcoord));
    [sizexa sizexb] = size(xdata{1});
    [sizeya sizeyb] = size(ydata{1});
    if sizexa ==2
        data(1,:) = [xdata{1}(1,:) xdata{1}(2,:)];
    else
        data(1,:)=xdata{1};
    end
    if sizeya ==2
        data(2,:) = [ydata{1}(1,:) ydata{1}(2,:)];
    else
        data(2,:)=ydata{1};
    end
    [dummy index] = sort(data(1,:));
    sorted_x = data(1,index);
    sorted_y = data(2,index);
    for k = 1:length(xcoord)
        [min_difference, array_pos]=min(abs(sorted_x(:)-xcoord(k)));
% locate the index where the x-coordinate is xccord
        if (min_difference < 4e-6)
            profile.y(k)=sorted_y(array_pos);
        end
        if ((profile.x(k)>=max_size) || (profile.x(k)<-max_size))
            profile.y(k) = 0.0;           % manually clean the edges
        end
    end

```

```
    end
y = sort(profile.y);
l = length(y);
for z = 0:(l-1)
    newy(z+1)=y(l-z);
end
profile.y = smooth(newy);
    % Clear stuff before next loop for incremental time
    clear xdata;
    clear ydata;
    clear zdata;
% close(fig1);          % Close the COMSOL plot figure

end
```

REFERENCES

- [1] Jacobs, P. "Rapid Prototyping & Manufacturing: Fundamentals of Stereolithography", Society of Manufacturing Engineers. Dearborn, MI, 1992.
- [2] Gabrielsen, A. Chen, P. and Ding, C. Mask Projection Stereolithography. Retrieved from Georgia Institute of Technology Rapid Prototyping in Engineering
- [3] Sun, C. Fang, N. Wu, D. M. and Zhang, X. "Projection micro-stereolithography using digital micro-mirror dynamic mask Sensors Actuators", Sensors and Actuators A Physical, 2005
- [4] <http://www.aniwaa.com/product/3d-printers/rapidshape-x30/> (Accessed Aug 5, 2016)
- [5] http://envisiontec.com/admin/machine_datasheet/Datasheet_machine39.pdf (Accessed Aug 5, 2016)
- [6] <http://www.3dsystems.com/3d-printers/professional/projet-1200> (Accessed Aug 5, 2016)
- [7] <http://carbon3d.com/> (Accessed Aug 5, 2016)
- [8] Tumbleston, J. R., D. Shirvanyants, N. Ermoshkin, R. Januszewicz, A. R. Johnson, D. Kelly, K. Chen, R. Pinschmidt, J. P. Rolland, A. Ermoshkin, E. T. Samulski, and J. M. Desimone. "Continuous Liquid Interface Production of 3D Objects." *Science* 347.6228 (2015): 1349-352. Web.
- [9] Jariwala, A. S., & Rosen, D. "Modeling and process planning for exposure controlled projection lithography", P.H.D Thesis, Georgia Institute of Technology, School of Mechanical Engineering, Atlanta, 2015.

- [10] Erdmann L., Deparnay A., Maschke G., Längle M., Bruner R., 2005, "MOEMS-Based Lithography for the Fabrication of Micro-Optical Components", *Journal of Microlithography, Microfabrication, Microsystems*, 4(4), pp. 041601-1, -5.
- [11] Mizukami Y., Rajnaik D., Rajnaik A., Nishimura M., 2002, "A Novel Microchip for Capillary Electrophoresis with Acrylic Microchannel Fabricated on Photosensor Array", *Sensors and Actuators B*, 81, pp. 202-209.
- [12] Jariwala A., Ding F., Zhao X., Rosen D., 2008, "A Film Fabrication Process on Transparent Substrate Using Mask Projection Stereolithography", D. Bourell, R. Crawford, C. Seepersad, J. Beaman, H. Marcus, eds., *Proceedings of the 19th Solid Freeform Fabrication Symposium*, Austin, Texas, pp. 216-229.
- [13] Jariwala A., Ding F., Boddapati A., Breedveld V., Grover M. A., Henderson C. L., Rosen D. W., 2011, "Modeling effects of oxygen inhibition in mask-based Stereolithography", *Rapid Prototyping Journal*, 17(3), pp. 168-175.
- [14] Jariwala, A., Ding, F., Zhao, X., & Rosen, D. W., "A Process Planning Method for Thin Film Mask Projection Micro-Stereolithography", *Proceedings of the ASME 2009 International Design Engineering Technical Conferences & Computers and Information in Engineering Conference*. San Diego, CA, Paper no. DETC2009-87532, 2009.
- [15] Limaye, A. S. and Rosen D. W., "Process planning method for mask projection micro-stereolithography," *Rapid Prototyping Journal*, vol. 13, pp. 76-84, 2007.
- [16] Decker C., "Photoinitiated Curing of Multifunctional Monomers," *Acta Polymerica*, vol. 45, pp. 333-347, Oct 1994.

- [17] Tang, Y. "Stereolithography Cure Process Modeling," PhD, School of Chemical & Biomolecular Engineering, Georgia Institute of Technology, Atlanta, 2005.
- [18] Boddapati, A. "Modeling Cure Depth during Photopolymerization of Multifunctional Acrylates," Masters of Science, School of Chemical & Biomolecular Engineering, Georgia Institute of Technology, Atlanta, 2010.
- [19] Boddapati, A. Rahane, S. B. Slopek, R. P. Breedveld, V. Henderson, C. L. and Grover, M. A. "Gel time prediction of multifunctional acrylates using a kinetics model," *Polymer*, vol. 52, pp. 866-873, 2011.
- [20] Zhao, X. "Process Planning for thick-film mask projection micro stereolithography," MS, Mechanical Engineering, Georgia Institute of Technology, Atlanta 2009.
- [21] Carothers, W. H. "Polymerization," *Chemical Reviews*, vol. 8, pp. 353-426, Jun 1931.
- [22] Carothers, W. H. "Polymers and polyfunctionality.," *Transactions of the Faraday Society*, vol. 32, pp. 0039-0053, 1936.
- [23] Flory, P. J. "Molecular size distribution in three dimensional polymers. I. Gelation," *Journal of the American Chemical Society*, vol. 63, pp. 3083-3090, Jul-Dec 1941.
- [24] Monneret, S. Loubere, V. and Corbel, S. "Microstereolithography using a dynamic mask generator and a non-coherent visible Light source," *Design, Test, and Microfabrication of Mems and Moems*, Pts 1 and 2, vol. 3680, pp. 553-561, 1999.
- [25] Bertsch A, Jiguet S, Renaud P, "Microfabrication of ceramic components by microstereolithography," *J Micromech Microeng* 14, 197-203, 2004

- [26] Peng, Q. Guo, Y. Liu, S. and Cui, Z. "Real-time gray-scale photolithography for fabrication of continuous microstructure," *Opt. Lett.* 27, 1720-1722, 2002
- [27] Limaye, A. S. "MULTI-OBJECTIVE PROCESS PLANNING METHOD FOR MASK PROJECTION STEREOLITHOGRAPHY," PhD, Mechanical Engineering, Georgia Institute of Technology, Atlanta, 2007.
- [28] Zhou. C. "OPTIMIZED MASK IMAGE PROJECTION FOR LARGE-AREA BASED ADDITIVE", P.H.D Thesis, University of Southern California, School of Industrial and System Engineering, 2011.
- [29] <http://web.mit.edu/nanophotonics/research.htm> (Accessed Aug 25, 2016)
- [30] Jariwala A., Jones H., Kwatra A., Rosen D. W., 2013, "Process Planning Method For Exposure Controlled Projection Lithography", *Proceedings of the 24th Solid Freeform Fabrication Symposium*, Austin, Texas, pp. 95-110.
- [31] Slopek, R., "In-Situ Monitoring of the Mechanical Properties during the Photopolymerization of Acrylate Resins Using Particle Tracking Microrheology", PhD thesis, Georgia Institute of Technology, Atlanta, 2008.
- [32] Li R., and Schork F., "Modeling of the inhibition mechanism of acrylic acid polymerization," *Industrial & Engineering Chemistry Research*, vol. 45, pp. 3001-3008, Apr 26 2006.
- [33] Gou L., Coretsopoulos C., and Scranton A., "Measurement of the dissolved oxygen concentration in acrylate monomers with a novel photochemical method," *Journal of Polymer Science Part a-Polymer Chemistry*, vol. 42, pp. 1285-1292, Mar 1 2004.

[34] <http://bobmay.astronomy.net/CassNotes/eccentricity.htm> (Accessed Aug 5, 2016)